GEOMORPHOLOGY OF THE CENTRAL INDIAN BASIN AND THE INFLUENCE OF TOPOGRAPHY ON THE DISTRIBUTION OF POLYMETALLIC NODULES

SUBMITTED TO THE
GOA UNIVERSITY
FOR THE DEGREE OF

DOCTOR OF PHILOSOPHY

BY
VIJAYKUMAR. N. KODAGALI

RESEARCH GUIDE

Mr. R. R. NAIR
DEPUTY DIRECTOR AND HEAD, GEOLOGICAL OCEANOGRAPHY DIVISION
NATIONAL INSTITUTE OF OCEANOGRAPHY

WORK CARRIED OUT AT
NATIONAL INSTITUTE OF OCEANOGRAPHY
DONA PAULA, GOA 403 004

OCTOBER 1992

CERTIFICATE

Mr. Vijaykumar N Kodagali has been working under my guidance since 1989. The Ph.D thesis entitled 'Geomorphology of the Central Indian Basin and influence of topography on the distribution of Polymetallic nodules' submitted by him contains the results of his original investigation of the subject. This is to certify that the thesis has not been the basis for the award of any other research degree or diploma of other university.

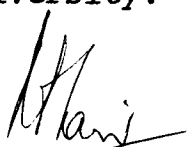

(Mr. R R Nair)

Research Guide
Deputy Director and
Head, Geological Oceanography Division
National Institute of Oceanography,
Dona Paula, Goa 403 004.

ACKNOWLEDGEMENTS

I take this opportunity to sincerely thank some of the many people who have helped me in completing this thesis.

I have been fortunate to be guided by Mr R R Nair, Deputy Director, NIO for this work. He initiated me into Multibeam data processing and provided constant encouragement, constructive criticism to this thesis. I am gratefully indebted to him.

My gratitudes to Dr B N Desai, Director, NIO for permission and facilities extended to carry out this work. I record my gratitudes to late Dr H N Siddiquie, former Director NIO for encouragement and guidance provided during the initial stages of this work.

My friend and colleague Mr Rahul Sharma has been constant source of encouragement during the course of this study. I record my appreciation for his all-round help. Special thanks are due to Mr M Shyam Prasad, Mr P S Rao and Dr N Ramaiah who have helped in keeping my morale high. I am also thankful to all the members of the PMN project who have helped in data collection and sampling. I have been benefitted from my association with Dr A V Mudholkar, Mr S

Afzalpurkar, Mr V Ramswamy, Dr R Mukhopadhyay, Mr B Nagendranath, Dr P C Rao, Mr Sridhar Iyer, Dr S M Gupta, Mr R Banerjee, Dr S M Karisiddiah, Mr N H Khadge, Mr D Pathak and other scientists in the project. Special mention must also be made of Dr V K Banakar, Dr J N Pattan and Dr Pratima Jauhari who also provided with the chemical data used in chapter 9. Dr V K Banakar is also thanked for the useful discussions we had on different topics of the thesis. I am highly indebted to Mr M Sudhakar for providing nodule abundance and grade data from the NIO-PMN data bank. Dr A B Valsangkar is thanked for the critical review of the thesis manuscript. I profusely thank Dr T R P Singh, EIL, New Delhi for the helpful discussions.

I am thankful to the Hydrosweep group comprising Mr G H Ranade, Dr B Chakraborty, Mr Y S N Raju and Mr T Sudhakar for cooperation and help in generating good quality multibeam data. I am grateful to Mr K A Kamesh Raju and Mr T Ramprasad who were associated with me during all stages of data processing, and had fruitful discussions with me. Assistance rendered by Pius George and S Jaishankar in data processing is acknowledged. The cooperation extended by the Marine Instrumentation group, Marine Survey group and the Mechanical Engineering group is gratefully acknowledged. The staff of photography section, drawing section of NIO and the office of the Geological

Oceanography Division is thanked for their help from time to time.

But for my father's persistent coaxing I would not have completed this work this early. I dedicate this work to him and my loving mother. I thank my brothers, sister and in-laws for their love and encouragement.

Last and not the least, this thesis would not have been possible but for the care and enduring support of my wife Jyoti. Also, my sons Rohit and little Karan tolerated my absence from home for long hours for last 6 months.

Vijay Kodagali

THIS WORK IS DEDICATED
TO
MY BELOVED PARENTS

Geomorphology of the Central Indian Basin and Influence of topography on the distribution of polymetallic nodules:

Contents

List of Tables

Chapter 1

Chapter 2

Chapter 3

Chapter 4

Chapter 5

List of Figures

Chapter 2.

Chapter 3

Chapter 4.

Chapter 5

Chapter 6.

Chapter 7.

Chapter 8.

Chapter 9

Total number of figures----- 49.

STATEMENT

As required under the university ordinance 0.413, I state that the present thesis entitled " GEOMORPHOLOGY OF THE CENTRAL INDIAN BASIN AND INFLUENCE OF TOPOGRAPHY ON THE DISTRIBUTION OF POLYMETALLIC NODULES" is my original contribution. To the best of my knowledge, the present study is the first comprehensive study of its kind from the area mentioned.

The literature concerning the thesis has been cited. Due acknowledgements have been made wherever facilities have been availed of.

(Vijaykumar N. Kodagali)

Chapter 1.
INTRODUCTION

Oceans have fascinated man all through the history. Sound of the waves and lure for adventure have had powerful influence on shaping the destiny of countries and mankind. From salt to gold and platinum to uranium, the ocean has the abundance of everything. Seas are the mineral-mines of the future.

Fast depleting land resources have pushed mankind into rigorous search for alternative sources. The deep seabed is the most promising and rewarding of the future living and non-living resources. Non-living resources of the deep seabed promise to make an enormous contribution to the world's resource base. Manganese nodules are the resources of immediate interest to mankind.

The discovery of marine manganese nodules dates back to the 'Challenger' expedition in 1873, on 18th February. This heralded the multidisciplinary investigation on these nodules world over. **Mero (1965)** suggested the manganese nodules as an alternative source of metals to the existing land deposits. The possible economic importance of these nodules in future has been attributed to the substantial concentration of certain elements e.g. nickel, copper, cobalt etc. Because of the availability of all these metals in nodules, the manganese nodules are popularly referred to

as 'polymetallic nodules'. The mineral resources of the deep sea bed beyond the limits of national jurisdiction, was declared as the 'Common Heritage of Mankind' by the United Nations Law of the Sea convention. This generated additional commercial interest in these nodule deposits on the deep-sea floor. Since then a large amount of data have been collected, mainly from the Pacific, on the mode of occurrence of the ferromanganese nodules, their chemistry and other related parameters in order to assess the economic feasibility of these deposits.

Though the Pacific ocean, especially the Clarion-Clipperton fracture zone area is regarded as the most promising area, the Indian Ocean also boasts of large reserves covering over 15 million sq. kms. Table 1.1 lists the area occupied by polymetallic nodules in three major oceans of the world.

Table 1.1

Distribution of nodule resources in different oceans.
(After Moore and Cruickshank, 1973)

Ocean	Area covered by nodules (in Million sq. km)	% share
Pacific	23	50
Indian	15	33
Atlantic	8	17

The ferromanganese nodules are reported to be generally present between 3500 and 6000 meters water depth in all the ocean basins. Initially the nodules were estimated to cover an area of nearly 46 million square kilometers in the world oceans **(Moore and Cruickshank, 1973; Table-1.1)**. Later studies indicate that nodules are present over an area of about 55 million km^2 accounting for about 15 percent of the total area of the world ocean floor **(Archer, 1985)**. However, all these areas will not be of economic interest in the future.

The estimated total reserves of ferromanganese nodules in the world oceans range from 1.7 to 3.0 trillion tons. **Moore and Cruickshank (1973)** calculated the reserves of these nodules in the Pacific, Atlantic and Indian oceans to be of the order of 1.7 trillion tons, of which 1.5 trillion tons are in the Pacific and 0.15 trillion tons in Indian and 0.50 trillion tons are in the Atlantic oceans. As regards the actual metal resources in the nodules, it is estimated that about 430 million tonnes of copper, nickel and cobalt together are available. Table 1.2 lists the metal resources in nodules of world oceans.

In addition to the assessment of the commercial viability of ocean-floor nodules, the studies carried out so far have enormously expanded the knowledge not only on the physical and chemical attributes of the nodules

themselves but also on the oceanographic parameters that directly or indirectly control nodule generation.

Table 1.2

Metal resources in nodules of the world oceans.
(from Archer, 1985)
(All figures in Million tonnes)

Nodules (wet)	-	25,000
Nodules (dry)	-	17,500
Copper	-	175
Nickel	-	215
Cobalt	-	40
Manganese	-	5,000

The ferromanganese nodule deposits occur mostly at the sediment-water interface in the deeper part of the oceans on red clay, siliceous and carbonate-rich sediment substrates. The slow detrital sedimentation rate in the deeper part of the ocean basins and the oxidizing Antarctic Bottom Water current are vital factors for the genesis of these nodules. Availability of nucleus also plays an important role in the nodule formation **(Horn et al., 1973)**.

Different theories have been proposed for the genesis of ferromanganese nodules, but none of them alone can explain the variable nature of chemistry, morphology, mineralogy and growth-rate of the nodules in different oceans or even within any single basin. Multiple sources

of metal supply for the formation of the nodules have been proposed by the majority of the workers. Comparing the slow growth rate (1-5mm/10^6year) of nodules vis-a-vis a much faster detrital sedimentation rate (1- 10mm/10^3years) at the same location, it is intriguing to see the persistence of ferromanganese nodules at the sediment-water interface. The role of bottom currents and deep-sea benthos in retaining the nodules at the sediment-water interface, has been considered viable by a number of workers, but these factors may not explain every situation of nodule occurrence. Buried nodules are however also common in sediment columns.

Investigations on the different aspects of ferromanganese nodules were confined mainly to the Pacific for a long time. Even in early eighties the density of data coverage on nodules in the Indian Ocean was much less than that of Pacific. India, realising the importance of polymetallic nodules plunged into nodule exploration in 1980 and since then lot of new data and information has been collected on Central Indian Basin nodules and it's morphology. As a result of extensive work carried out in the field of survey and exploration in Central Indian Basin and also by meeting other financial criteria, India was registered as a 'Pioneer investor' and subsequently became, in 1987 first country to be allotted a

mine site measuring 1,50,000 sq. kms for exclusive development work. This has rendered India as a leader in the new and challenging field of deep seabed exploration.

During the surveys for polymetallic nodules by the National Institute of Oceanography since 1982, large amount of echosounding data has been collected. This has thrown more light on the hitherto unknown morphology of the Central Indian Basin. With the acquisition of multi-beam swath bathymetric system (Hydrosweep), a major part of the deep seabed in the allotted area has been mapped. This has provided accurate topographic map of the seafloor which will help determining the mineable blocks. Before commencing commercial mining, a detailed picture of the seafloor is essential. The seamounts, hills and valleys have to be identified to mark inaccessible areas. Morphometric study, slope angles etc. will help in pre-determining the dredge paths. Bathymetry is also known to influence the distribution of polymetallic nodules. Keeping all these in mind, detailed morphologic study and influence of topography on distribution of polymetallic nodules in Central Indian Basin is carried out in this thesis.

Objectives:

The main objectives of the present study are

1. To study the geomorphology and morphometry of the Central Indian Basin, and
2. To establish relationship between seafloor topography and distribution of polymetallic nodules in the study area.

Depth data for the study was collected from the echosounding (both single beam and sophisticated multibeam techniques). For navigation, dual channel satellite navigator was used for single beam echosounding and Global Positioning System (GPS) for multibeam studies. The nodule sampling was carried out using the free fall grabs, dredges and Petersson grabs. Underwater photographic data was collected using the cameras mounted on the free fall grabs.

During the course of the present study, a number of new techniques and computer programs were developed. Procedure for underway data processing was evolved. Program to plot bathymetric profiles, sampling stations on bathymetric profiles, to generate slope angle data from digitised depth data and from multibeam sounder (Hydrosweep) data, cluster analysis to plot dendograms, calculation of statistical parameters, improvement on existing post-processing package- Hydromap for Hydrosweep data etc. are some of the

programs developed during the course of present study which will make underway data processing easier and faster. For the assessment of the seafloor environment and all related parameters, a system called 'SPHINCS'(Seabed Photographs Interpretation and Cataloguing System) was prepared which uses a specially developed format for the storage of the data acquired from the seabed photographs using dBase III+ database management system.

Based on the enormous echosounding data collected, a comprehensive bathymetric map of the Central Indian Basin is prepared which will serve as a base map in future for the researchers and navigators. Also, detailed morphology of the basin from multibeam sounder data depicting the presence of 79^0 E fracture zone, east-west lineations and a graben is presented. Numerous seamounts have been identified in the basin. Detailed morphology of a seamount and that of three chains of seamounts is described. Morphometric studies on some part of the basin is also carried out.

Topographic control of the polymetallic nodule distribution is studied using the echosounding data and the nodule sampling data. Nodule distribution in different topographic domains is studied. Influence of regional and local topography, 79^0 E fracture on the nodule distribution

is deliberated. Factors controlling the nodule distribution based on photographic evidences is also presented. The importance of detailed bathymetric studies prior to and for selection of mine sites is discussed and a method for identifying unfavorable blocks in the mine site is given.

Thus, this study addresses a wide range of new and unknown aspects covering geomorphology of Central Indian Basin, nodule distribution and topography and nodule mining and will fill the void in these fields.

Chapter 2.
Physiography and Geomorphology of Central Indian Basin

2.1 Physiography of the Indian Ocean.

Indian ocean is considered to be the most complex of the three major oceans **(Schlich, 1982)**. It has many features which are unique (like the 90 East Ridge) and a host of other physiographic features not found in other oceans. The major physiographic features of Indian ocean are shown in figure 2.1.

The western part of this ocean is bounded by India to the north and Africa to the northwest. The Ninety East Ridge in the east, the Kerguelen-Heard Plateau in the southeast and the Antarctic continent in the south mark the limits of the western Indian Ocean. The western Indian Ocean is dominated by a complex system of active mid-oceanic ridges which extends from the Gulf of Aden on the northwestern extremity with the Sheba Ridge, the Carlsberg Ridge, and the Central Indian Ridge that continues to the Rodrigues Triple Junction of 25^0S and 70^0E. Here, Central Indian Ridge bifurcates into two distinct branches, the southeast Indian Ridge and the southwest Indian Ridge, which separate the African plate and the Indian-Australian Plate from Antarctica.

Different types of topographical features such as banks, plateaus, ridges, seamount chains or rises are

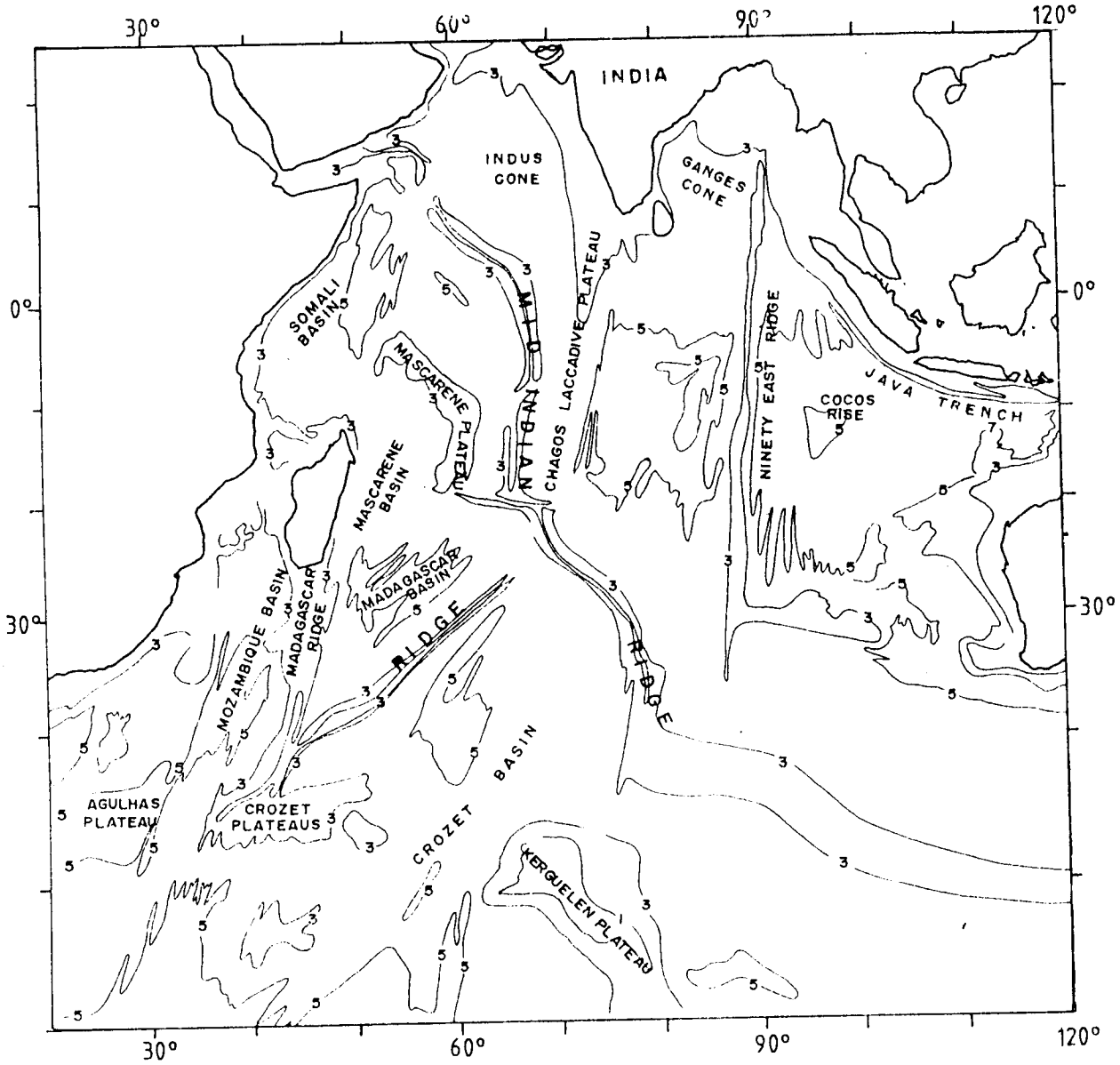

Fig. 2.1 Physiographic provinces of the Indian Ocean.

present in the Indian Ocean. These features were called as Oceanic Ridges by **Udinstev (1975)**, microcontinents by **Heezen and Tharp (1966)**, and are grouped as aseismic ridges by **Laughton et al. (1970)**. These may represent the continental fragments which have been separated from the main continental blocks by seafloor spreading (like the Madagascar island, Seychelles island, Seychelles Bank, Kerguelen Plateau, Agulhas Plateau etc.) or to the uplifted blocks of oceanic crust (like Chagos-Laccadive oceanic Plateau, Crozet Plateau, Ninety East Ridge etc.). The submarine plateaus or aseismic ridges, striking north-south, and located in different parts of the western Indian Ocean, along with the active ridges and the surrounding continents, divide the Indian Ocean in to a number of deep ocean basins such as the Arabian Basin, the western and eastern Somali Basins, the Mascarene and Madagascar Basins, the Mozambique Basin, the Agulhas Basin, the Central Indian Basin and the Crozet Basin (Fig. 2.1).

Available seismic data shows that the structure of basins of the Indian Ocean is similar in many respects to the basins of other world oceans. However, the basins lying north and west in Indian Ocean are peculiar in that they have exceptionally high supply of sediments. Indus and Ganges cone regions have been witnessing heavy crustal

downpouring resulting in huge sediment thickness **(Closs et al., 1969, Naini and Leyden, 1973)**. Indus cone sediments have been derived from erosion of Himalayan mountain chain and extend in the Arabian basin to the northern Carlsberg ridge with 1000-2500 m sediment thickness and to the Central Indian Basin, with over 2000 m thickness **(Ewing et al. 1969, Udinstev, 1975)**. Thus Arabian basin and Northern part of Central Indian Basin account for over 40% of total Indian ocean sediments. The basins in the Indian Ocean are of only low relief variations characterized by relatively thin homogeneous sediments, acoustically transparent, with only few internal reflectors.

2.1.1 Origin

Indian Ocean is a 'Young' ocean surrounded by continental areas of Africa, India, Australia and Antarctica. These land masses were all single continent or clusters of closely related subcontinental nuclei around the Precambrian era. In early Cretaceous, India, Antarctica and Australia formed the eastern part of Gondwana landmass. Around 100-150 Million Year (ma), a spreading center just east of north became active in Central Indian and Wharton Basins. At 20 ma, India moved north-north east with respect to Antarctica. Around 80 ma, there was some change in direction of relative motion with India separating from fixed Australia-Antarctica region in

a more North easterly direction. The pole of relative motion was 70^0 from ninety east transform fault. Around 64 ma and 53 ma, the spreading center just west of ninety east transform fault jumped 11^0 to south. Around this time, Antarctica started to separate from Australia. Ninety east transform fault marked the relative motion between India and Antarctica. A new plate was formed between India and Australia with active boundary in the vicinity of northern section of Ninety East Ridge. This plate boundary was active between 53 ma and 32 ma before present and might have caused an echelon faulting on the northern section of Ninety East Ridge. The relative motion on either side of ninety east transform fault stopped around 32 ma and India and Australia became part of same plate. The direction of movement between Australia, India and Antarctica changed to north east-south west. North south transform fault joining South east Indian ridge to Antarctica-Australia ridge became 'S' shaped series of active spreading centers and transform faults with relative motion in NE-SW direction. This geometry of active plate boundaries has continued till present. Little movement is inferred between Africa, America and Antarctica and present South pole during Tertiary but India must have moved 50^0 across or 5500 km between early Eocene to Miocene, coinciding with formation of

Himalayas. This works out to a spreading rate of 11 cm /year for India and for Australia a rate 8 cm/year between Oligocene and Present.

Chagos-Laccadive plateau separates Central Indian Basin from Indian Ridge and Ninety East Ridge separates this basin from Wharton basin. **Mckenzie and Sclater (1971)** recognized distinctive magnetic anomalies in Central Indian Basin. The anomalies reported are numbers 5-16 and 21 to beginning of 33. Spreading rates envisaged are 2.5 cm/year (anomaly number 5-16), 4 cm /year (16-22), 8 cm/year (22-27), 12 cm/year (27-29) and 5.7 cm/year (29-33) respectively. The anomalies cannot be traced over long distances in east-west direction and hence it is suggested that Central Indian basin is made up of series of short east-west segments offset by north-south trending fracture zones at 79^0E, 83^0 E (Indira fracture zone), 86^0 and a new fracture zone (75^0 45' E) **(Kamesh Raju and Ramprasad 1989, Kamesh Raju 1990)**. Extension of 79^0 E fracture zone up to $14^0$30' S has been identified based on multibeam sonar data **(Chapter 3 and Kamesh Raju et al., 1992)**.

As a consequence of the theory of seafloor spreading, in the Indian Ocean **(LePichon and Heirtzler, 1968)** identification and correlation of characteristic anomalies

can be made on magnetic profiles across the mid ocean ridges. This has enabled isochronous lines to be drawn, giving spreading rate of ocean floor on either side of ridge as a function of position along the ridge. This rate varies from about 1 cm/year in Gulf of Aden to 3 cm/year south of Australia. Tentative scheme for evolution of Indian ocean **(Lepichon and Heirtzler, 1968)** is that initial separation of Africa from India, Australia and Antarctica along the line of South west Indian ridge started in lower cretaceous (140 ma) and completed by Albian (100 ma). By early Eocene axis of splitting had shifted twice, first to east-west direction that separated India from Antarctica and second to NW-SE direction along major mid-ocean ridge as seen presently from Gulf of Aden to South east Indian Ridge. Two episodes of fast spreading are identified in this latter phase, one pre Miocene and other post-Miocene. Northward movement of Indian subcontinent is confirmed by estimates of minimum crustal shortening of 500 km in Himalayas and by transcurrent faulting of appropriate sign in both western and eastern structural belts that terminate the Himalayas **(Gansser, 1966)**.

2.2 Geomorphology- Introduction.

Geomorphology is the science concerned with the study of landforms at the surface of the earth and at the seafloor. The main task of the geomorphologist is to

describe and explain the different features. The word 'Geomorphology' means form and development of earth (**Fairbridge, 1968**). In classical geomorphology, variations of earth's surface are divided in to different orders. The Continental platforms and ocean basins are the first order features.

Background

Three major morphological features of the Indian Ocean are the major active ridge systems- the Central Indian Ridge (CIR), South East Indian Ridge (SEIR) and South West Indian Ridge system (SWIR). Also, there are several fracture zones which offset these ridge systems. The three ridge systems join at the Indian Ocean Triple junction. Prior to the International Indian Ocean expedition (IIOE, 1959- 1966), there was not much work done on Indian ocean as regards it's morphology and bathymetry. First report on physiography of Indian Ocean was by **Heezen and Tharp (1966). Le Pichon and Heirtzler (1968) and Laughton et al (1971)** contributed further information to this. First general atlas of geology and geophysics of Indian ocean was prepared based on these studies **(Udintsev, 1975)** which, till date is the only one of it's kind. However, later years witnessed increasing interest in Indian Ocean, as a result of which detailed bathymetric surveys were

carried out in different parts of Indian Ocean. Most of these studies are concentrated either at the mid-ocean ridge systems- triple junction or at and near the continental margins of different countries. The continental margins of India have been extensively covered by geological and geophysical surveys **(Siddiquie et al., 1987)**. Other parts of the Indian Ocean, especially the Central Indian Basin had not been surveyed extensively. Central Indian Basin (CIB) lies between the Central Indian ridge and 90 degree east ridge and is bounded in the south by SEIR and Indian Ocean Triple junction. CIB has complex evolutionary pattern because of existence of aseismic ridges and fracture zones. Varied spreading rates of CIR, SEIR and SWIR also have contributed to it's complexity.

The National Institute of Oceanography, Goa India as a part of the program on polymetallic nodules exploration embarked on the detailed bathymetric survey of Central Indian Basin. Initially, the survey was carried out using the single beam echosounders and later, after acquiring the multibeam swath bathymetric system, detailed surveys in part of the CIB has been carried out. Morphology of the basin as revealed single beam echosounding data is presented here.

2.3 Morphology of the CIB from single beam echosounding data.

2.3.1 Data acquisition.

Over 4,20,000 line kilometers of single beam echosounding data was collected during the period 1981 to 1990. For this purpose services of two research vessels from India namely ORV Sagarkanya and RV Gaveshani and also four chartered vessels MV Fernella and MV GA Reay (both from UK), MV Skandi Surveyor (Norway) and DSV Nand Rachit (India) were utilised. 3.5 KHz and 12 KHz echosounding system (manufacturers M/S Raytheon , USA), 12, 20, 30 KHz deep sea and narrow beam echosounders (manufacturers Honeywell Elac, Germany) were used for echosounding. Raytheon system comprises of a high power transmitter, receiver, correlation echoprocessor and line scan recorder. Depth is calculated by determining the to and fro travel time of the sound pulses. The time is multiplied by the velocity of sound (standard taken as 1500 m/sec.). Actual depth is half of this product. The depth is presented in analog form on the line scan recorder. Honeywell Elac narrow beam echosounders used on ORV Sagarkanya have beam width of only 1.5^0. Figure 2.2 shows a typical analog record obtained from Honeywell elac echosounder in the Survey area. Quantum of data collected from each of the vessels and the equipment used for data acquisition is

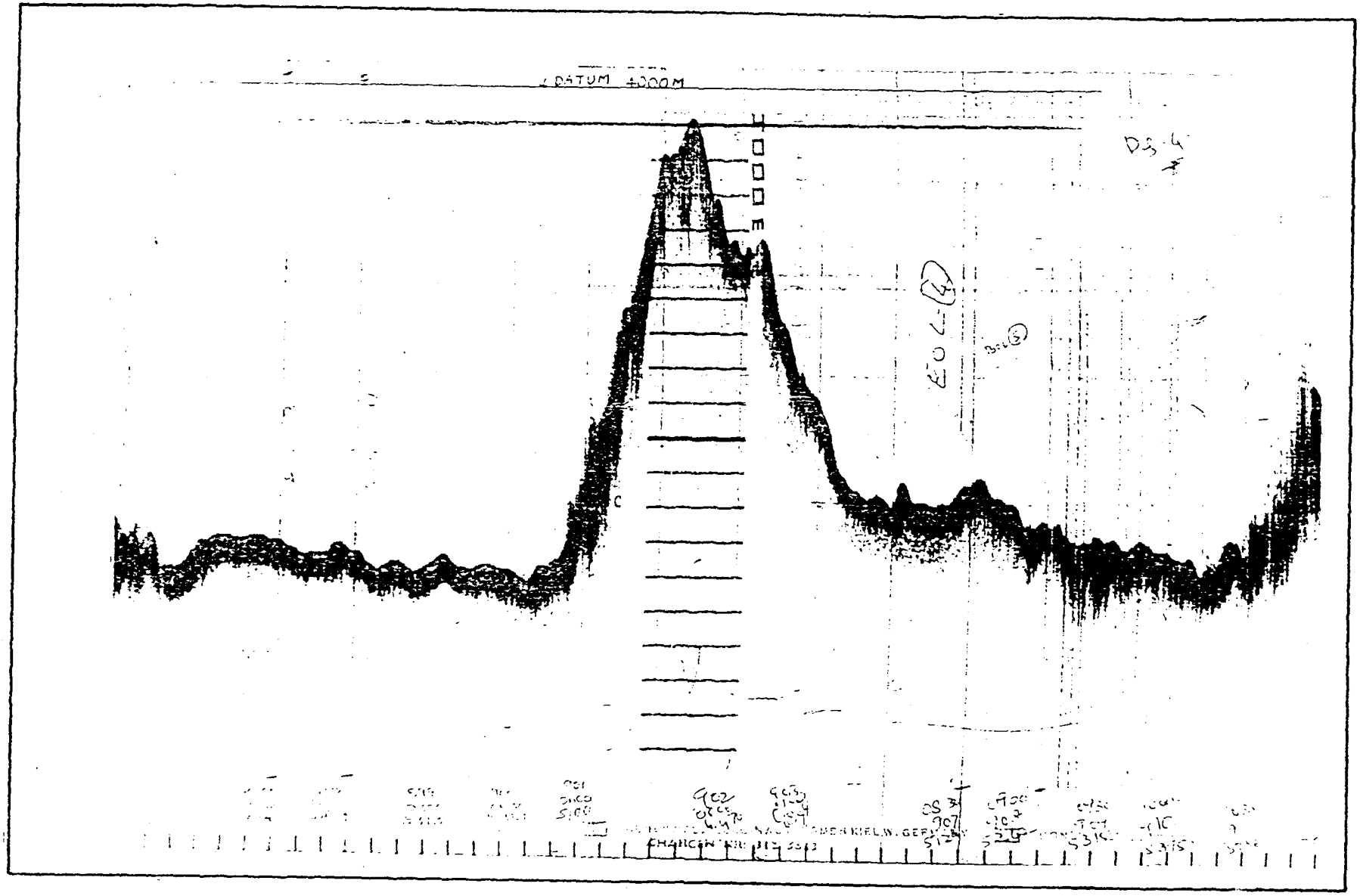

FIG. 2.2 TYPICAL ECHOSOUNDING RECORD - HONEYWELL-ELAC NARROW BEAM SOUNDER.

shown in Table 2.1. Spacing of echosounding lines in the initial stages of survey was 60 nm which was brought down to 30 nm in to 30 nm in the second phase and was fu nautical miles in some areas. Fig.2.3 shows the survey tracks in the study area. As seen in figure, lines are clustered around in the central part of CIB (15 nm track spacing) whereas the rest of the area is covered by 30 nm spaced lines. Most of the tracks are north-south while few tracks are east-west.

Table 2.1

Amount of echosounding data collected on different ships during 1982-1990.

Sr. No.	Name of Ship	No of cruises	No.of shipdays	Equipment used.	line kilo meter data collected
1.	RV Gaveshani	8	164	Simrad ES	40242
2.	MV Farnella	8	363	Raytheon ES (3.5 and 12)	100954
3.	MV Skandi surveyor	17	720	""	116559
4.	MV Ga Reay	3	135	""	31840
5.	MV Nand Rachit	4	135	""	35000
6.	ORV Sagarkanya	8	330	Honeywell Elac Narrow beam and Deep sea sounders	99499
	Total	48	1747		424094

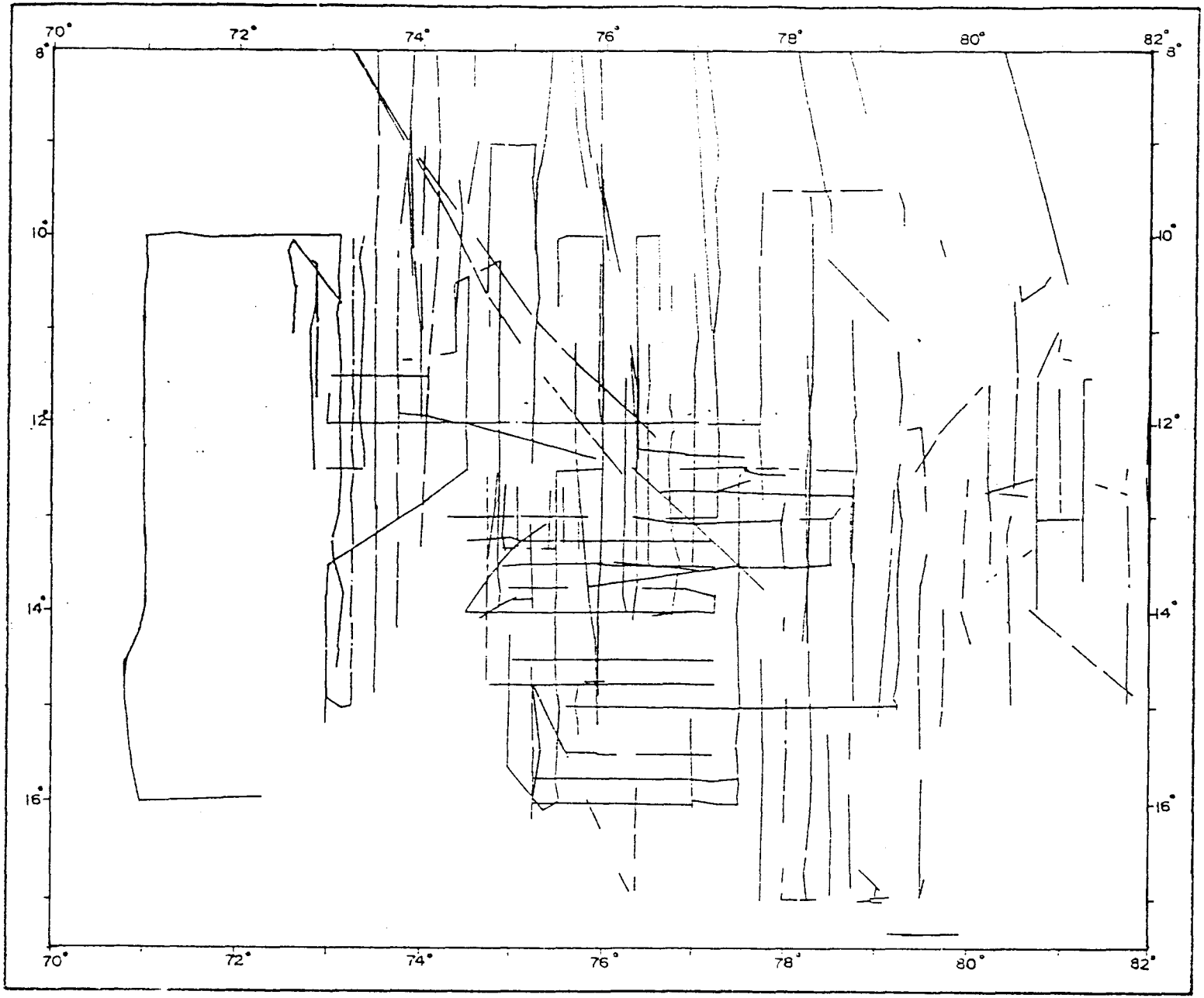

FIG. 2.3 ECHOSOUNDING SURVEY TRACKS IN CIB FROM DIFFERENT VESSELS

2.3.2 Position fixing:

Magnavox dual channel satellite navigator (MX 1107) was used for accurate navigation on the chartered vessels. Magnavox satellite receiver acquires and tracks two signals from a satellite passing overhead. The satellites-called transit are from the United States Navy Navigation Satellite System (NNSS). Transit satellites are operative since 1964, though commercially available since 1968. Transit satellites are in approximately circular polar orbits at altitudes about 600 nautical miles. They form a bird cage within which the earth rotates. Each satellite has a orbital period of 1-3/4 hours. Whenever a satellite passes above the horizon of the user, an opportunity to obtain position fix exists. (Magnavox 1107, operating manual, 1982).

Satellites radiate stable 400 & 150 MHz signals which are phase modulated with information of several types. Satellites travel roughly 4 miles/sec. and this motion with respect to an observer on the earth causes a Doppler shift in the radiated 400 and 150 Mhz signals. This Doppler shift is measured by the satellite receiver providing an indication of the change in slant range between observer and satellite. Slant range data are combined in the navigation computer with estimates of the

boat's position during the satellite pass to determine the position of the receiver on the earth. The transmission of two signals at different frequencies both of which are Doppler shifted and both of which carry navigational data is done to minimize the effect of ionospheric interference with the Doppler shift. MX 1107 used in the present study employs dual channel receiver obtaining a sharp increase in position fix accuracy compared to single channel receiver which would receive only one of the transmitted frequencies.

Between two satellite fixes (good passes), the dead reckoning time (DRT) position is calculated by this system by utilising the speed and heading inputs from the speed log and the gyro. Whenever a good pass is received, the position is updated. The occurrence of good pass is about 7-8 per day. Normally, every three or four hours, satfix update is obtained.

On all the chartered vessels, the dual channel satellite navigator was used for navigation while on ORV Sagarkanya, the navigation was carried out by the Integrated Navigation System (INS). INS consists of a navigation computer and attached peripheral equipments. This system provides accurate positioning from integration of Magnavox satellite navigators, Radio navigation system,

sonar, gyro and other navigational sensors. INS is a fully integrated system intended for both near shore and deep sea oceanographic surveys. It can also log navigation and other underway data on magnetic tape for which processing facilities exist on board.

2.3.3 **Data processing:**

Large amount of position-depth data collected was processed on UNIVAC 1100/60 computer at the Computer center of MECON (Metallurgical and Engineering consultants), Ranchi. Fig- 2.4 shows the flow chart of the package employed for data processing.

For position data-processing, only the good fix data was used. The data between two good fixes was interpolated for every one minute. Thus, a navigation data file for position at every minute was created.

Voluminous echosounding data was digitised using the digitizer. Care was taken to digitise as many points on the echosounding analog record as possible, especially when the depth variations were frequent. A time-depth file was created after digitising. By interpolating depth values between two digitised depth values, one minute interval time-depth file was created. Underway (depth) and navigation data were merged to create a one minute master

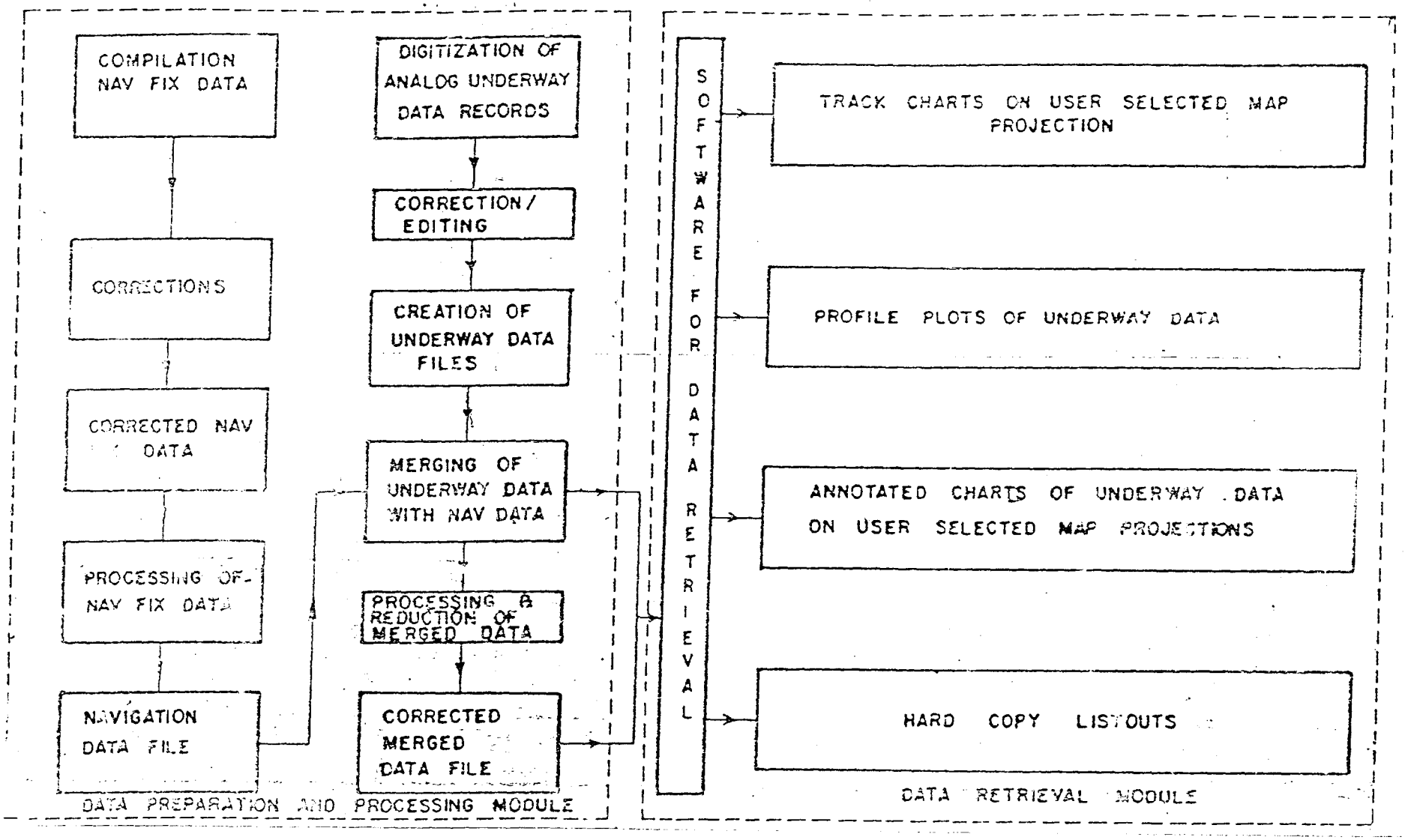

FIG. 2.4. FLOW CHART OF THE SCHEME EMPLOYED FOR NAVIGATION AND BATHYMETRIC DATA PROCESSING.

file for position-depth. On this depth data, transducer and Mathews corrections **(Carter, 1980)** were applied. The merged and corrected position-depth files were generated for the each cruise. These merged files were used for generating track plots, cross section profiles and annotated depth plots on user selectable map projections.

A hand drawn contour map of the Central Indian Basin was prepared using the annotated depth data plots. Fig. 2.5 shows the manually drawn depth contour map of the area with contour interval of 100 m. Numerous geomorphic features hitherto not reported from the basin are observed on this map. However, the manually prepared depth contour map for such a huge area (over 4,00,000 sq.kms) using large amount of data can be less accurate. The annotated depth data plot from which this contour map is drawn itself has limitation as all depth points cannot be transferred on to a map owing to limitations of space. In hand drawn contouring, the contourer has to imagine what the relief must be and then portray this abstraction on the map. Since drawing of contours is subjective, quality is partly related to time, care and thought devoted to the subject by the contourer. It is also, the function of experience of the contourer and correctness of his hypothesis. For this reason, alternatively, GMS (GECO mapping system) software on the ND 570 computer at

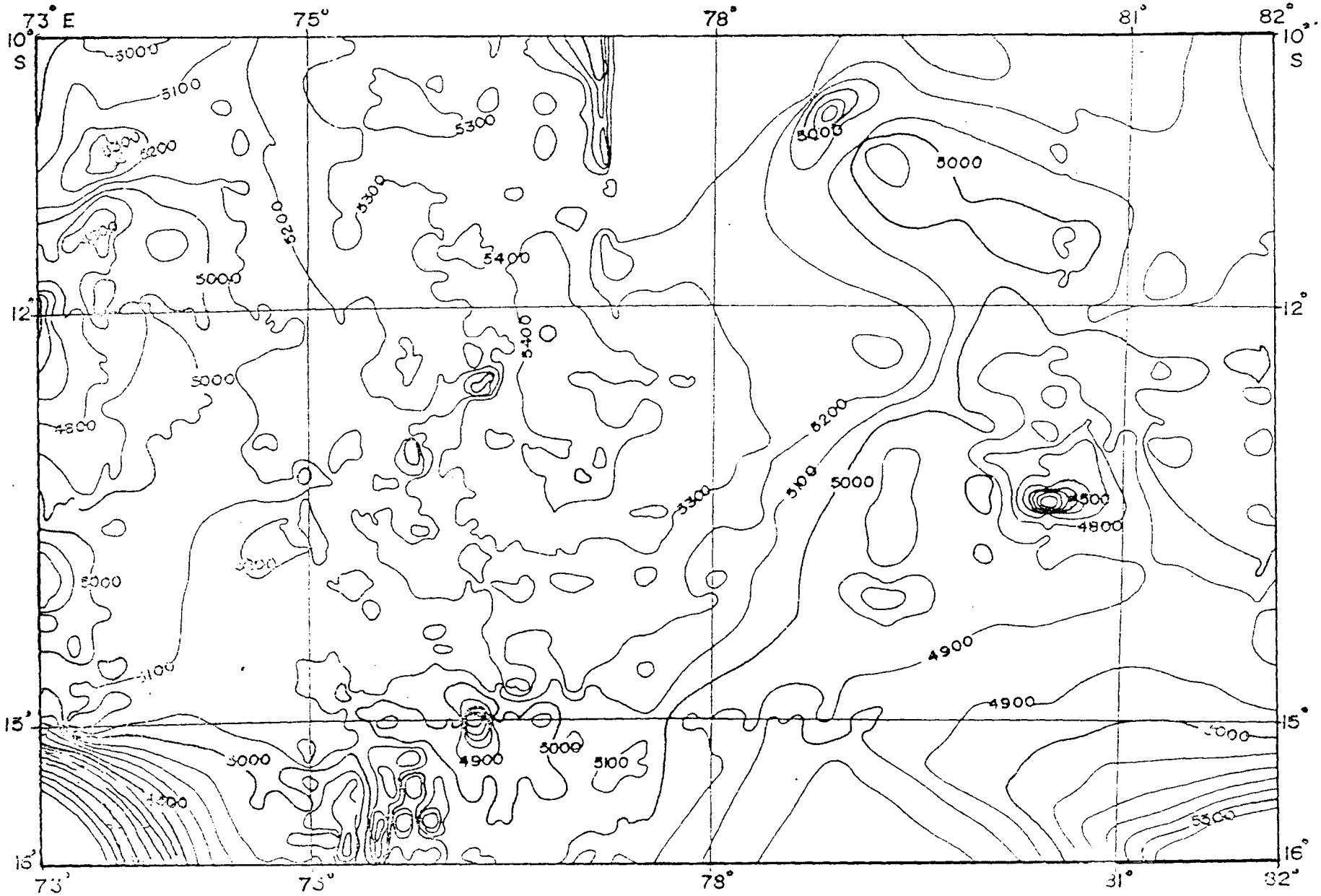

FIG. 2.5 HAND DRAWN DEPTH CONTOUR MAP OF CIB (CONTOUR INTERVAL 100 MQ. SCALE 1 CM= 43.4 Km.

National Institute of Oceanography was also used. Using the master position depth data files from all the 48 cruises as input for GMS, a detailed and more accurate 100 m interval depth contour map (fig 2.6) was generated. It is interesting to observe here that both the hand drawn (Fig 2.5) and the computer drawn (Fig 2.6) are closely comparable. Although, the data set used for drawing depth contour map on the computer is much larger than that for the hand drawn map, the trends and the prominent features are comparable. This map is the only one of it's kind for the Central Indian Basin as no detailed bathymetric surveys of this order have been carried out in CIB so far.

2.3.4 Discussion:

The depths in the basin range from 2900 m to 5700 m. It is observed that the average depth in the basin is around 5200 m. The depth increases from west to east. Lower depths are predominating in the western part of the basin whereas in the eastern part the average is higher. Generally, the topography in the basin is medium to rugged. On the basis of relief, the study area can be divided into three divisions as follows.

1. Plain areas.
2. Medium relief areas and
3. High relief or rugged areas.

1. Plain areas:

The central part of the Central Indian Basin between latitudes 10^0 S-14^0 S and longitudes 74^0-76^0 E is the plain area. The average depth in the region is about 5200 m and slope is around 20 degrees. There are, nevertheless few seamounts and abyssal hills in this region. This area is marked as 'P' in fig.2.6.

2. Medium relief areas.

Medium relief areas in the basin exist in the eastern part of the basin (Between longitudes 79^0E to 82^0). The average depths are higher- 5325 m. There are quite a few seamounts in this area- especially between 12^0 to 14^0 S latitudes and 80^0 to 82^0 E longitudes. South-eastern part of the basin (South of 15^0) is also a medium relief area but the average depth here is slightly higher- 5400 m. In fig. 2.6 the medium relief areas are marked as 'M'.

3. High relief or rugged areas.:

The western part of the Central Indian Basin can be categorized as high relief area. The shallowest depth of the basin is recorded in this basin (2900 m). The maximum depth is about 5050 m and the average is 4600 m. There are numerous abyssal hills and seamounts. Due to proximity of

BATHYMETRIC MAP CIB

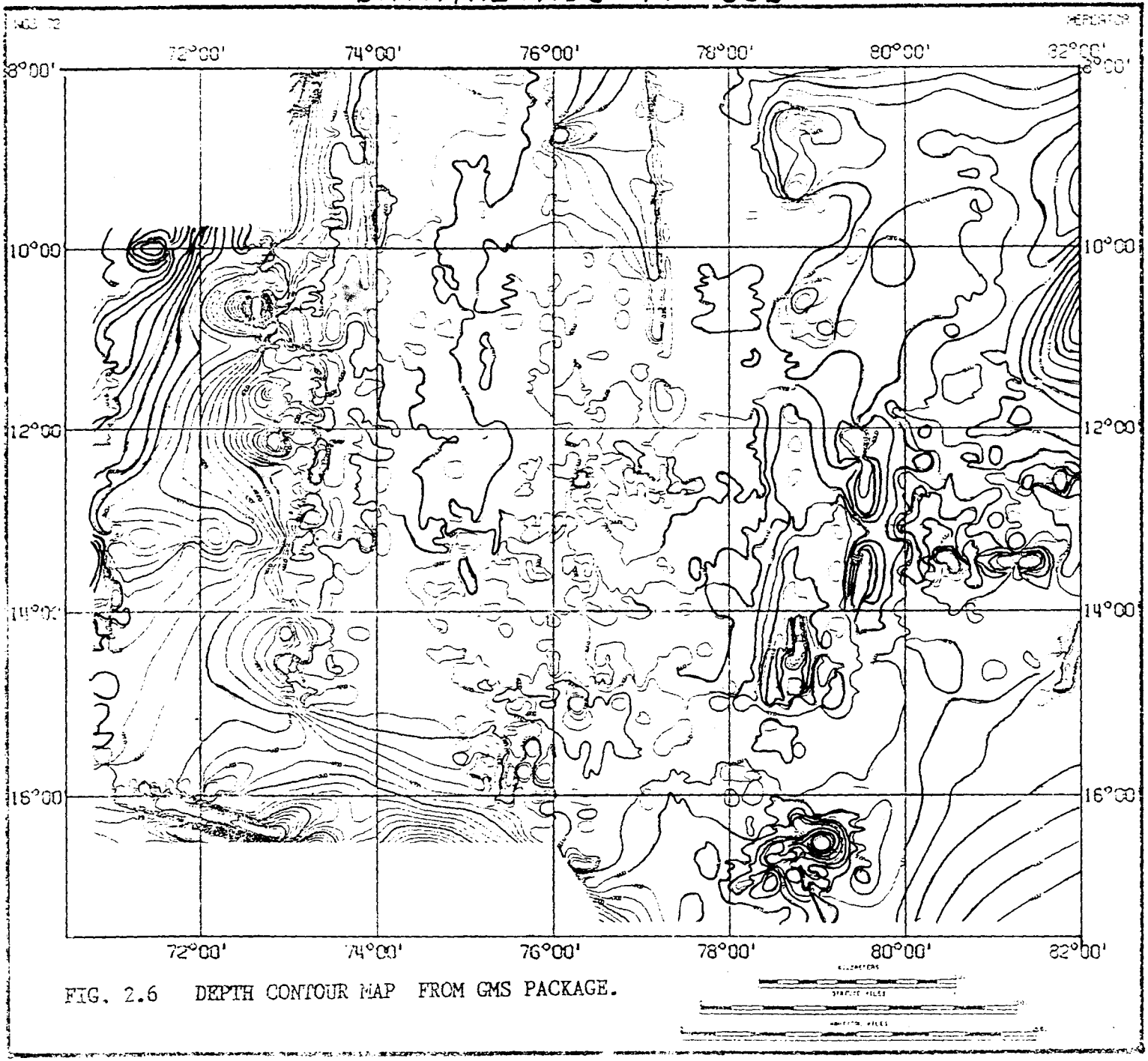

FIG. 2.6 DEPTH CONTOUR MAP FROM GMS PACKAGE.

this region to the Central Indian Ridge and the Chagos-Laccadive ridge, the area is highly rugged and morphology is complex. The amount of echosounding data available in this region is comparatively less than that in Eastern and central parts of CIB. In fig. 2.6, the rugged areas are marked as 'R'.

2.3.5 Prominent features:

There are, as indicated in the previous paragraphs, numerous abyssal hills and seamounts in the study area which are brought to light from the contour map. The Central Indian Basin was not known to contain these many features till now, the primary reason being that echosounding data collection of this magnitude was not done earlier. There are 10 seamounts of heights over 1000 m. The locations, heights and depths at the top of prominent seamounts and abyssal hills as deciphered from single beam echosounding study are given in table 2.2. Most of the seamounts have conical tops and their heights do not exceed 1500 m. No guyots are observed in this region. The western part of the basin contains more number of seamounts than the eastern and central region. Seamount at 11^0 10'S , 73^0 02' E (no.2, table 2.2) is tallest with height of 1450 m. Seamounts appear to be clustered at some

same places and follow trend of nearly North-South. **Mukhopadhyay and Khadge (1990)** reported about six

Table 2.2
Location and heights of major seamounts and abyssal hills in the Central Indian Basin.

S.No.	Latitude (^{0} S)	longitude (^{0} E)	Height (m)	Depth on top (m)
1.	14^0 30.3′	073^0 2.5′	1200	3800
2.	11^0 10.3′	073^0 2.2′	1450	3570
3.	15^0 35.5′	075^0 15.1′	1000	4000
4.	12^0 46.3′	075^0 29.8′	600	4500
5.	14^0 26.3′	075^0 24.7′	800	4300
6.	12^0 38.6′	075^0 15.2′	650	4400
7.	13^0 15.5′	075^0 29.1′	700	4525
8.	12^0 19.0′	075^0 45.8′	1000	4120
9.	15^0 45.3′	075^0 42.1′	450	4600
10.	13^0 00.6′	075^0 46.1′	900	4300
11.	15^0 00.0′	076^0 14.8′	700	4400
12.	12^0 35.0′	076^0 16.0′	1275	4130
13.	12^0 20.3′	073^0 45.1′	1150	4100
14.	11^0 05.6′	077^0 08.1′	900	4200
15.	12^0 31.0′	076^0 19.0′	1000	4100
16.	13^0 52.3′	078^0 18.3′	800	4320
17.	14^0 15.0′	079^0 13.0′	850	4350
18.	13^0 30.3′	080^0 30.0′	1240	3800
19.	14^0 33.0′	078^0 27.0′	1180	3800
20.	14^0 38.0′	078^0 43.3′	1080	4140
21.	14^0 43.3′	078^0 45.0′	850	4350

seamounts in the northern region- 0^0 to 8^0 south latitudes, which are taller and have shallower depths at the top. The CIB seamounts observed here have lesser heights. Morphology of some of the seamounts (from Single beam echosounding and also from Multibeam swath bathymetric data) and morphometry of some areas are described in detail in the

subsequent chapters. The basin also has, in addition to the seamounts, over 100 abyssal hills (heights 300-1000 m). Owing to the large scale in fig.2.5 and fig.2.6, some of the smaller features are not represented on the map.

Another important feature observed from this study is presence of a ridge like feature of 300-400 m height (between 8^0 S and 11^0 S latitudes and along 77^0 E longitude). This ridge is oriented North-South and is narrow. The depths range from 4800-5150 m. Area surrounding the ridge is generally plain. The quantity of data on the ridge is less and this needs to be investigated further preferably with Multibeam sonar. Though a fracture zone has recently been reported from this area at 75^0 45′ E trending North- South using the magnetic data **(Kamesh Raju and Ramprasad 1989, Kamesh Raju 1990)**, the same has not been represented topographically on the contour map. They have also speculated the southern extension of 79^0 E fracture zone. The single beam echosounding data has not been able to confirm this. However, the multibeam data has shown unmistakable evidence for southern extension of 79^0 E fracture zone **(details in chapter 3)**.

The data used for preparation of the bathymetric map is mostly from 30 nautical mile spaced echosounding lines. Obviously a lot of interpolation is done to prepare the map

and features of less than 30 nautical miles (approximately 55 km) dimension, and the exact depth of those with their center not falling on the echosounding line are missed from this map. Also, the positioning system used for this survey (Magnavox dual channel satellite navigator) has an accuracy of up to 300 m. However, this map will serve as a base map for navigators and marine researchers for future surveys as there is no comprehensive, detailed map of the Central Indian Basin available till now.

Chapter 3
GEOMORPHOLOGY OF PART OF CENTRAL INDIAN BASIN FROM MULTIBEAM ECHOSOUNDING DATA.

3.1 Introduction.

The bathymetric map of Central Indian Basin as presented in chapter 2 though unique and first of it's kind, is more of a reconnaissance map. As there is a lot of interpolation done in areas between the survey lines, there is some ambiguity and features of less dimension are not represented on this map. Central Indian Basin (CIB) being potential manganese nodule mining area, the National Institute Of Oceanography, Goa has been carrying out exploration activities in this region since 1982. After the allocation of 1,50,000 sq. km of area in CIB by the International seabed authority, the exploration activities have been intensified in the allotted area. 50% of the allotted area has to be surrendered phase wise to the United Nations in three years. To identify the unproductive areas and topographically unsuitable terrains, a more detailed bathymetric picture of the area is necessary. Also, to aid exploration activities that will be intensified with the help of deep towed equipments (Underwater Television and Underwater photography and sub bottom profiling) a detailed depth contour map is prerequisite. To meet these requirements and to obtain more comprehensive bathymetric picture of the allotted

area, use of state of art technology like the multibeam swath (MBS) bathymetric system was felt essential. Hydrosweep- the multibeam swath bathymetric system manufactured by M/S Krupp Atlas Elektronik, Germany was acquired and installed on ORV Sagarkanya in early 1990. This state of art bathymetric survey system and the geomorphology of part of Central Indian Basin (About 1,20,000 sq.km of area) as revealed by the MBS studies is discussed in the ensuing paragraphs.

3.2 Multibeam Echosounder : Hydrosweep system.

The last two decades have witnessed tremendous advancement in bathymetric survey. Single beam echosounders have given way to a variety of high resolution swath bathymetric mapping systems thus enhancing accuracy and reliability of bathymetric maps. Multibeam system revolutionizes our understanding of the ocean bottom and it's major structural features by providing highly detailed bottom maps. Depth resolution is much greater than that can be achieved by employing single beam conventional echosounders. The cost effectiveness of the multi beam system is very high. To map an area of 1,50,000 sq.kms by conventional echosounders the number of ship days required will be over 400 days (for a line spacing of 30 nautical miles). Even then the accuracy of the results will be far less. Per day cost of running the ship ORV Sagarkanya is

about 200,000 rupees. Thus expenditure is curtailed and good quality data generated by using this equipment, as the same area can be covered in less than 80 days.

Basically the multibeam echosounders measure depths simultaneously from a series of beams pointing at discreet angles of incidence in the athwartship direction. Hydrosweep system covers 45 degree on either side of the ship by a fan of 59 preformed beams thus providing capability of achieving a total swath width equal to twice the water depth **(Grant and Schreiber, 1990 and Gutberlet and Schenke, 1989)**. By spacing the survey lines at twice the water depth, a complete coverage of the seabed from this system can be obtained with no need of interpolation in between. The system is capable of measuring depths from 10 m. to 10000 m. Technical details of the equipment are given in Table 3.1. Fig.3.1. gives a schematic configuration of Hydrosweep system. This system has two sets of identical acoustic transducers mounted in 'T' shape on the hull of the ship. One set is installed along longitudinal fore-aft axis and is used for transmission during the normal survey and other set is installed perpendicular to the first one for reception .

Conventional echosounders use a constant value for sound velocity to calculate the depth. The value of sound

Table 3.1

Technical details of Hydrosweep system

Frequency of operation	15.5 Khz
Transmission array size	3* .3 m
Reception array size	3*.3 m
Band width	.3-2 Khz
Side lobe level	25 db
No. of preformed beams	59
Depth range	10-10000 m
Beam spacing	1.5 degree.
Data storage	1600 bpi
Swath width coverage	200% depth
Operational Ship speed	2-15 knot
Maximum permissible--	
roll	20 degree.
Pitch	+/- 10 degree
Heave	+/- 5 m.
Sea state	6

velocity in the water column varies and influences the travel time of acoustic pulse and thereby the system accuracy. This problem is compounded in the multibeam echosounders as there is additional effect on divergence of outermost slant beams which may result in errors. To overcome this problem, some multi beam survey systems employ time consuming and expensive method of using sound velocity probes regularly during the survey and inputting the sound velocity value to the system. Hydrosweep uses a unique patented calibration process. Fig.3.2. shows schematically the calibration process of Hydrosweep. During survey vertical depths from center beam are stored. At regular interval, after 1000 m. of travel, fan of beam is electronically rotated through 90 degrees to transmit

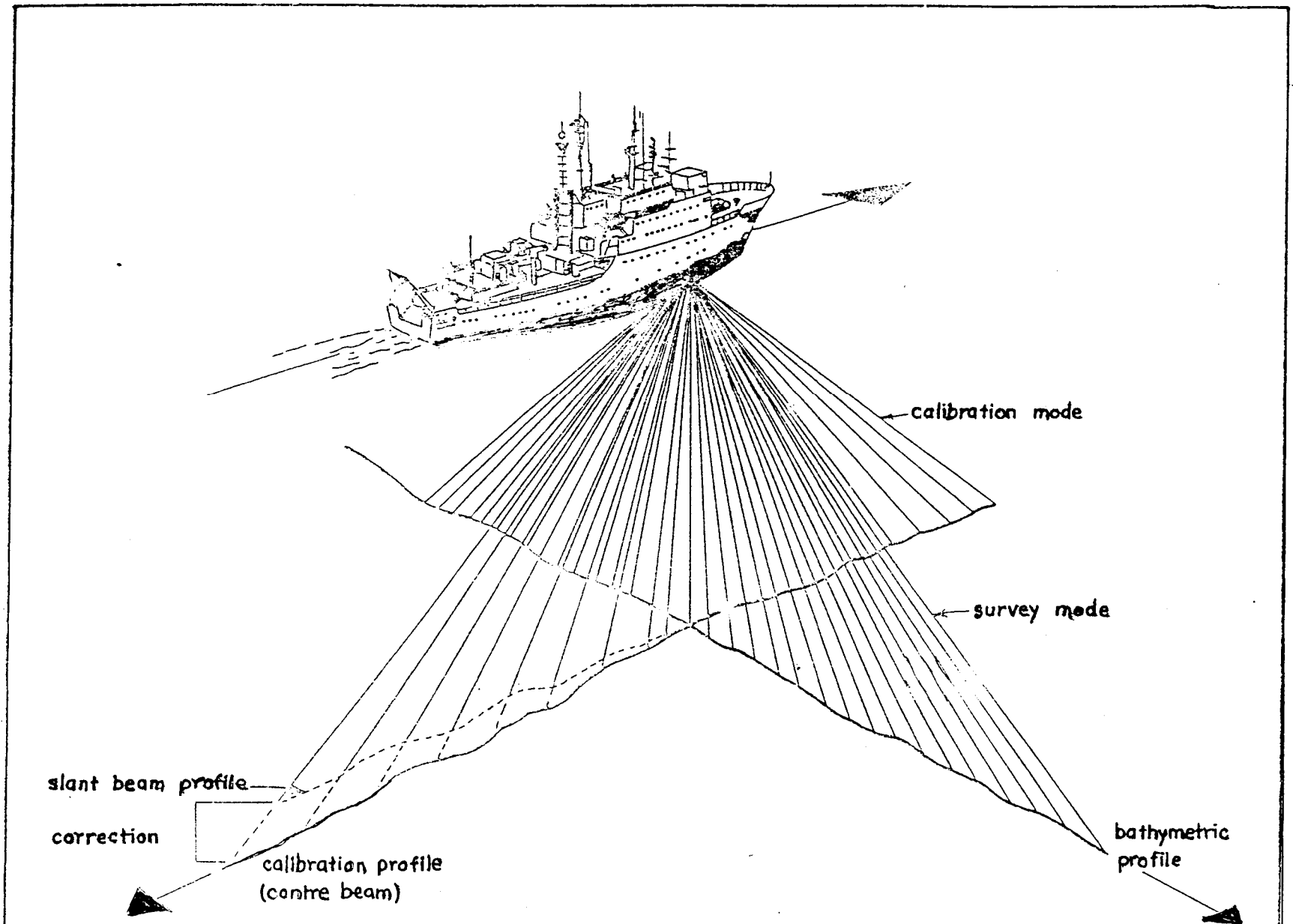

Fig3.2. CALIBRATION PROCESS OF HYDROSWEEP SYSTEM

along ship's longitudinal axis and resulting profile is compared with the earlier one. A correction factor is applied to produce a best fit result. Calibration provides an average sound velocity value for the entire water column. This value is used till the next calculation from calibration process is obtained.

Data collection in Hydrosweep is monitored through operator's console. Either a graduated color coded depth contour map or cross section profile can be displayed on color display unit. On-line contour map is also printed on the ink-jet printer. Data (position, depths and distances from the center) are stored on magnetic tape for further processing. For depths of over 5000 m. data of about 120 hours can be stored on one magnetic tape.

Data thus stored on the magnetic tape is used for post processing on Hydromap- the dedicated post processing system for Hydrosweep data. Hydromap consists of a EPR 1300 computer with color video display unit, a four color printer and a eight pen plotter. Individual hydrosweep survey lines can be processed on Hydromap to produce track-coverage maps, isoline maps etc. By combining hydrosweep data from different lines, a depth grid can be created which can be used to generate depth contour maps, cross section profiles and three dimensional figures. EPR 1300

computer of the hydromap system can also be used for programming by using languages like **FORTRAN** and **META** with plot subroutines of **CALCOMP** and **PLOT**. The computer uses the MOS (multi user operating system) and has no compatibility with standard **DOS** or **UNIX** of **IBM PCs**.

The original hydromap post processing package was inadequate to handle large data sets like the one used in the present study. Only about 40 hours data could be combined to generate one combined map. New software was developed to add any amount of data to generate big maps covering large areas (**Kodagali 1990, SK 58 cruise report**). Also, new computer programs were developed to plot cross section profiles at user selectable scale and vertical exaggeration, to plot staion/areas on the Mercator chart, to plot the depth contour map for a part of the grid generated, to split the big hydrosweep data files into line wise data files which will help in storing and later retrieval of the processed data from magnetic data tapes.

Position fixing:

Prerequisite for accurate bathymetric survey is a good navigation system. On Sagarkanya, Hydrosweep gets navigation data from the Integrated Navigation System (INS) with Global positioning System (GPS). GPS is the most accurate positioning system available in market today with

accuracy up to 30 m. About 24 satellites have been sent in the space by US Navy and minimum of three of these satellites will be available to the receivers on the earth and accurate position of the receiver on ground is calculated using the data sent from these satellites which are within the range of the receiver. GPS satellite transmissions are now available for 24 hours/day in the Central Indian Basin and hence there is no need of carrying out position postprocessing.

3.3 Results and discussion:

The geomorphology of three areas in the Central Indian Basin as revealed from Multibeam system (MBS) data is described here. This is for the first time that the CIB has been covered by multibeam surveys so extensively. The first area covers the area P2 allotted by the United Nations PREPCOM. (Between latitudes 10^0 15′ S, 14^0 45′ S and longitudes 78^0 E, 79^0 25′ E covering an area of about 72,000 sq. kms). Area II covers an area of about 49,000 sq.kms (between latitude 10^0 28′ S and 14^0 32 S and longitude 75^0 to 76^0), while Area III is a small block of 2200 sq.kms (between latitudes 9^0 48′ and 10^0 26′ S and longitudes 73^0 35′ E and 73^0 55′E).

3.3.1 Multibeam Survey- Area I (79^0 E Fracture zone).

Hydrosweep was used along a total of 16 north south survey lines (each around 270 nm long) with 5 nautical miles spacing. As the general depth in the area is over 5100 m, the coverage in the area will be about 10,200 m. 5 nautical mile (about 9300 m) spacing between the survey lines ensured that not only the coverage was full but also there was a slight overlap of 700-800 m. Fig.3.3 shows the coverage map obtained in the area. The small lines across the survey lines indicate the coverage obtained during that part of the survey and as seen from the figure the coverage is complete.

Depth contour map (contour interval 100 m) generated from combining hydrosweep data along the 16 lines is given in Fig 3.4. The depths in this area range from 5100 to 5400 m., with average being 5200 m. This area corresponds to the 'medium relief' category region as described using the single beam echosounding data (Fig.2.6,chapter 1). Even with the present data, this area can continue to be clubbed under the 'medium relief' category. Within this area, the northern part (10^0 15' to 12^0 S) is comparatively plain than the southern portion which is studded with few clusters of seamounts and abyssal hills.

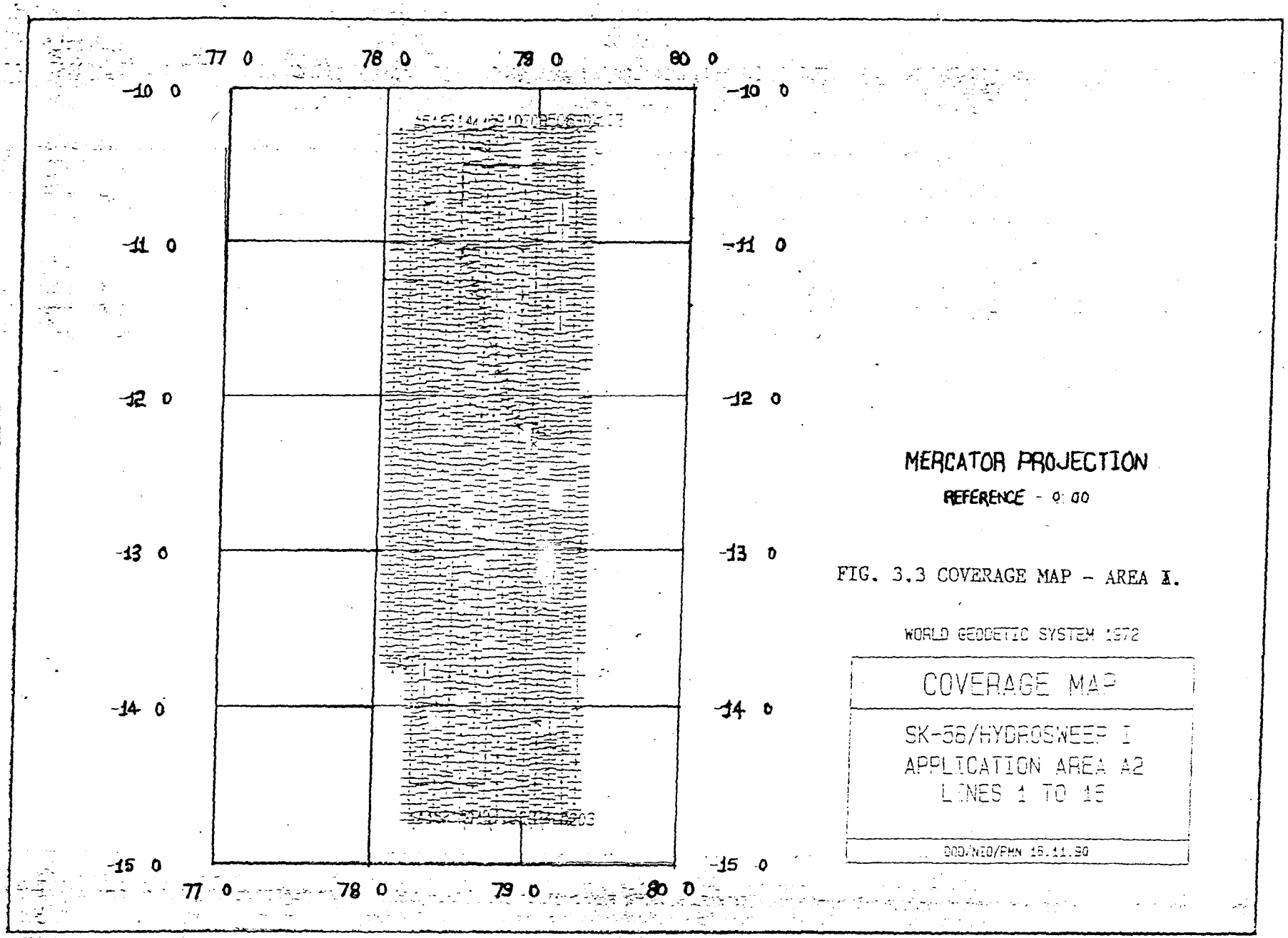

FIG. 3.3 COVERAGE MAP - AREA A.

WORLD GEODETIC SYSTEM 1972

COVERAGE MAP

SK-56/HYDROSWEEP I
APPLICATION AREA A2
LINES 1 TO 15

DOD/NGO/PHN 16.11.90

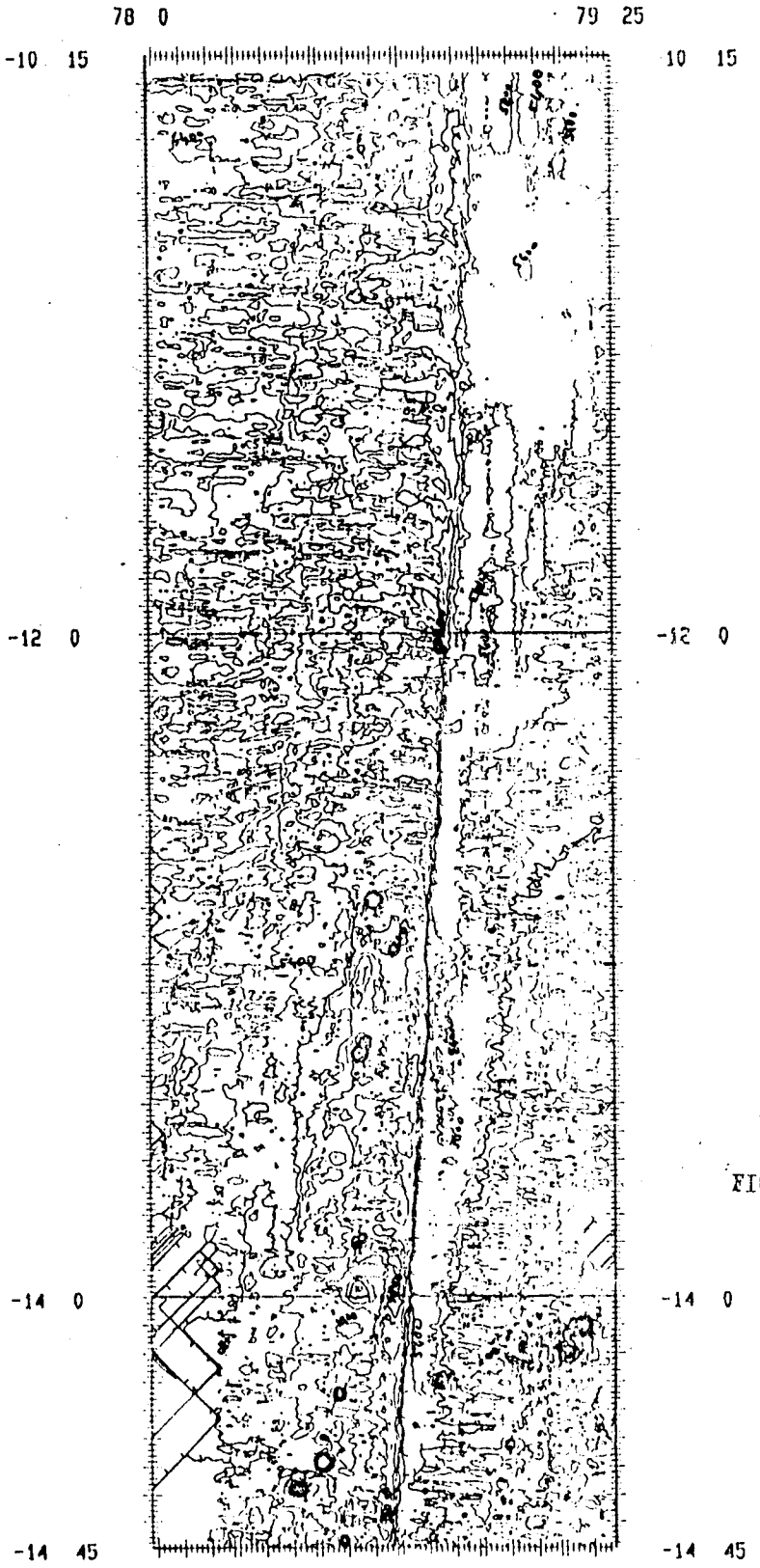

MERCATOR PROJECTION

REFERENCE + 0.00

SCALE 1 CM= 24.5Km

FIG. 3.4 DEPTH CONTOUR MAP AREA I.

CONTOUR INT. 100 M

WORLD GEODETIC SYSTEM 1972

DEPTH CONTOUR MAP

AREA A1
INDIAN OCEAN
ORV SAGARKANYA
HYPR/HSALL

DOO/NIO/PRN 15. 4.91

Fracture zone and the seamounts.

The most significant and striking feature of the map is the presence of linear trend along 79^0 E longitude. This is an unmistakable evidence for the southern extension of 79^0 E fracture zone, deciphered earlier from magnetic data **(Kamesh Raju and Ramprasad, 1989)**. The depths on the west of the fracture zone is around 5100 m where as on the eastern side (the downthrown side), it is about 5400 m. Thus the overall relief along the fracture zone is around 5400 m. It is less at the southern side while is more at the northern latitudes. Along the fracture zone, the gradient is very high, indicated by very close north-south trending contours. The fracture zone has a typical ridge-trough topography, which is clearly seen in cross section profiles across the fracture zone in Fig.3.5. These profiles have been drawn using the depth value grid created for drawing the combined depth contour map (Fig.3.4). Profile EW-1 along the 13^0 15′ S latitude has high relief of 585 m and the southern most profile EW-5 (along 14^0 15′ S latitude), has a relief of about 385 m. Relief across a fracture zone is a factor of evolution of sedimentary fill in elongate bathymetric trough typical of many fracture zones. Other conspicuous feature is the East-west bathymetric lineaments which are more pronounced in

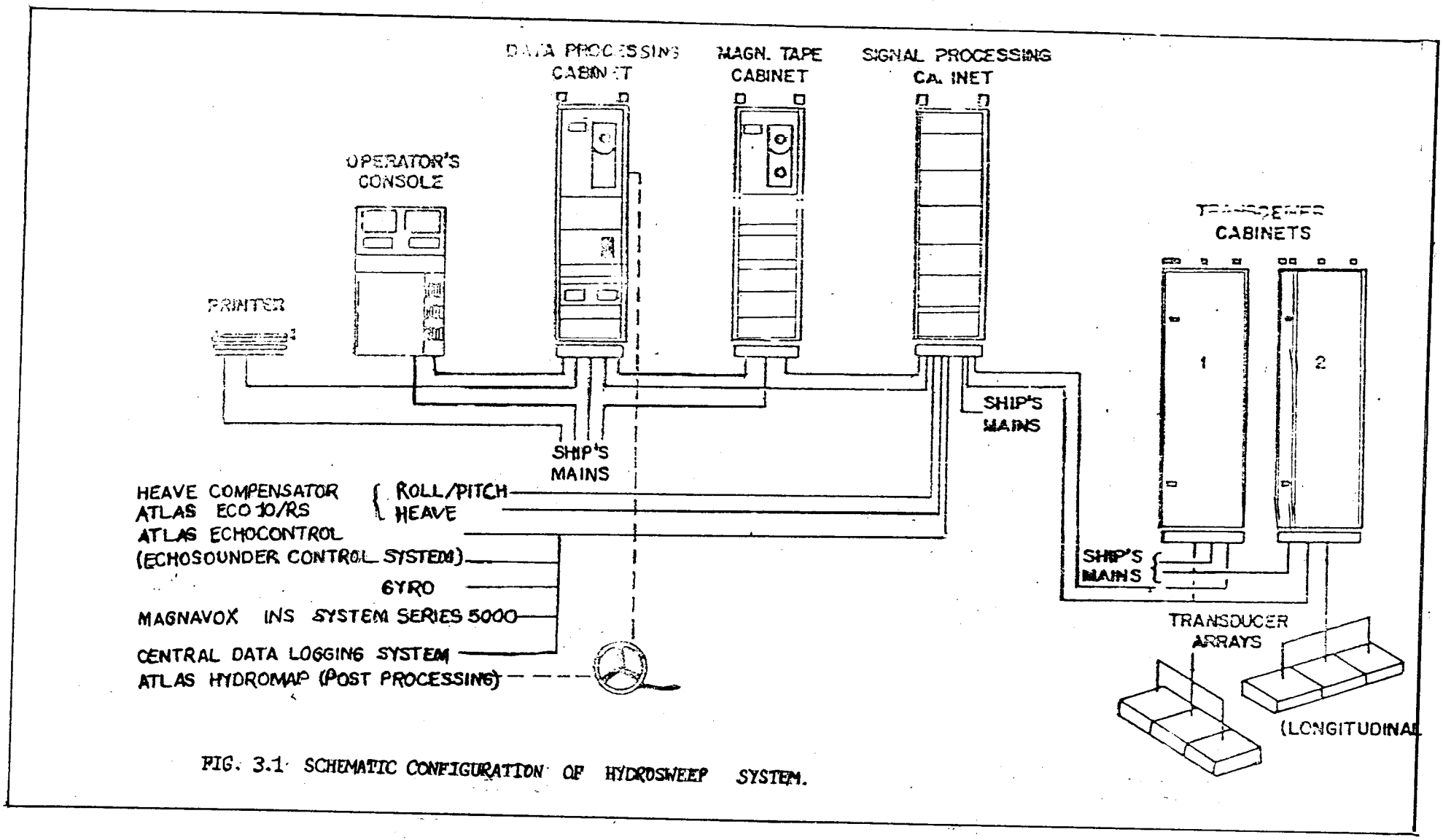

FIG. 3.1 SCHEMATIC CONFIGURATION OF HYDROSWEEP SYSTEM.

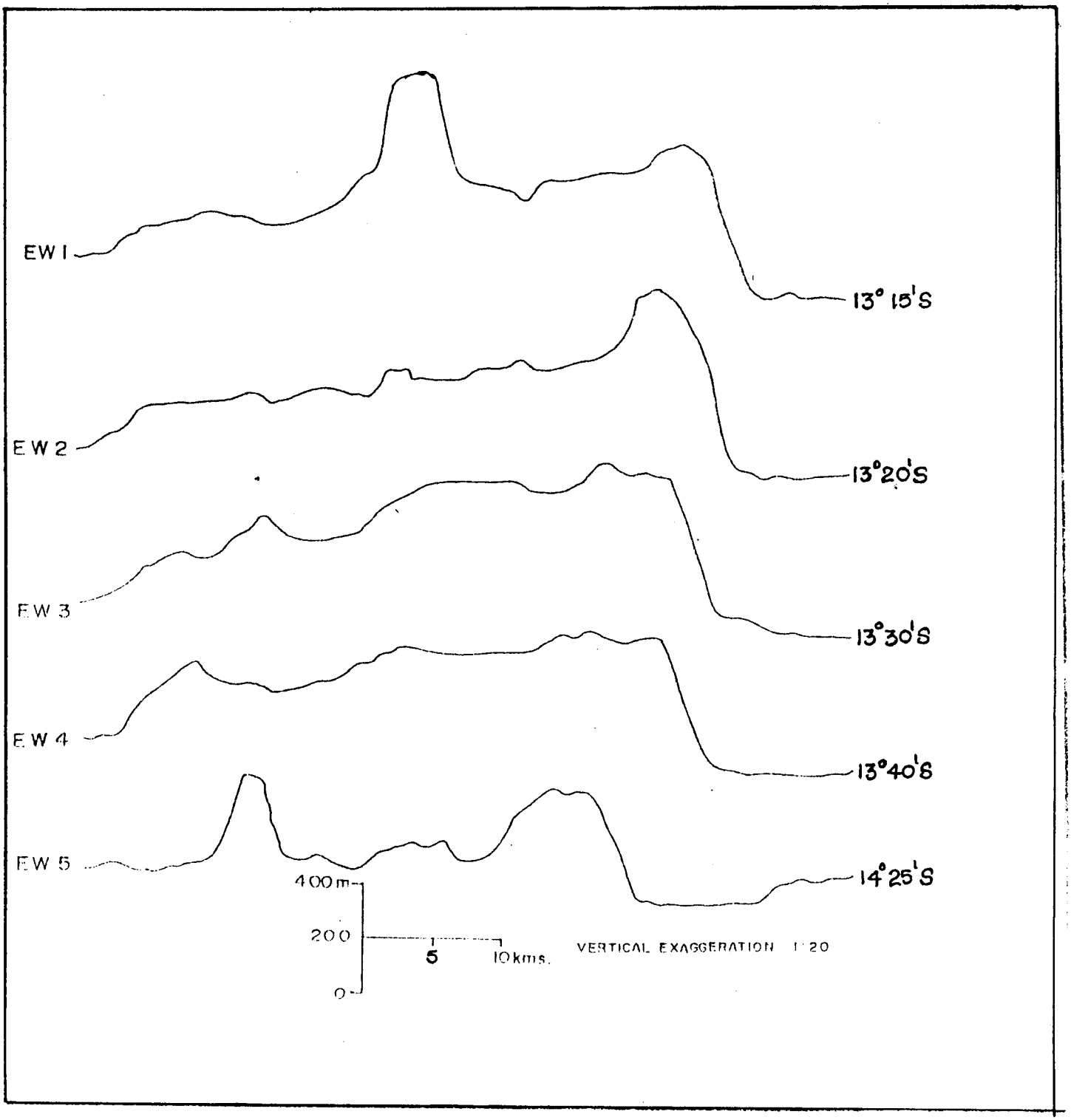

FIG. 3.5 BATHYMETRIC PROFILES SHOWING THE RIDGE TROUGH TOPOGRAPHY ACROSS FZ.

southeastern and north western quadrants of the map. Bathymetric character of these lineaments in the southeastern quadrant between 13^0 S and 14^0 S latitudes and a similar bathymetric character in the northwestern quadrant between 11^0S and 12^0S latitudes, show a correlation of the bathymetric signature with the crustal age **(anomaly A24, as described in Kamesh Raju et al., 1992)** and indicate the right lateral offset of the oceanic crust across the 79^0 E fracture zone. Age difference of volcanic crust on either side of a fracture zone results in a depth difference and also in different subsidence rates on two sides. The E-W trending bathymetric lineaments appear to flex towards south against 79^0E fracture zone in the west. The magnitude of these flexures tend to reduce south of the area where there is high concentration of seamounts. The overall change in the bathymetry across the fracture zone is over 300 m, depicting a ridge and trough topography, this resembles the major topographic character of the Pacific fracture zones **(Sandwell and Schubert, 1982)**. In the case of 79^0 E fracture zone, the bathymetric expression is confined to 5-6 miles in the south and widened to over 30 miles in the north.

Fracture zones are linear bands of mountainous topography which offset and are perpendicular to the crest of mid Ocean ridge system. They include very long ridges

and troughs. Fracture zones are extensions of transform faults between plates of oceanic crust moving away from centers of seafloor spreading **(Menard and Atwater, 1969)**. They are also characterised by wide variety of structures, most of them associated with scarps, which may have troughs at it's foot and a ridge near it's crest **(Searle, 1979)**. The fracture zones in the CIB are known to have changed their orientation from N-S to N 45^0E, during anomaly times 18 to 20, as a consequence of the global plate reorganization in the Indian Ocean resulting in major spreading direction changes on SEIR and CIR **(Patriat and Achache, 1984; Patriat and Segoufin, 1988)**. The spreading direction is near N-S, during anomaly times A21-A26 from an E-W trending SEIR. The E-W bathymetric lineaments observed in the bathymetric map (figure 3.4) may represent the dominance of N-S spreading prevalent during the anomaly times A21-A26.

Studies of microseismicity at the intersections of transform faults, spreading ridges and fracture zones demonstrate that while numerous microearthquakes occur along the transform faults and spreading ridges, the fracture zones are seismically inactive **(Francis, et al., 1978; Forsyth and Rowlett, 1979; Rowlett, 1981)**. It was also suggested that fracture zones are not zones of weakness and the fractured crust is only a remnant surface

expression of past tectonic activity along the transform fault. Furthermore, it was also shown that there is no significant slip along the fracture zones and the lithosphere bends in the vicinity of the fracture zone, in order to contain the topographic expression **(Sandwell and Schubert, 1982)**. The flexures of the bathymetric contours, which can be seen on the high precision multibeam bathymetric map, probably reflect the surface expression of the lithospheric flexure across the 79^0E fracture zone. Studies of multibeam bathymetry using *Seabeam* near a slow slipping transform fault **(Vema fracture zone, Macdonald, et al., 1986)** and fast slipping transform boundary **(Clipperton transform fault, Gallo, et al., 1986)** have shown the existence of a transform tectonised zone of varying dimensions along the length of the active transform fault. The varying width of the zone of smooth topographic expression, perhaps resulted from the fracturing in the transform fault environment and subsequent sedimentation, represent the fossil transform tectonised zone.

Apart from the fracture zone and the east-west topographic lineaments, there are few clusters of seamounts and abyssal hills in the area. The seamounts are mainly occurring in the southern latitudes, associated with the fracture zone. There are as many as 14 major seamounts and abyssal hills. The locations of these features, their

Table 3.2.

Details of major seamounts and abyssal hills as deciphered from MBS data in area I.

S.No.	Center Position	Minimum depth (m)	Height (m)	Area (sq.km)
1	14^0 10′ S 79^0 17′ E	3925	1175	76
2	14^0 05′ S 79^0 18.8′E	3975	1150	84
3	14^0 08.5′S 79^0 43′ E	4125	900	32
4	14^0 39.7′S 78^0 35.7′E	4640	500	53
5	14^0 43.4′S 78^0 35′ E	4425	675	20
6	14^0 29.4′S 78^0 31.2′E	4390	700	63
7	14^0 33.6′S 78^0 27′ E	3925	1175	75
8	13^0 50′ S 78^0 38′ E	4170	850	38
9	13^0 59′ S 78^0 37′ E	4610	400	160
10	13^0 16′ S 78^0 38′ E	4440	600	40
11	14^0 26′ S 79^0 05′ E	4650	375	40
12	14^0 17′ S 78^0 34.5′E	4180	850	30
13	12^0 48′ S 79^0 41.5′E	4520	500	66
14	12^0 41.5′S 78^0 40.6′E	4580	520	15

height and area occupied by them is tabulated in table 3.2. As seen from the table there are 3 major seamounts with heights around 1150-1175 m. The abyssal hills are in the range 500 to 850 m. Detailed morphology of some of the seamount chains obtained from MBS data is given in chapter 4. Seamount clusters in the southern portion of the area

might have originated from the fracture zone. Fracture zone provide easy conduits for seamounts **(Batiza, 1982)**. Although, fracture zones are not necessary for seamount formation, there may be local perturbations to plumbing system or other zones of weakness in the crust that control the location of seamounts **(Epp and Smoot, 1989)**. It appears that the fracture zone at 79^0 E provided conduits for seamount formations.

3.3.2 Multibeam survey- Area II (east-west lineaments).

This area lies between latitude 10^0 28′ S and 14^0 32 S and longitude 75^0 to 76^0, covering an area of about 49,000 sq. kms. 12 North-south lines (each 240 nm) with a spacing of 5 nautical miles (Fig.3.6) were covered in this area thus obtaining full coverage. A combined depth contour map generated from the data is given Fig 3.7 The depth in the region are in the range 5000-5300 m. with an average of 5200 m. This area, based on the single beam echosounding data was classified completely as plain area (chapter.2). However, a cursory observation of contour map of the area reveals that there are two distinct regions- the northern part (10^0 30′ S to 12^0 10′ S latitudes) is completely plain but the area south of 12^0 15′ latitude, area has to classified as medium to high relief region. There are no

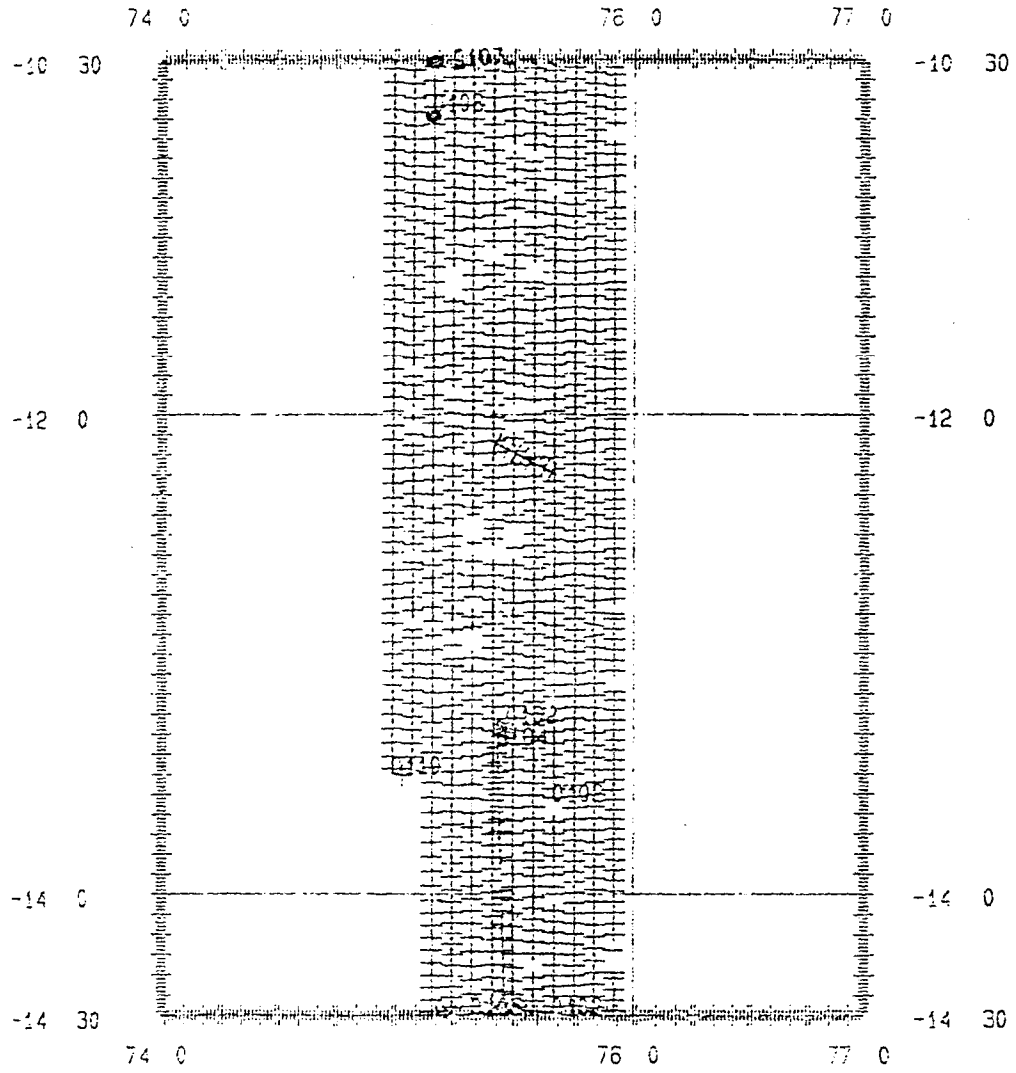

MERCATOR PROJECTION

REFERENCE -12: 30

FIG. 3.6 COVERAGE MAP AREA II.

WORLD GEODETIC SYSTEM 1972

SAGARKANYA 69

COVERAGE PLOT
ALL LINES

DGD/NIO/PNN 20.11.91

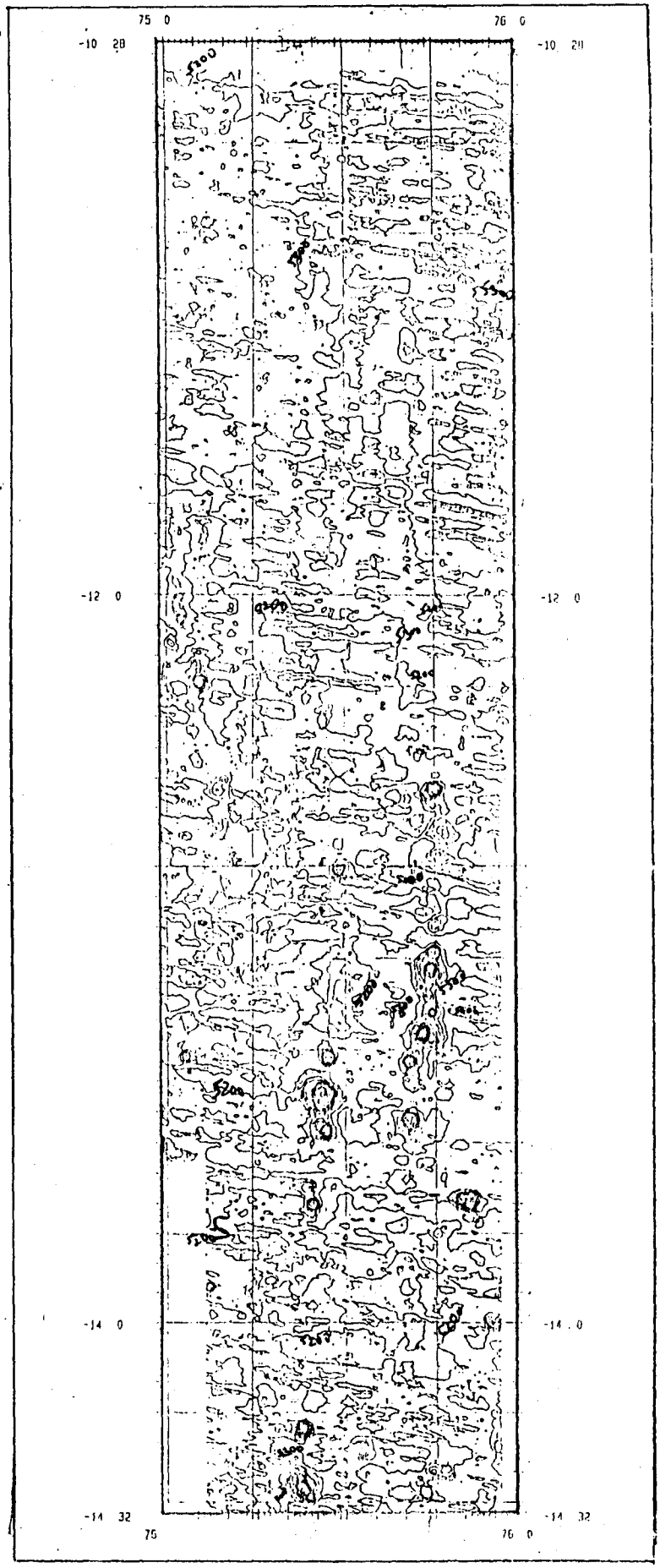

FIG. 3.7 DEPTH CONTOUR MAP AREA II. CONTOUR INT. 10
SCALE 1 Cm= 19.22 km.

seamounts noticed in the northern region where as the in the south, there are numerous seamounts and abyssal hills.

Lineaments

The east-west topographic lineaments which were observed in area I are present in this area also. Lineament is a term used in geomorphology for extensive linear topographic features which may reflect the trend of underlaying structure, often recognizable on land by aerial photos (**Hills, 1972**). Lineaments occur in pairs of strikingly similar appearances on both sides of the axis of mid ocean ridges. Each lineament exhibits a second order relief consisting of highs and lows that alternate along the strike of the lineament. Their evolution is primarily due to processes operating within 5 km to either side of the ridge axis. In this zone, lineaments form by progressive faulting over a long period of time two paired lineaments start to form at slightly different times. This is related to instantaneous position of primary zone of extrusion which migrates continuously across the rift valley floor (**Allmendinger and Riis, 1979**). Process of formation of lineaments is completed in the crestal ranges. Beyond, the pattern is frozen and lineaments are transferred downslope with only subsidence and relief reduction by faulting. Constant width of lineaments probably reflects the depth near the axis of a transition

from brittle to ductile crust at approximately 1 km. Precision and agreement in location of lineaments has always been a matter of argument. Recognition of large lineaments must be based on actual topographic maps and geological and geophysical evidences. However, here both in area I and II, the detection of lineaments by MBS depth contour map has been unambiguous. The lineaments are narrower and longer (10 to 15 nm length), with depth difference of 100 to 140 m and are more pronounced in the northern (plain) half than the southern (medium to rough) half. Flexuring of the lineaments as observed in area I is not observed here. Though, magnetic studies have revealed presence of a fracture zone at 75^0 45' **(Kamesh Raju and Ramprasad, 1989)**, it does not have a topographic signature and is not observed on this map. The lineaments are more clearly seen in larger scale map (Fig.3.8 , contour interval 25 m).

The southern half of the area has numerous seamounts and abyssal hills. The location, depth on top, height and area of the major ones are tabulated in table 3.3. Some of the seamounts have double peaks and some are cratered volcanoes. Five of the features have heights above 1000 m. The shallowest point is 3900 m (seamount no 2). No. 2, 7 and 10 are large and occupy an area of 145 and 170 sq. km respectively. Other features cover an area of 15 to 80 km^2.

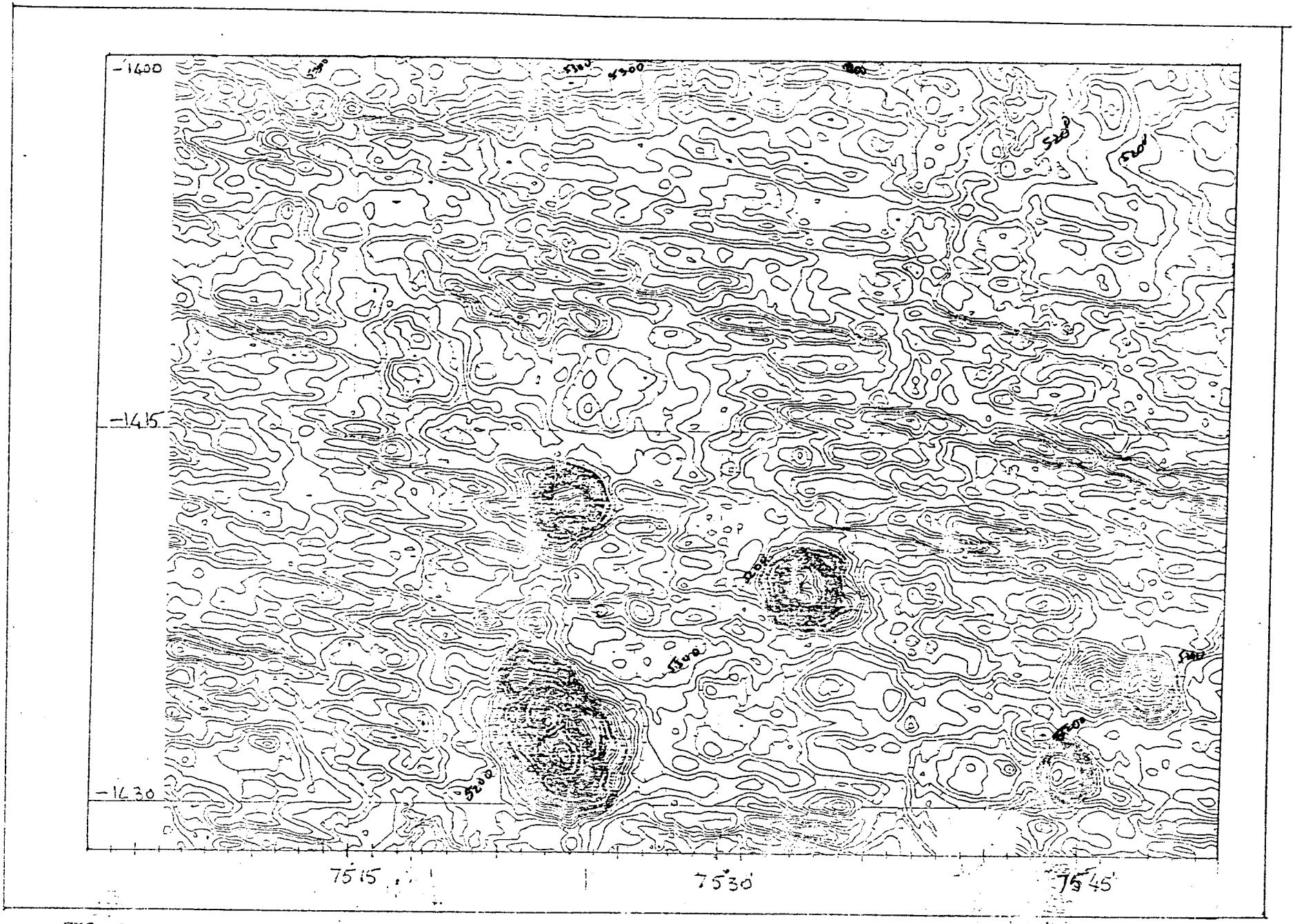

FIG. 3.8 DEPTH CONTOUR MAP OF PART OF AREA II CONTOUR INT. 25 M. SCALE 1CM = 3.9 KM.

Table 3.3.

Details of major seamounts and abyssal hills as deciphered from MBS data in area II.

S.No.	Center Position	Minimum depth (m)	Height (m)	Area (sq.km)
1	13^0 26′ S 75^0 42′ E	4530	650	25
2	13^0 22′ S 75^0 26.5′E	3900	1200	275
3	13^0 27.5′S 75^0 26.5′E	4300	700	30
4	13^0 15.1′S 75^0 26.6′E	4100	900	30
5	10^0 31.2′S 75^0 07′ E	4825	475	45
6	12^0 32′ S 75^0 46.1′E	4150	1050	60
7	13^0 00.0′S 75^0 46′ E	4190	900	145
8	13^0 12.2′S 75^0 44.5′E	4080	1150	95
9	13^0 17.5′S 75^0 42.1′E	4450	800	43
10	14^0 27.8′S 75^0 23′ E	3990	1200	170
11	14^0 19.2′S 75^0 22.7′E	4150	1000	55
12	14^0 21.6′S 75^0 33.2′E	4250	950	63
13	14^0 00.3′S 75^0 56.8′E	4500	700	53
14	13^0 39.5′S 75^0 51.5′E	4400	800	75
15	14^0 28.7′S 75^0 44.5′E	4800	450	15
16	13^0 39.8′S 75^0 25.3′E	4800	450	12
17	13^0 32′ S 75^0 07.5′E	4450	800	25
18	12^0 45′ S 75^0 30′ E	4700	550	40

There are two distinct chains of seamounts - both trending nearly north-south. One of the seamounts is along longitude

75^0 26′ E (no. 2,3 and 4,6,9,10) and other longitude 75^0 45′ E (no.1,6,7,8,9, and 12). Morphology of features in these two chains is described in chapter 4.

3.3.3 Multibeam survey- Area III (Graben).

This is the smallest of the three areas covering about 2200 sq. km (between latitudes 9^0 48′ and 10^0 26′ S and longitudes 73^0 35′ E and 73^0 55′E). General depth in the area is in the range 5100-5250 m with average being 5200 m. Fig.3.9 shows the depth contour map of this area. The significant feature in this map is the presence of two parallel faults resulting in a graben. The faults have $N8^0$-$E8^0$ trend. The western fault runs over the full length of the map and it's northern and southern extensions are outside the limits of the map. East of this fault is the downthrown side. The amount of downthrow ranges from 200-350 m. The other fault on the eastern side is smaller one having the same (nearly North-south) trend. This fault is about 35 km long and amount of throw is 160-200 m. Western side is the down thrown side for this fault thus making the central portion of the map the downthrown side for both the fault zones. Fig.3.10 shows five east-west cross sections across the map. Four of these sections are across the graben while one is north of the graben across the major western fault and the seamount. Latitude of the profile, Downthrow, minimum depth of each fault along the profile

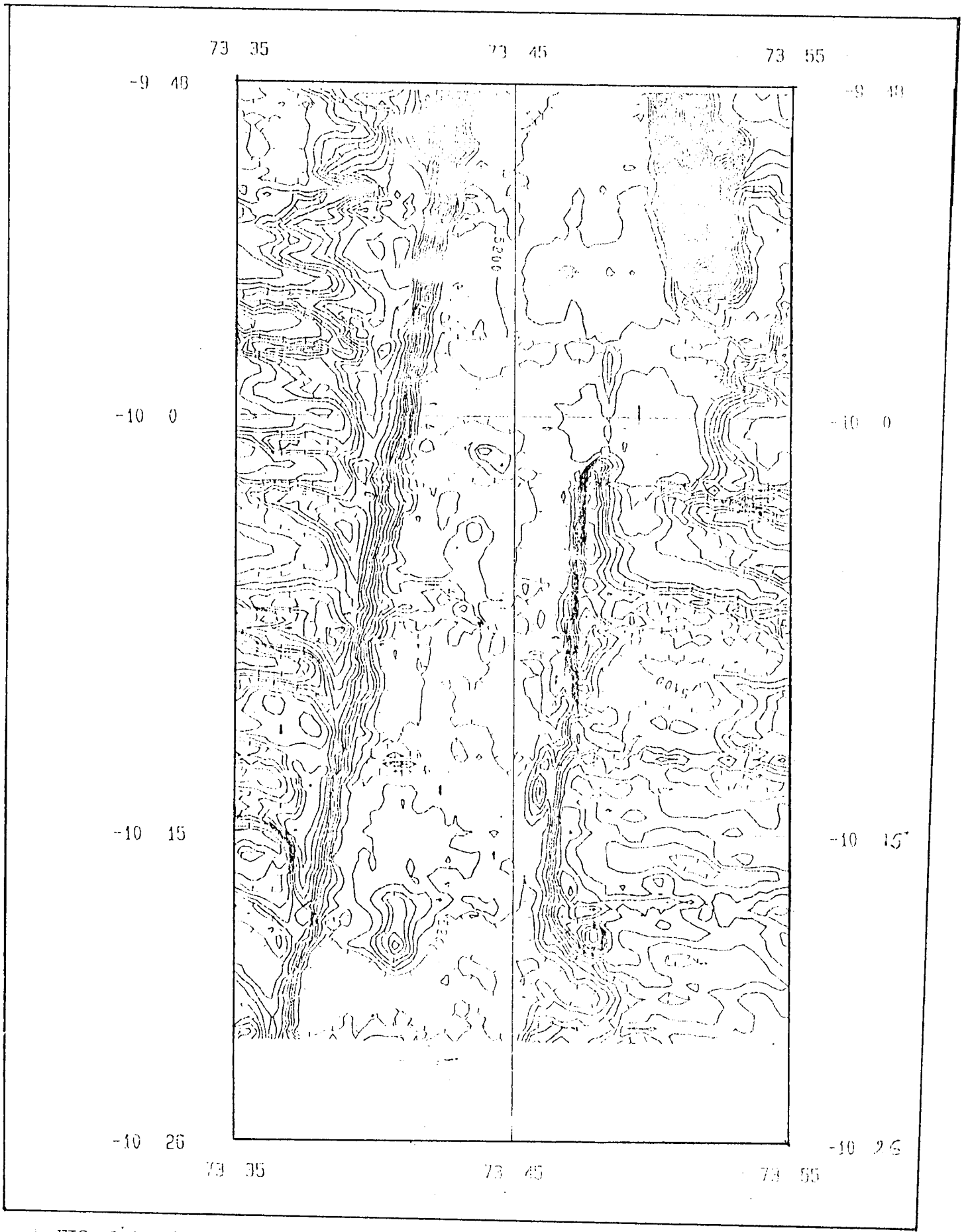

FIG. 3.9 DEPTH CONTOUR MAP OF AREA III. CONTOUR INT. 25 M. SCALE 1 CM= 3.28 KM.

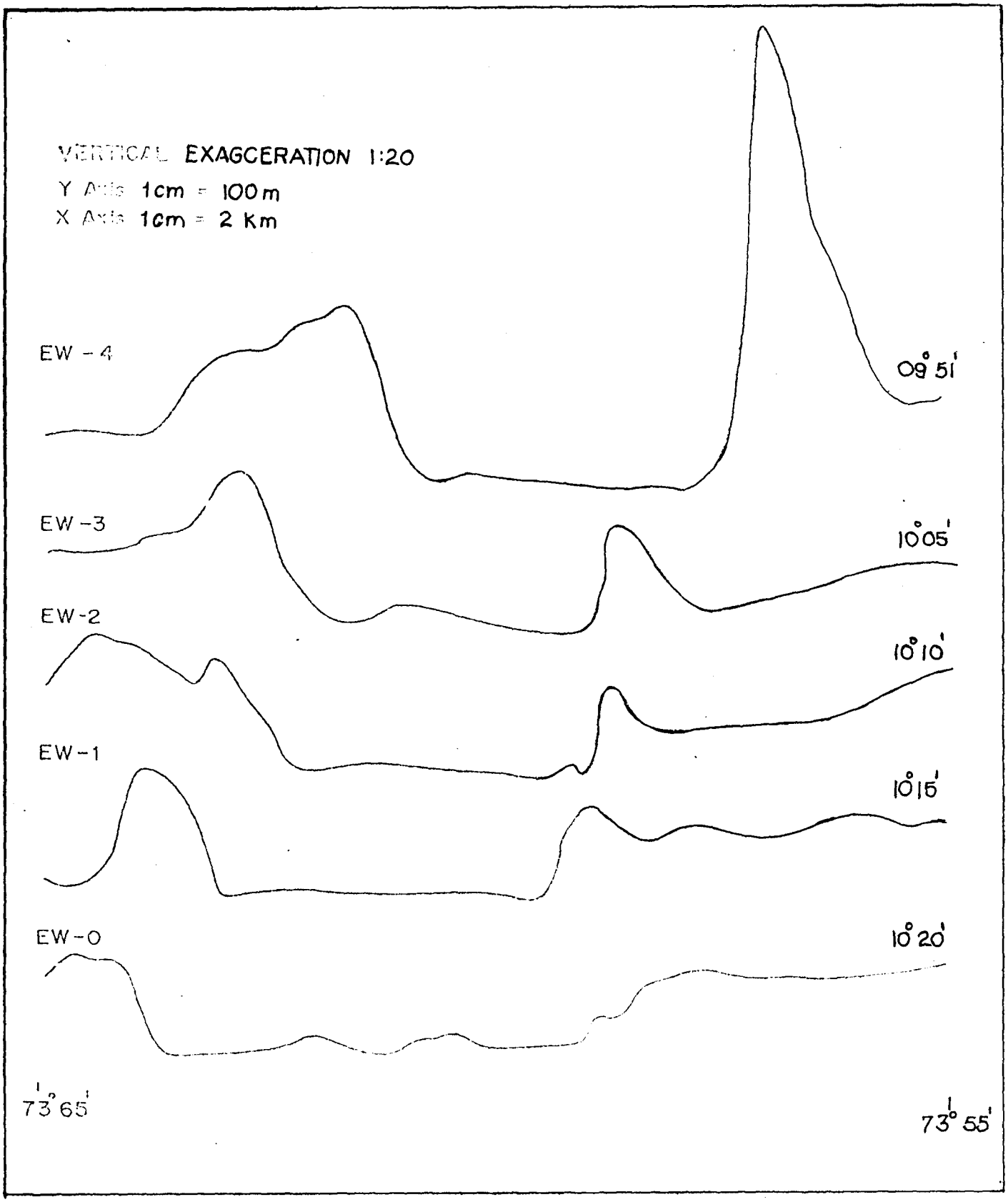

FIG. 3.10 CROSS SECTION PROFILES ACROSS THE GRABEN FEATURE.

and the basal width of the graben are shown in table 3.4. The graben base is almost flat, though minor undulations of 30-40 m are seen in profiles EW-0, EW-2 and EW-3.

Table 3.4

Details of fault downthrow and basal width of the graben in the 5 cross section profiles (Fig.3.10)

Profile No.	Across Latitude	Fault				Basal width of graben
		Western		Eastern		
		Minimum Depth (m)	Downthrow amount (m)	Minimum depth (m)	Downthrow amount (m)	(Km)
EW-0	9^0 51'S	4900	360	(Seamount of height 1050 m with basal width 6.5 km)		
EW-1	10^0 05'S	4860	330	4973	220	11.5
EW-2	10^0 10'S	4935	270	5015	200	12.2
EW-3	10^0 15'S	4930	260	4990	200	13.2
EW-4	10^0 20'S	5030	200	5060	160	19.0

Graben is a fault block, generally elongate that has been lowered relative to the two blocks on it's either side without major disturbance or pronounced tilting **(Fairbridge, 1968)**. Movements of blocks in graben are relative, all the blocks have moved but center block has moved more. Downthrow area between two parallel faults is produced by trough faulting **(Whitten and Brooks, 1976)**. Mid ocean rift valleys are a large scale grabens. Parallel

faults may have resulted from tension from breaking up of continental masses, deep seated lateral compressions or displacement of **SIMA** in the substratum. Certain grabens are undoubtedly related to lateral displacement along the intersecting wrench (transcurrent) faults. Red sea and dead sea graben have composite origin. Due to mantle upwelling form a hotspot, continental lithosphere thin and isostatic uplift results in crustal deviatoric stress, enhanced if underlying material is visco-elastic, rifting and graben formation begins when crustal tension reaches about 2 kilobar **(wedge subsidence hypothesis, Bott 1981)**. Amount of subsidence depends on graben width, friction on faulting, amplitude of applied tensile stress and sediment loading. Graben on the continental shelf are locations of hydrocarbon deposits, especially on the coast of Norway. Though there are many grabens reported from continental shelf and slope **(Viking graben, Fagerland Nils 1983)**, in deep sea they are rare, except for the active or dormant rift valleys. This is the first such occurrence in the Central Indian Basin.

Association of volcanism with graben is well known and it may be related to their origin. In this area also, there is a large seamount (Cross section EW-4, fig 3.10) on the north eastern corner of the map. It is exactly north of the eastern fault. The seamount is elongated, and it's northern

extension is outside the map limits. Height of the seamount is 1050 m and depth at the top of the mount is 4200 m. It has a pointed conical shape and it's basal width is 6.5 kms. This seamount may be genetically related to the existence of the graben.

Chapter 4
Morphology of some seamounts from Central Indian Basin.

4.1 Introduction and Background.

Seamounts are the important physiographic features beneath the sea and have evoked considerable interest amongst the geomorphologists world over. They are the surface manifestations of magma eruption within the oceanic crust triggered by tectonic activities and deep seated mantle upwelling **(Mukhopadhyay and Khadge, 1990)**. Till recently, our understanding of the geologic nature of the seamounts has been based upon the land-based studies on oceanic islands. In Central Indian Basin (CIB), such oceanic islands are non existent. Even in case of oceanic islands, the subaerial portion of the seamount is generally less than one percent of volume of the seamounts, the knowledge on gross morphology, stratigraphy and internal structure of the seamounts has been correspondingly limited. Last few years have witnessed increased interest on seamounts resulting many investigations and increased bathymetric surveying **(Keating, 1989, Handschumacher, 1973 and Walgate, 1984)**.

Seamounts have profound influence on mixing processes in the deep oceans. A seamount can influence up to three times its height above the neighboring abyssal plains and to a horizontal distance equal to three times it's width

(Gould et al., 1981). They are also a sort of markers to plate movements. **Handschumacher (1973)** suggests that the Emperor chain in Pacific Ocean might have formed along the boundary between the stable portion of ocean crust and the active spreading ridge migrating parallel to the boundary. The study of seamounts is essential in areas where manganese nodules of commercial interest occur. Considerable area around the seamounts have high abundance with lesser concentration of elements **(chapters 6 and 7)**. However, seamounts can be hazardous to future deep sea mining operations. Therefore, it is necessary that such features are studied in detail and their extent marked to avoid obstacles to mining.

There are numerous seamounts reported from world oceans, especially from Pacific and Atlantic. The Hawaiian-Emperor chain of the Pacific is reported to contain over 1000 seamounts of varying size **(Pratt 1963, Davies et al., 1972, Larina 1975 Irish 1976 and Walgate, 1984)**. Pacific ocean alone has more than 12,000 big and small seamounts **(Batiza, 1982)**. Morphologic studies have described individual seamounts and seamount chains in various tectonic regimes, like multibeam studies of small seamounts in the Philippine Basin **(Hollister et al, 1978)**, East Pacific rise seamounts **(Batiza and Venko, 1983)**, Atlantic seamounts **(Taylor et al., 1975)**, Henderson seamount in

eastern Pacific **(Taylor et al, 1980)**, Loihi seamount in Hawaiian chain **(Malhoff et al, 1982)**. Multibeam surveys on guyots in the gulf of Alaska has been carried out by **Smoot (1981)** and on Emperor seamounts by **Smoot (1982)**. The seamounts can best be detected with good quality bathymetric data. Probably because of lack of such data from the Indian Ocean, very few seamounts have been reported. Even the International Hydrographic charts of the Central Indian Basin show less number of seamounts. Morphology of one of the seamounts as revealed from single beam echosounding data and also from the multibeam data and morphology of three seamount chains from multibeam studies is described in this chapter.

4.2 Morphology of uncharted seamount from Central Indian Basin.

Area and methods.

A seamount with a height of 1275 m with its peak at a water depth of 4135 m at 12^0 35′ S, 76^0 16′ E was surveyed in detail during one of the cruises of ORV Sagarkanya (SK-20). This seamount had not been charted earlier. The general bathymetry around the region is quite rugged and a couple of abyssal hills are also present to the north of the seamount. Echosounding data on the seamount was collected using a Honewell Elac narrow beam sounder (NBS) and a deep sea sounder (12 KHz) run simultaneously. The NBS

has distinct advantages over conventional sounders in delineating features on the seabed (**Belderson et al 1972**). The NBS recorder was adjusted to 4000-6000 m range to obtain an enhanced resolution. Seven east-west lines, each about 25 nautical miles long and two cross lines were run traversing the complete length and breadth of the seamount. The distance between the east-west lines was 3 nm (approximately 5.4 km). Navigation was performed using the Integrated Navigation system with Magnavox dual channel satellite navigator.

Echosounding data collected during the survey also from the previous cruises were used for preparing the depth contour map of the area. Echosounding data was digitized, interpolated and merged with the navigation data on the Norsk data (ND 520) computer using the Geco Mapping system (GMS) package. Depth contour map and the isometric display of the area were also generated from GMS package. Slope angles were computed using the digitized depth values (from a computer program developed for the purpose) for different lines and a slope angle map of the area was also prepared.

Results and discussions.

Unlike the majority of seamounts from the Pacific (Meteor, Koko etc.) this is not a flat topped guyot. Basal width of the mount is 24 km and the height is 1275 m. It

occupies an area of about 190 km. Two features, a seamount and an abyssal hill lying side by side are recognised from the contour map and isometric display (Fig.4.1 and Fig.4.2). Fig.4.3 shows the bathymetric profiles drawn across the seamount from different east-west lines. Table 4.1 gives the mean, minimum and maximum depths at each lines and for the entire area. Line 4 has the minimum mean depth of 4975 m. On either side of the mount, the depths extend down to about 5400 m. The average depth in the area is 5214.1 m. Southern tip of the seamount appears in line 3 with maximum height of 250 m. the peak of is observed on line 4 (1275 m). In this profile, western flank of the mount appears to be gentler and lengthier, whereas the eastern flank is steeper and shorter. On the northern side of the seamount (line 6, fig.4.3), two features are evident (with heights 800 m and 600 m). Feature on the east (76^0 21'E) on this line appears to be an extension of the seamount whereas the feature at 76^0 12' E is another abyssal hill. The extension of the seamount on this line is confirmed by observing the flank morphology (Steeper eastern flank and gentler western flank). At about 250 m from the top of the mount, there is conspicuous presence of a flat step like feature on the western flank ('a' on line 4,5 and 6 in Fig.4.3). The seamount thus appears on

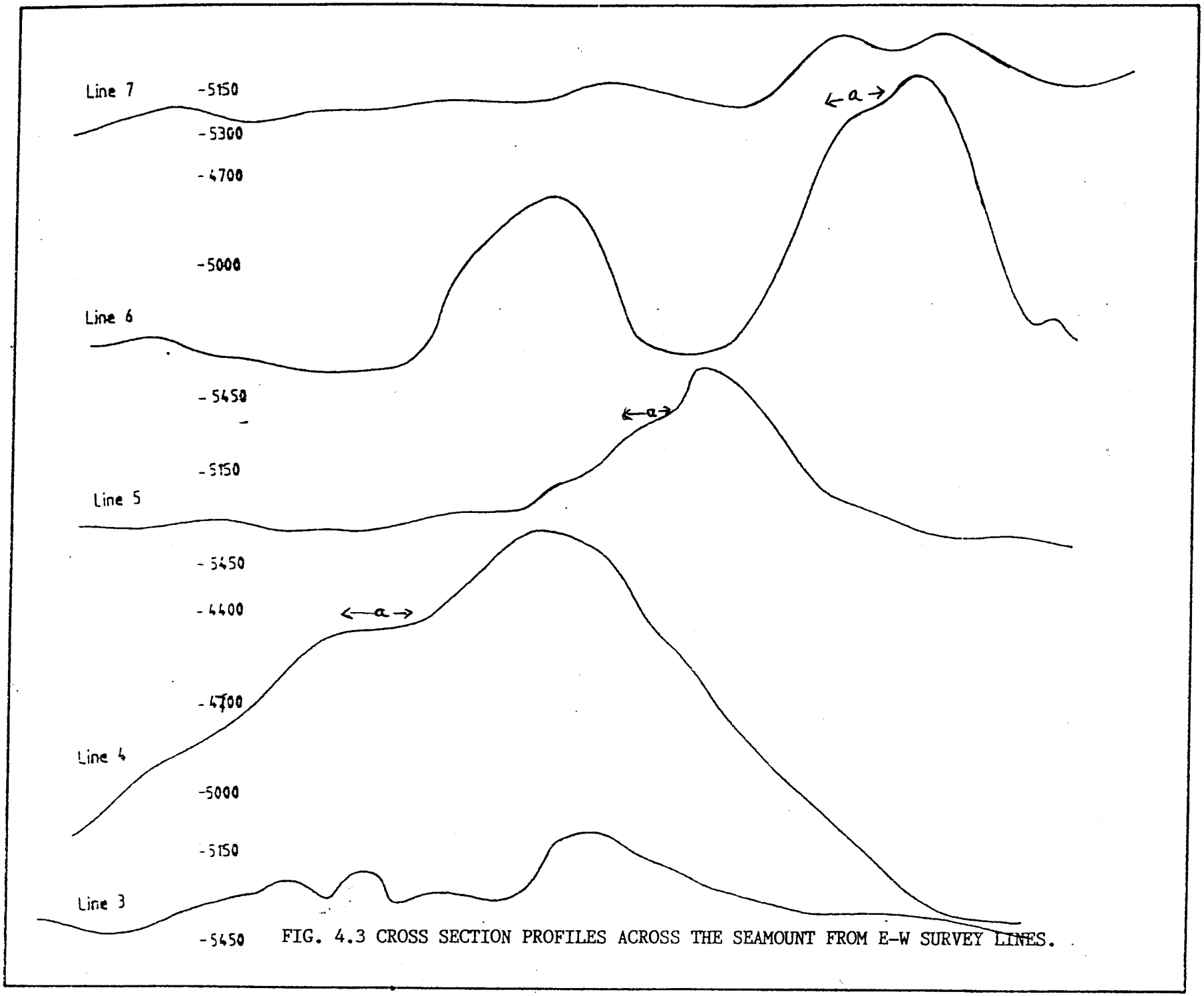

FIG. 4.3 CROSS SECTION PROFILES ACROSS THE SEAMOUNT FROM E-W SURVEY LINES.

Table 4.1

Mean, maximum and minimum depth and slope angles along each lines and entire area.

Line No.	Depth (in m) mean	maximum	minimum	slope angle (in degrees) Mean	maximum	minimum
2	5392	5423	5000	1.1	4.68	<1.0
3	5301	5401	5000	2.37	10.58	<1.0
4	4975	5416	4114	3.55	13.48	<1.0
5	5250	5408	4796	2.11	9.16	<1.0
6	5082	5387	4466	5.55	27.97	<1.0
7	5276	5395	5000	2.21	12.46	<1.0
8	5266	5370	4790	1.67	14.29	<1.0
9	5266	5420	4699	4.09	35.1	<1.0
Entire area	5214.2	5420	4114	2.85	35.1	<1.0

lines 3,4,5 and 6 with small signature of about 75 m on line 7. The trend of the mount is approximately NNE-SSW.

Slope angles were also computed on all lines using the digitized depth values. The mean, maximum and minimum slope angle data for different lines and entire area is tabulated in table 4.1. Slope angle map for the area is presented in Fig.4.4 Mean slope for the entire area is 2.85^0 which higher than the average reported elsewhere in the area (chapter 4, 1.305^0). Lines 4 and 6 where the peak of the seamount is encountered reported higher mean angles. For the entire area, 45% of the angles were found to be in the range $0\text{-}1^0$. Steeper angles (over 7^0) appeared 15% of the time, the rest were in the range $1\text{-}7^0$.

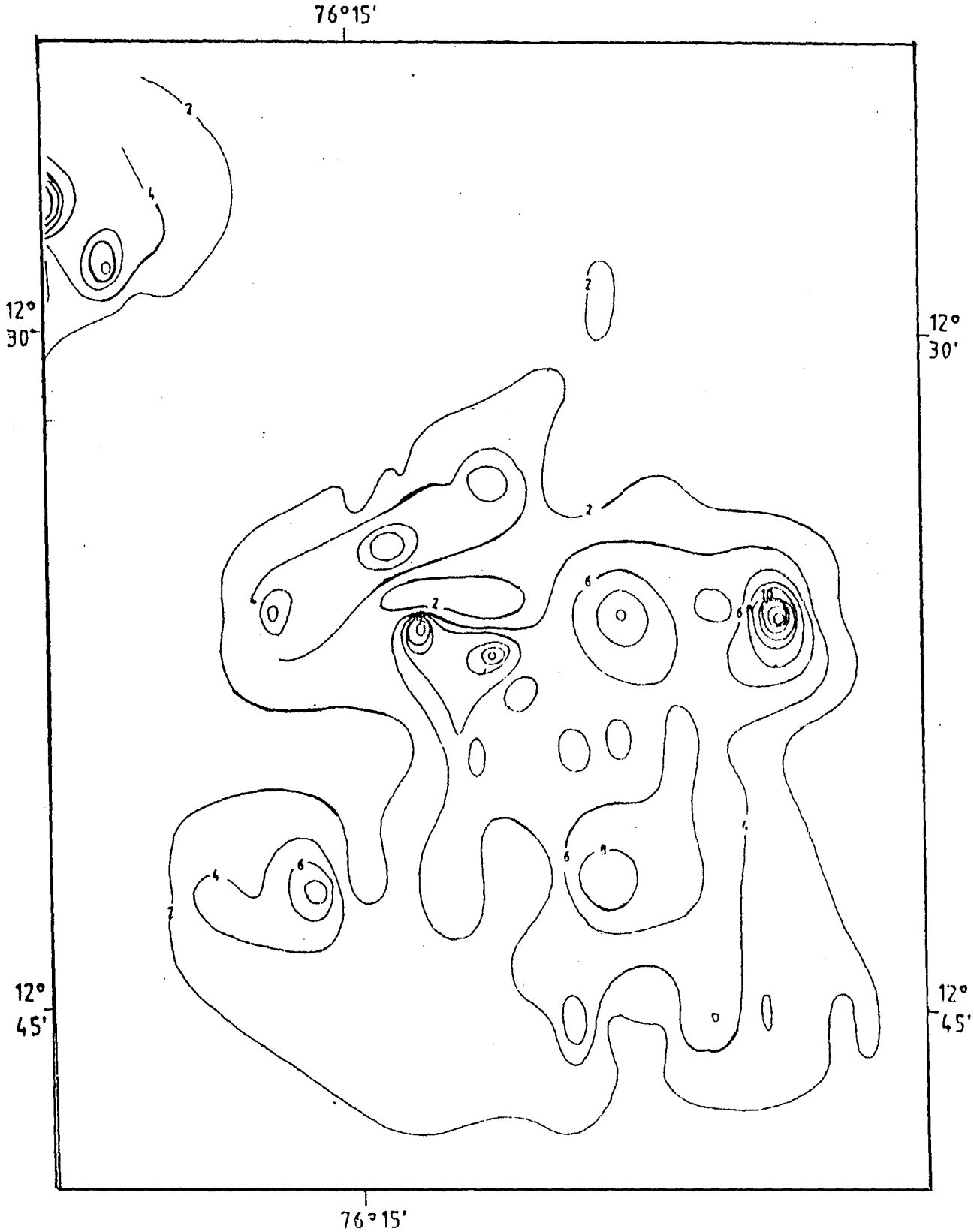

FIG. 4.4 SLOPE ANGLE MAP OF THE SEAMOUNT AREA. SCALE 1 CM= 2.3 KM.

Shape of the seamount is irregular and rugged. As the area is far away from land, the sedimentation rates are less and hence the seamount is less eroded. The flat tops for seamounts are developed by wave action and reef growth when the features are near the surface **(Pratt, 1963)**. As top of the seamount is over 4000 m from the surface factors like wave action and reef growth are not seen here. The seamount heights are generally related directly to the age of the lithosphere **(Morov, 1982)**. CIB being comparatively young, the seamount heights are less. Trend of this uncharted seamount is perpendicular to the south west Indian ridge and parallel to the fracture zones in the area (Chapter 3). The nearest fracture zone is the one along 75^0 45'E longitude **(Kamesh Raju and Ramprasad, 1990)**. The present plate positions result from recent openings along the north-south fracture zones that existed in this area during the interval of rapid spreading in the late Cretaceous to early Tertiary **(Fischer et al, 1971)**. Volcanism initiated from leaky transform faults might have resulted in the seamount. The dredging carried out on this seamount yielded ferromanganese encrustations on basalts confirm the volcanic origin. Seamount might have later subsided because of effects of seafloor spreading. Subsidence in the CIB is confirmed by the results of DSDP site 215 **(Borch et al, 1972)**. In Pacific Ocean, the

response of the seamounts to subduction related tectonic processes is a function of two factors- seamount age and degree of fracturing of the surrounding seafloor. Smaller seamounts- less than 40 km diameter are disturbed as much or more than the surrounding area. Larger seamounts (over 40 km diameter) show less evidence of fracturing prior to subduction **(Fryer and Smoot, 1985)**. The seamount described here has a maximum diameter of 24 km and seafloor surrounding it is quite rugged with varying slope angles. Non hotspot volcanoes are likely to be preferentially located on fracture zones.

4.3 Morphology of the 'uncharted' seamount - revisited with Multibeam system.

The seamount described in previous paragraphs was resurveyed using the multibeam swath bathymetric system 'Hydrosweep' on ORV Sagarkanya in November 1990. For this survey, Global Positioning System (GPS) was employed for accurate navigation.

Methods:

Hydrosweep data was collected from north-south survey lines spaced at 5 nautical miles. The line spacing of 5 miles accounted for a 100% coverage on the seafloor. Hydrosweep data from 5 survey lines falling within the

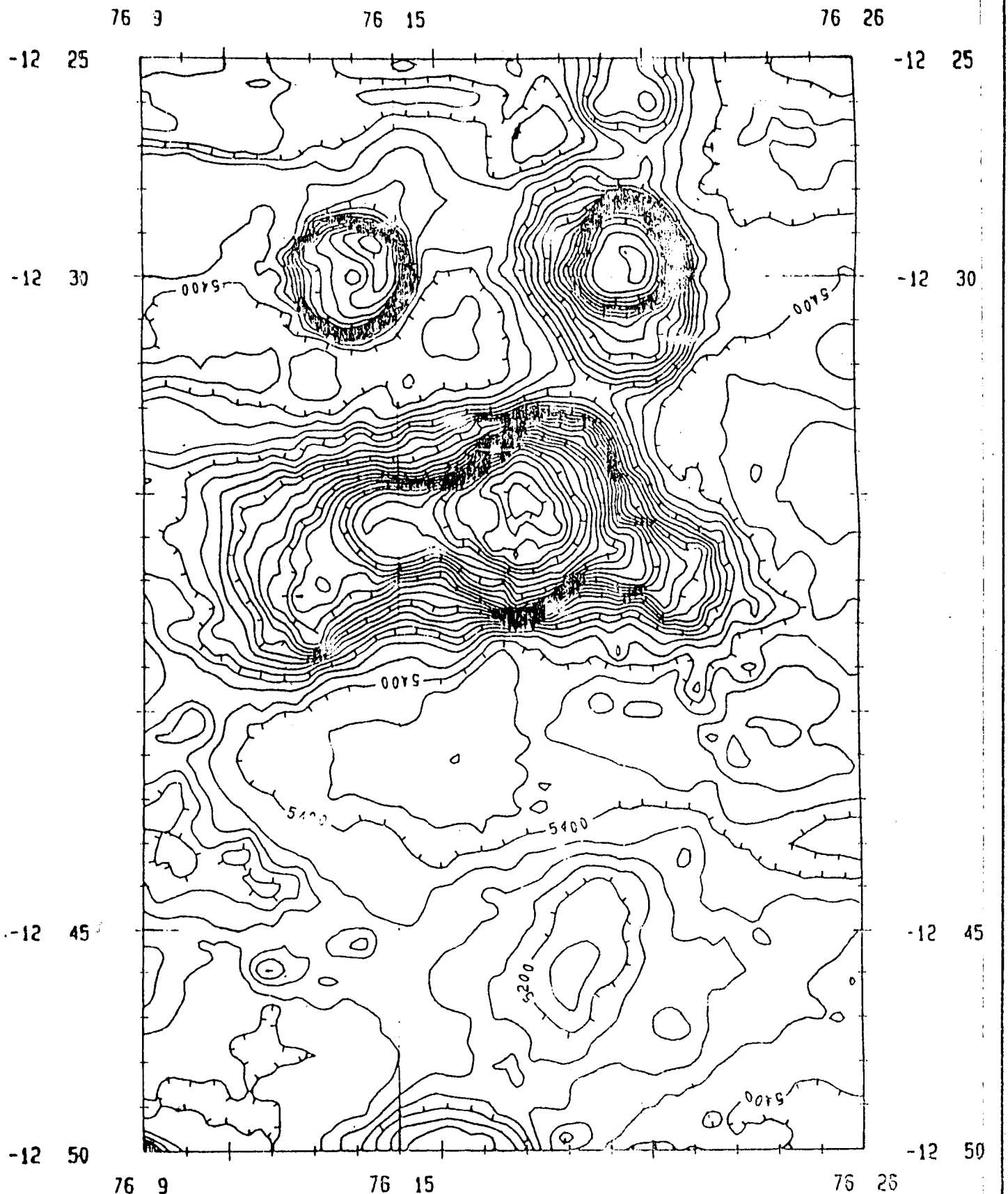

FIG. 4.5 DEPTH CONTOUR MAP OF THE SEAMOUNT DRAWN FROM MBS DATA. CONTOUR INTERVAL 25 M.

Scale 1cm = 2.23 Km

seamount area was processed onboard on the Hydromap post-processing system. A grid of depth values was generated from this data and this grid was used to draw depth contour map of the seamount area (Fig.4.5) and to generate isometric view of the seamount (Fig.4.6). East-west cross profiles across the seamount were drawn using the gridded depth values (Fig.4.7). The gridded depth values were converted to slope angles by a program developed on Hydromap system **(details of the technique are described in chapter 5)**. This grid of slope angle values was used for generating slope angle map of the area (Fig.4.8).

As seen from the depth contour map (Fig.4.5), there are three positive features in the area surveyed. The biggest feature is the seamount at 12^0 35′ S and 76^0 18.5′ E. It has a height of 1350 m with maximum basal width of 22.2 kms. The total area covered by this seamount is about 330 km^2. The water depth at the top of the mount is 3950 m. Three dimensional view of the seamount is given in fig. 4.6. There are two abyssal hills on the north of this seamount adjacent to one another. Table 4.2 gives the shape statistics of these features.

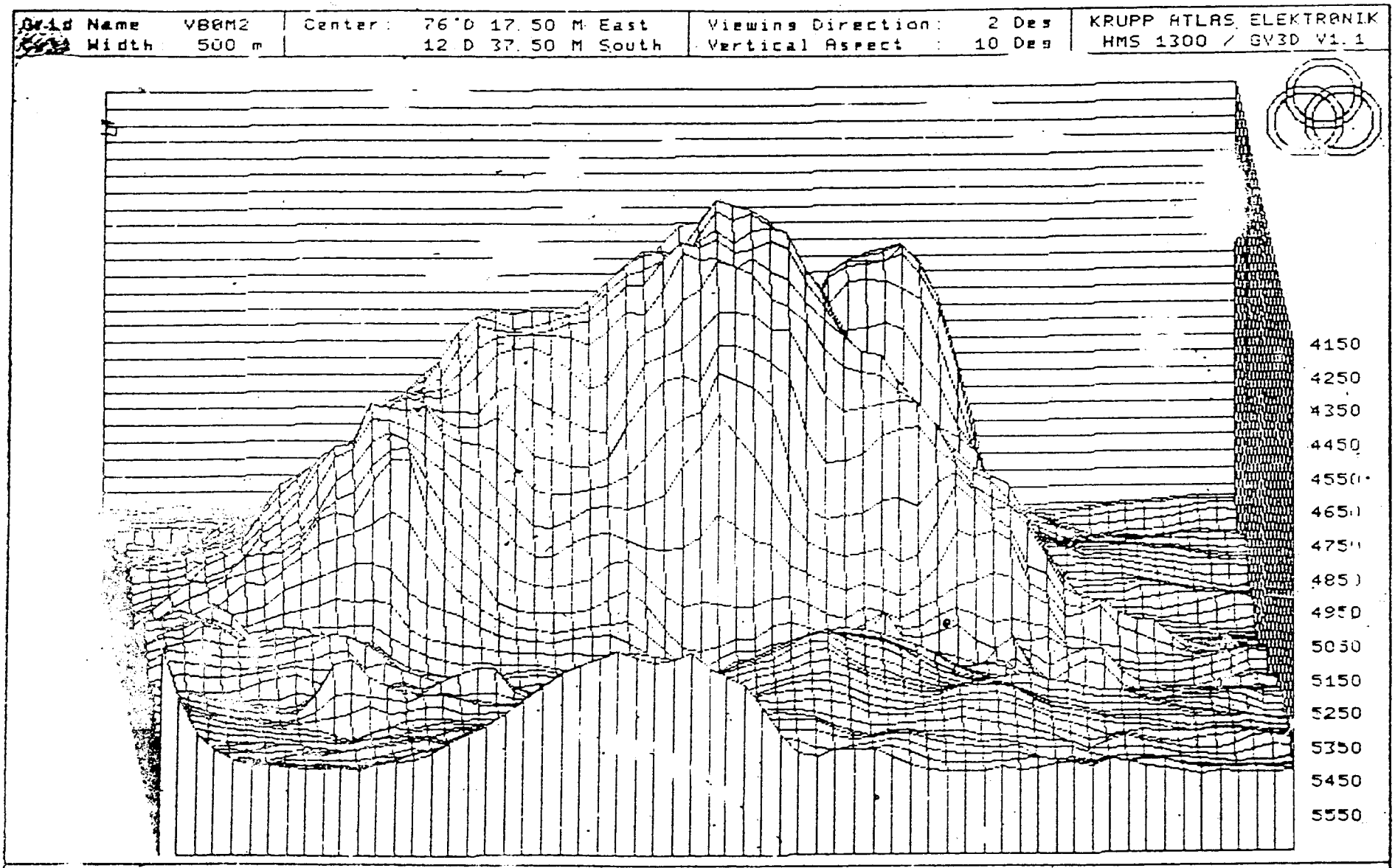

FIG. 4.6 ISOMETRIC VIEW OF THE SEAMOUNT FROM MBS DATA.

Table 4.2

Shape statistics of the seamount and abyssal hills:

Feature	Central position	Ht. in M. (h)	Basal width (W_b) $*10^3$ m	Summit width (W_s) $*10^3$ m.	Area (sq.km)	H-W ratio ($2h/W_b$)	Flatness (W_s/W_b)
Seamount	$12^0$35.5'S $76^0$18'E	1300	22.2	4.9	330	0.117	0.22
Abyssal Hill	$12^0$29.5'S $76^0$20.2'E	850	11.1	3.1	102	0.15	0.286
Abyssal Hill	$12^0$29.6'S $76^0$13.5'E	550	7.4	3.35	49	0.15	0.45

Five east-west cross section profiles across the area are shown in Fig-4.7. Profiles EW-3, EW-4 and EW-5 show clearly the morphology of the seamount. The western flank of the mount is gentler and lengthier, whereas the eastern flank is comparatively steeper. The step like feature on the western flank, as reported earlier **(Kodagali 1989b)** is manifested in the multibeam data as well (see 'a' in Fig-4.7). This feature is about 300 m from top of the mount and it's maximum width is about 3 km (in profile EW-4). Also, there is a small well developed caldera on this mount as seen in profile EW-4.

The two abyssal hills on the north of the seamount are comparatively small in size. The eastern hill appears as an extension of the seamount and is wider (basal width 11 kms and height 850 m). This abyssal hill also has a steep eastern flank and gentle western flank, as well as a

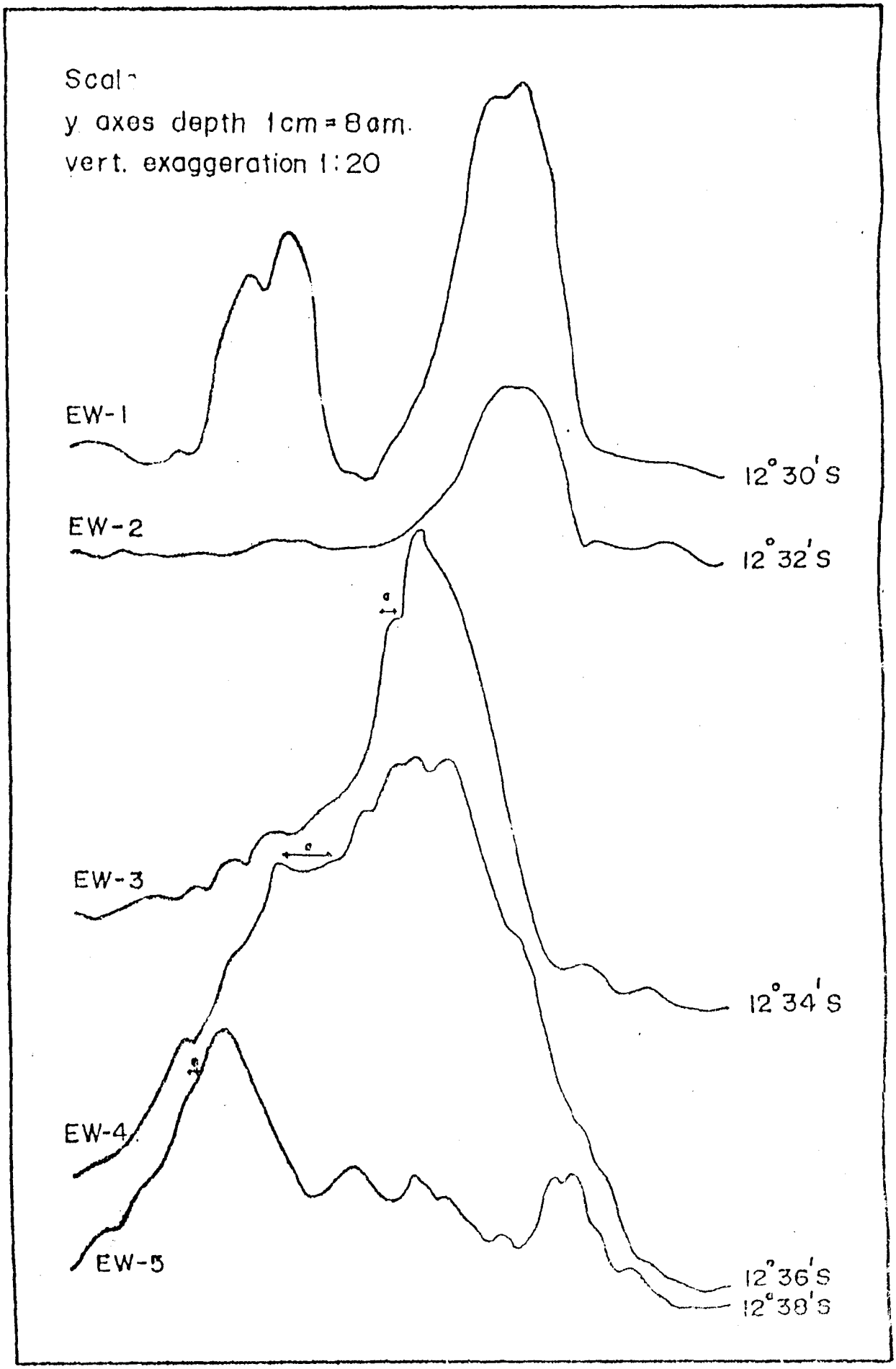

FIG. 4.7 CROSS SECTION PROFILES ACROSS SEAMOUNT DRAWN USING THE GRIDDED DEPTH VALUES.

caldera on it's top (profile EW-1). The other abyssal hill is more symmetric with both the eastern and western flanks being gentler but is much smaller (basal width 8 kms and height 500 m). This small hill has a relatively higher summit width of 3.35 km (Table 4.2).

Height-width (H-W) ratio (ratio of height to basal radius) and flatness coefficient (f= ratio of summit diameter to basal diameter) were calculated for the three features (table 4.2). The seamount has a low H-W ratio (0.117) whereas for the abyssal hills it is 0.15. Flatness (F) is highest for the smaller abyssal hill (0.45). Summit diameter of smaller abyssal is quite high compared to it's size. Generally it is observed that mean flatness decreases as a function of height. Larger sized seamounts have preferentially pointy cone shape **(Smith 1988)**. Mean H-W ratio of these features determined by this study (.125) is lower than that observed in Pacific **(Smith 1988 and Jordan, Menard and Smith 1983)**.

The grid of depth values which was used for generating depth contour map was also used to generate slope angle grid. From this grid, slope angle map was prepared (Fig.4.8). The maximum slope angle in this area is about 38^0. Pockets of high angles are present in all the three features. The average slope of the seamount is about 10.5^0

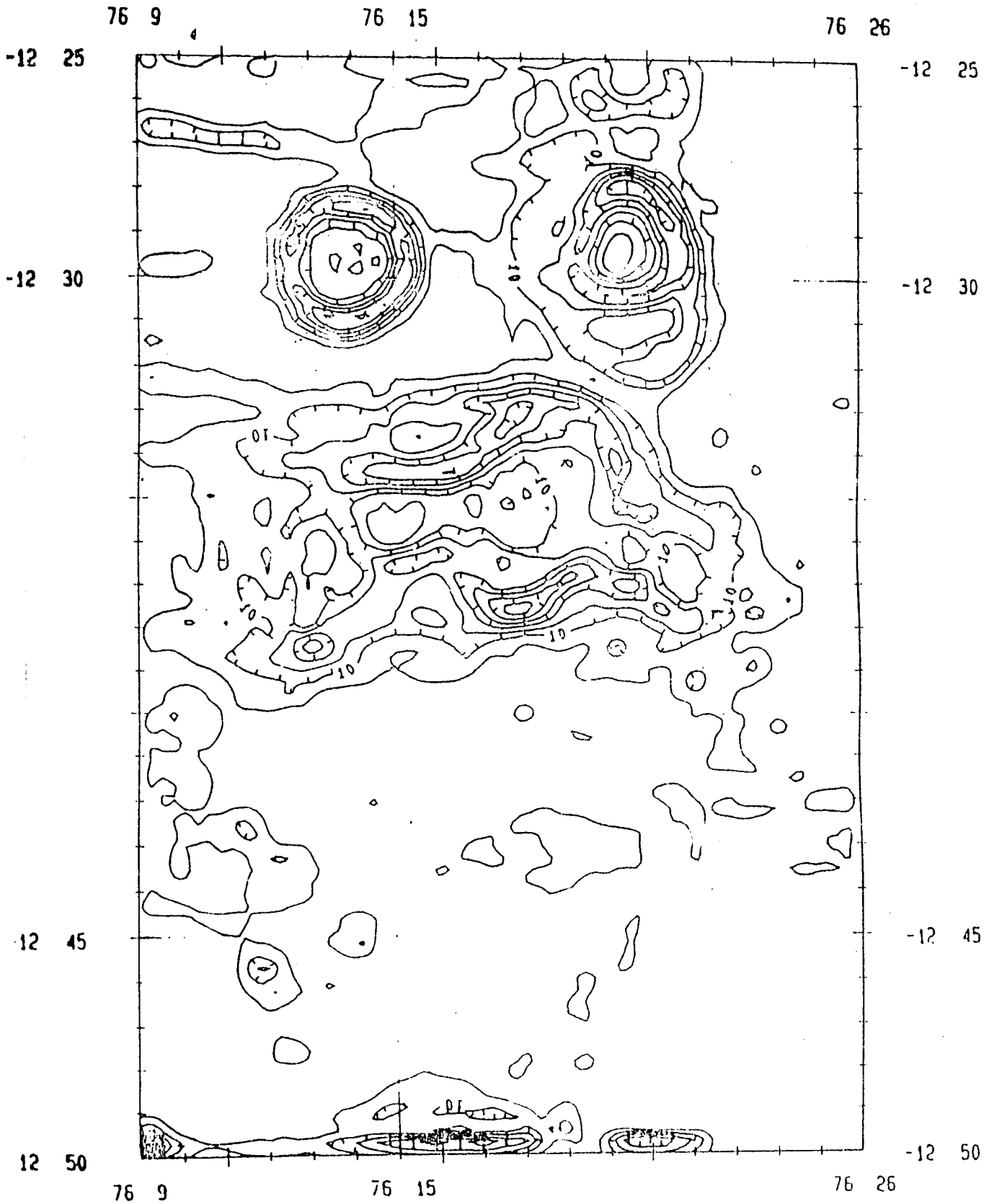

FIG. 4.8 SLOPE ANGLE MAP OF SEAMOUNT FROM MBS DATA. CONTOUR INTERVAL 2 DEGREE.

Scale 1 cm = 2-3 km.

and is slightly higher (13^0) for the abyssal hills. To the south and east of the seamount, the slope angles are less than 3^0 on an average. The average angle estimated from this study is higher than the average value reported earlier using the narrow beam echosounding data.

4.4 Comparison of single narrow beam and multibeam echosounding data on the seamount.

This seamount has been mapped by narrow beam echosounding (NBS) data and also by multibeam swath (MBS) bathymetric data. Depth contour maps generated by MBS and NBS are almost comparable (Fig. 4.1 and Fig.4.5). A comparison of different parameters observed from the two different surveys is given in table 4.3. Pointy cone shape and the step like feature on the western flank of the mount are recognized from both the surveys. The caldera on top of the seamount could be deciphered only from the detailed MBS survey (Fig.3,profile EW-4). In the previous survey, the seamount was reported to encompass an area of 189 sq kms, but the MBS survey has revealed that the seamount is much larger covering an area of 330 sq kms. Similarly, the average slope angle values are higher.

Table 4.3

Morphology of the seamount: comparison between narrow beam and MBS surveys.

Seamount	Narrow beam survey	Multi beam survey	Difference from MBS
Center position	$12^0$35′ S $76^0$16′ E	12^0 35′ S 76^0 18.5′ E	on longitude +2.5′
Height	1275 m.	1350 m.	+75 m
Depth at the top	4135 m.	3950 m.	-185 m
Basal width	24 Kms.	22.5 Kms.	-1.5 km
Area	189 Sq.kms	330 sq.Kms.	+141 km
Slope angle			
Maximum	35.1^0	38^0	~ 3^0
Average	2.8^0	10.5^0	~ 8^0

The Global positioning system (GPS) used for this survey is more accurate compared to transit satellite system used in the previous survey. The accurate center position of the seamount is 12^0 35′ S and 76^0 18.5 ′E, a shift of 2.5 nautical miles longitudinally. It can be concluded that, results of detailed mapping for small areas by narrow beam sounders are broadly comparable to that from multibeam swath bathymetric system provided closer grid echosounding is done. However, exact extension and minor morphologic features can only be obtained from MBS data.

Discussion:

The shape of the mount is that of a pointed cone. The shape is a primary constructional form **(Hollister, Glenn and Lonsdale 1978, Lonsdale and Speiss 1979)**. Development

of summit craters, filling the depression with sediments and development of calderas might produce a shape which may look flat topped in cross section. Development of cone or flat top is controlled by geological factors such as conduit geometry, magma chemistry and flow volume **(Batiza and Venko 1983 and Fornari, Ryan and Fox 1983)**. It is possible that the low sedimentation rate (1-2 mm/1000 years) has resulted in caldera remaining unfilled giving pointed cone shape to this mountain. Also, it is observed that features with less height have higher flatness compared to the seamounts. Mean flatness decreases with increasing height **(Smith 1988)**. Hence, it is likely that factors like conduit geometry, flow volume are highly variable in case of smaller features.

Distribution of the bathymetric features, such as seamount shapes vary significantly from one province to another. For example the Pacific Hawaiian chain of seamounts are invariably flat topped **(Keating 1989)**. Indian Ocean seamounts are mostly pointed cones with small calderas present in a few cases. The origin of these depressions (calderas) is uncertain probably reflecting different mechanisms. These are however related to tectonic activity and not landsliding **(Taylor, Wood and O'Hearn 1980)**. **Kamesh Raju and Ramprasad (1989)** have suggested existence of a possible fracture zone at 75^0 45′ E in

Central Indian Basin. Although the fracture zones are not necessary for seamount formation **(Epp and Smoot 1989)**, local zones of weakness control the location of seamount chains. It is likely that this seamount as well as others in area around 76^0 are genetically related to this fracture zone.

4.5 Morphological investigation of three seamount and abyssal hill chains in the Central Indian Basin from Multibeam sounder data.

Menard (1964) defined seamounts as equant, seafloor features higher than 1 km. smaller features were defined as abyssal hills. The term abyssal hill is however used to denote ridge parallel faulting. Loosely, term seamount can be referred to volcanic constructional features with height above 700 m. It is used as synonymous to volcano or central volcano **(Batiza et al., 1989)**. Central volcanoes are isolated features on the abyssal seafloor while the volcanoes are fed by linear conduits. Seamounts are known to have diverse shapes and varying sizes **(Batiza and Venko, 1983, Fornari et al., 1987)**. Morphology of seamounts varies with local and regional tectonic settings and thermal properties of underlying lithosphere. Factors influencing the morphology are sediment cover, chemical composition of the magma, conduit geometry **(Batiza and Venko, 1983, Wood**

1984), flow rate, gravity pull of ascending magma and it's viscosity **(Lacey et al., 1981)**.

Central Indian Basin (CIB) has a number of seamounts and abyssal hills (chapter 2), identified from multibeam sonar (MBS) data. Morphology of seamounts in CIB is also known to vary greatly **(Mukhopadhyay and Khadge, 1990, based on single beam echosounding data)**. MBS studies carried out in the CIB have thrown more light on the morphology of seamounts. Three chains of seamounts trending NNE-SSW have been studied and their morphology presented here.

4.5.1 Chain A:

This chain is present to the west of the 79^0 E fracture zone. The contour map showing the fracture zone and the chain of seamounts is shown in figure 3.4 (chapter 3). This chain trending NNE-SSW has nine seamounts and abyssal hills. Their center position, height and other morphological parameters like summit depth, basal width, summit width, Height-width ratio, sigma and flatness coefficient are tabulated in table 4.4.

Heights of the these features range from 500 to 1175 m. The seamounts and abyssal hills of this chain individually occupy an area of 11- 75 km maximum. The

Table 4.4

Position, minimum depth, height and other morphological features in Chain A

Feature No.	Center Position	Minimum depth (in m)	Height (h) (in m)	Area (sq.km)	Length (l) (in nm)	Width Base (W_1) (in nm)	Width summit (W_2) (in nm)	H-W ratio ($2h/W_1$)	Sigma ($2h/(W_1-W_2)$)	flatness (F) (W_2/W_1)
1	12° 48' S 79° 41.5'E	4520	500	66	4.2	4.8	1.8	.112	.180	.375
2	12° 41.5'S 78° 40.6'E	4580	520	15	1.4	2.5	0.5	.226	.281	.2
3	13° 16' S 78° 38' E	4440	600	40	3.5	3.5	1.5	.185	.323	.428
4	13° 50' S 78° 38' E	4170	850	38	3.2	3.6	0.15	.255	.266	.041
5	14° 17' S 78° 34.5'E	4180	850	30	3.0	3.0	0.8	.306	.417	.266
6	14° 29.4'S 78° 31.2'E	4390	700	63	4.3	4.5	2.0	.168	.302	.444
7	14° 33.6'S 78° 27' E	3925	1175	75	4.3	5.3	0.4	.239	.259	.075
8	14° 39.7'S 78° 35.7'E	4640	500	53	3.7	4.4	1.0	.123	.159	.227
9	14° 43.4'S 78° 35' E	4425	675	20	2.5	2.5	0.9	.291	.455	.360

largest is the seamount no. 7 both in terms of height and the area (1175 m and 75 sq km.). The summit widths vary from .15 nm to 2 nm. Feature nos. 1, 3 and 6 are flat topped with higher summit widths more than 1.5. Largest feature (no. 7) and feature no. 2 are perfectly pointed and conical (summit width 0.4 nm only). Height-width ratio (H-W) is the ratio of height to maximum basal radius and is another morphological parameter helpful in describing oceanic features. On this chain, the H-W ratios are in the range .112 to .306. H-W ratio and summit width are observed to have good negative correlation, higher the summit width, lower will be H-W ratio (r=-.63). H-W ratio also shows good correlation with height and summit depth (r=-.57, .56 respectively). Table 4.5 gives the coefficient of correlation matrix showing correlation between different morphological parameters. Sigma (ratio of height to difference of basal and summit radii) for the features indicate that sigma (range .159 to .455) is high whenever the H-W ratio is high (r=0.82).

Table 4.5

Correlation matrix for different morphological parameters Chain A

number of features = 9

****

Depth	1.00								
Height	-.98	1.00							
Area	-.29	0.31	1.00						
Length	-.30	0.29	0.93	1.00					
W(base)	-.27	0.29	0.99	0.90	1.00				
W(summit)	.45	-.49	0.38	0.48	0.30	1.00			
H-W	-.57	0.56	-.57	-.50	-.60	-.63	1.00		
Sigma	-.26	0.24	-.60	-.42	-.67	-.13	0.82	1.00	
Flatness	.52	-.56	-.00	0.15	-.098	0.90	-.34	0.25	1.00
	Depth	Height	Area	Length	W(base)	W(summit)	H-W	Sigma	Flatness

****

Flatness, the ratio of summit width to basal width is also a pointer to the seamount shape. If the ratio 'f' is nearer to zero, the seamount will be pointed cone, whereas, for flat topped features, f will be higher (>.3). In this chain, abyssal hill and seamounts have f in the range of 0.041 to 0.444. Feature nos. 3, 1 and 6 have 'f' higher than 0.375 and have wider summit (flat topped). Of the remaining, the lowest value of 'f' is observed for the largest feature (no.7, .075). It is observed universally that, the preferred shape for the large sized seamounts is the pointed cone (Smith, 1988) and this is confirmed in this case also. Other features have 'f' between .2-.36,

the shape varying between conical, sharp peak to sloping summits. 'f' shows strong correlation to summit width (0.91) and to some extent to depth and height (.53,-.56). Higher, the mount, the flatness will be less. Correlation of f to summit width (r=0.91) in this case is much higher than reported earlier based on wide beam echosounding data **(Mukhopadhyay and Khadge, 1990 r= 0.715)**. It was reported by them that 'f' is insignificantly correlated with summit height (r=0.428) where as in this case it is slightly higher and has inverse correlation (r=-0.56).

4.5.2 Seamount and abyssal hills- Chain B and Chain C

Chain B and chain C are observed in area II as described in chapter 2. Fig. 3.7 (chapter 3) gives the depth contour map (contour interval 100 m) of the area showing the two chains. Position, depth, height, area and other morphological parameters basal width, summit width, H-W ratio, sigma and flatness ratio for chain B and chain C are tabulated in table 4.6. As the two chains are quite close by and are parallel (about 18 nautical miles apart), they are discussed together here.

Chain B has 7 distinct features (4 seamounts and 3 abyssal hills) and they are along 75^0 26' E longitude.

Table 4.6

Position, minimum depth, height and other morphological features in Chain B and C.

Feature No.	Center Position	Minimum depth (in m)	Height (h) (in m)	Area (sq.km)	Length (l) (in nm)	Width Base (W_1) (in nm)	Width summit (W_2)	H-W ratio ($2h/W_1$)	Sigma ($2h/(W_1-W_2)$)	flatness (F) (W_2/W_1)
Chain B (along 75° 26' E)										
1	12° 45.5'S									
	75° 29 E	4700	550	43	3	4	1.1	.148	.204	.275
2	13° 15.1'S									
	75° 26.6'E	4100	900	30	3	3.5	.4	.278	.313	.114
3	13° 22' S									
	75° 26.5'E	3900	1200	275	8	10	.5	.129	.136	.05
4	13° 27.5'S									
	75° 26.5'E	4300	700	30	3	3	1.1	.252	.398	.366
5	13° 39.8'S									
	75° 25.3'E	4800	450	12	1.8	1.8	.4	.270	.346	.222
6	14° 19.2'S									
	75° 28.5'E	4150	1000	55	3.8	4	.8	.270	.337	.200
7	14° 27.8'S									
	75° 23' E	3990	1200	170	7	7	1	.185	.216	.143

Table 4.6 continued.....

Chain C (along 75° 44')

Feature No.	Center Position	Minimum depth (in m)	Height (h) (in m)	Area (sq.km)	Length (l) (in nm)	Width Base (W_1) (in nm)	Width summit (W_2) (in nm)	H-W ratio ($2h/W_1$)	Sigma ($2h/(W_1-W_2)$)	flatness (F) (W_2/W_1)
1	12° 32' S 75° 46.1'E	4150	1050	60	4	4.2	.4	.270	.298	.096
2	13° 00.0'S 75° 46' E	4190	900	145	6	7	.65	.139	.153	.092
3	13° 12.2'S 75° 44.5'E	4080	1150	95	4.5	6	.8	.206	.238	.133
4	13° 17.5'S 75° 42.1'E	4450	800	43	3.5	3.5	.5	.247	.288	.142
5	13° 26' S 75° 42' E	4530	650	25	4	4	.75	.135	.166	.188
6	14° 21.6'S 75° 33.2'E	4250	950	63	4	4.5	1.0	.228	.292	.222

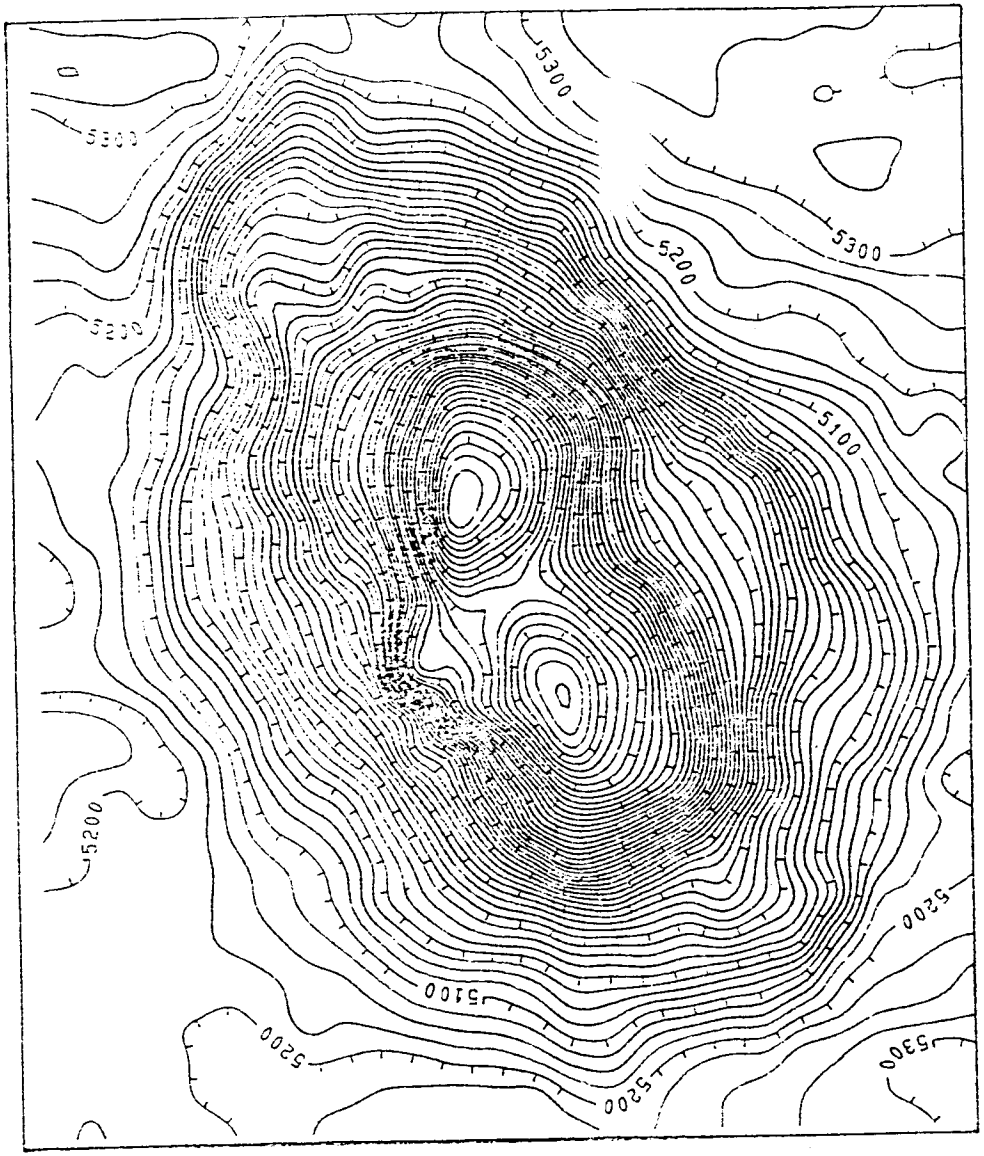

MERCATOR PROJECTION

REFERENCE -12: 30

SCALE 1 CM= 0.95 KM.

FIG. 4.9 DEPTH CONTOUR MAP OF CRATERED SEAMOUNT CONTOUR INT. 25 M.

WORLD GEODETIC SYSTEM 1972

SAGARKANYA 69

AREA-P1
SEAMOUNT S69N4-1
CONTOUR INT.25M.

DOD/NIO/PMN 19.11.91

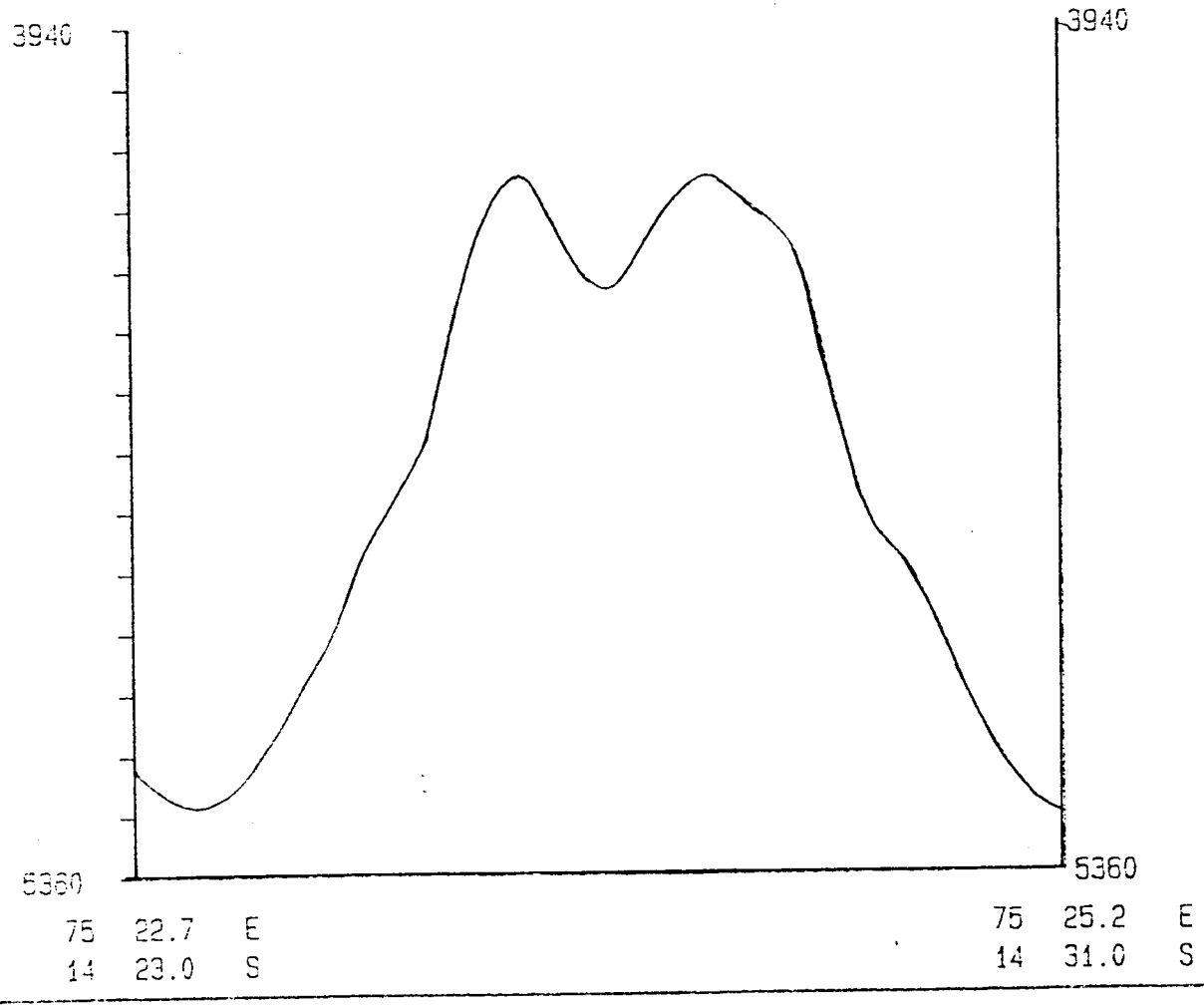

NAT.INST.OF OCEANOGRAPHY

GOA-INDIA -403 004

VERT.EXAG=10

FIG. 4.10 CROSS SECTION PROFILE ACROSS DRAWNDD TOP OF SEAMOUNT CHAIN B

POLYMETALLIC NODULES PROJECT

CROSS SECTION

VNK
SMT S69N4-1
ORV SAGARKANYA
N-S3

DOD/NIO-PMN 19.11.91

Trend of this chain is almost N-S ($N3^0E$-$S3^0W$).Chain B has two very big seamounts (area 275 and 170 sq. km respectively with height 1200 m each). One of these seamounts (at 14^0 27.8'S and 75^0 23' E ,S.No.7 in table 4.6) is a cratered volcano. Depth contour map of this seamount is shown in fig.4.9. Fig. 4.10 gives the N-S cross section profile across the cratered top. The width of the crater is .9 km and the depth 180 m. Other seamount is having a low smaller summit width and low 'f' and has pointed cone shape. In contrast feature nos. 1 and 4 have high summit width and high 'f' indicating their flat top nature. Flatness shows good correlation with almost all other morphological parameters except H-W ratio (r in other cases ranges from 0.61 to .70). Summit width is not correlated with any feature other than 'f'.

Chain C has 6 features (3 seamounts and 3 abyssal hills) and has a trend more towards east ($N10^0E$-$S10^0W$). The depth of the features is between 500-1150 m. Feature no. 2 is the largest in terms of size occupying 145 sq km area. One interesting observation on this chain is that 'f' increases gradually from north to south. Feature nos. 1 and 2 have 'f'<.1, indicating pointed cone shape. Southern most feature no 6 has the highest 'f' of 0.22, showing slightly flat top. 'f' shows good correlation with summit width

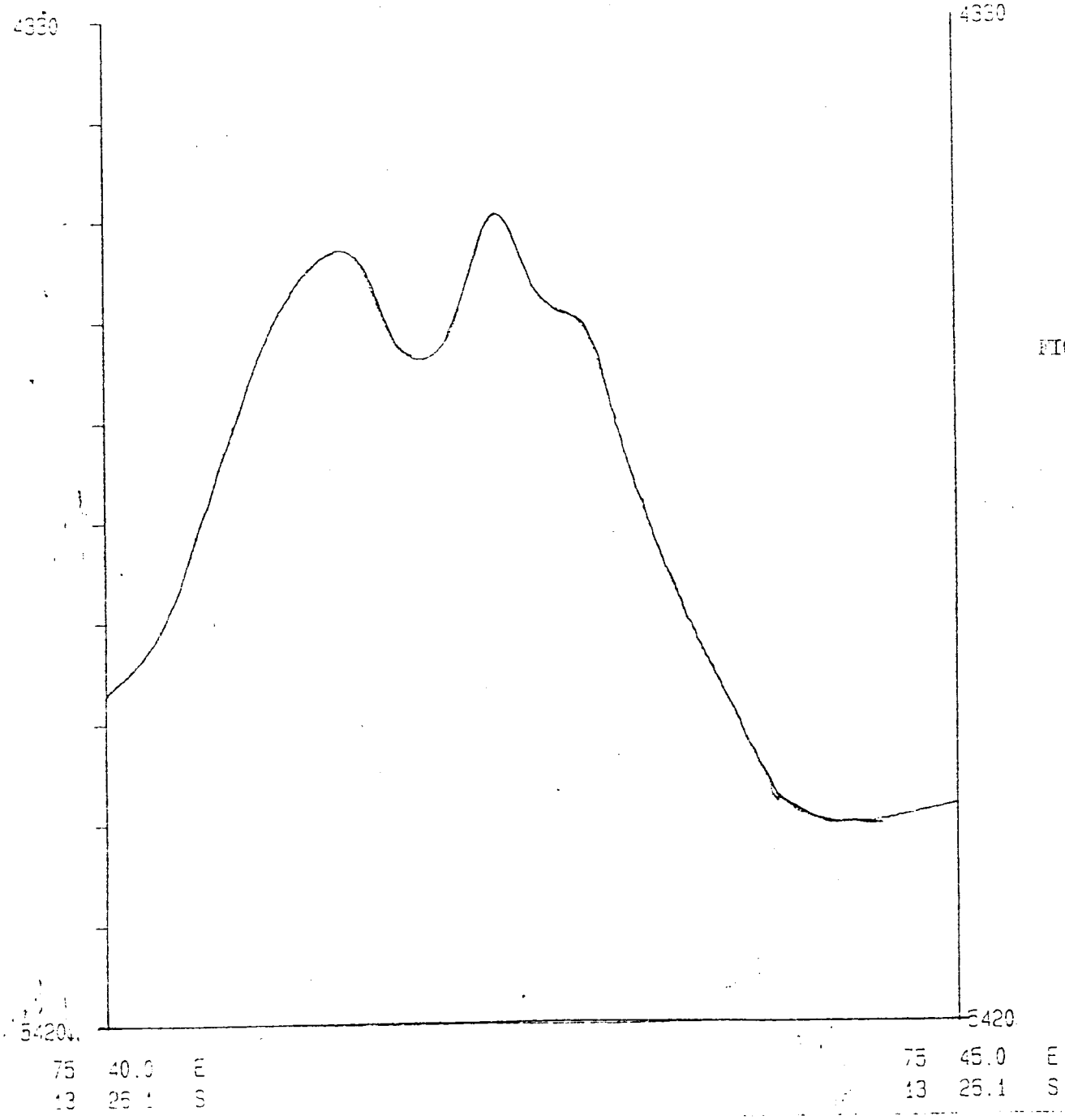

FIG. 4.12 CROSS SECTIONM PROFILE
ACROSS CRATERED TOP OF SEAMOUNT
CHAIN C. . V.E= 1:10.

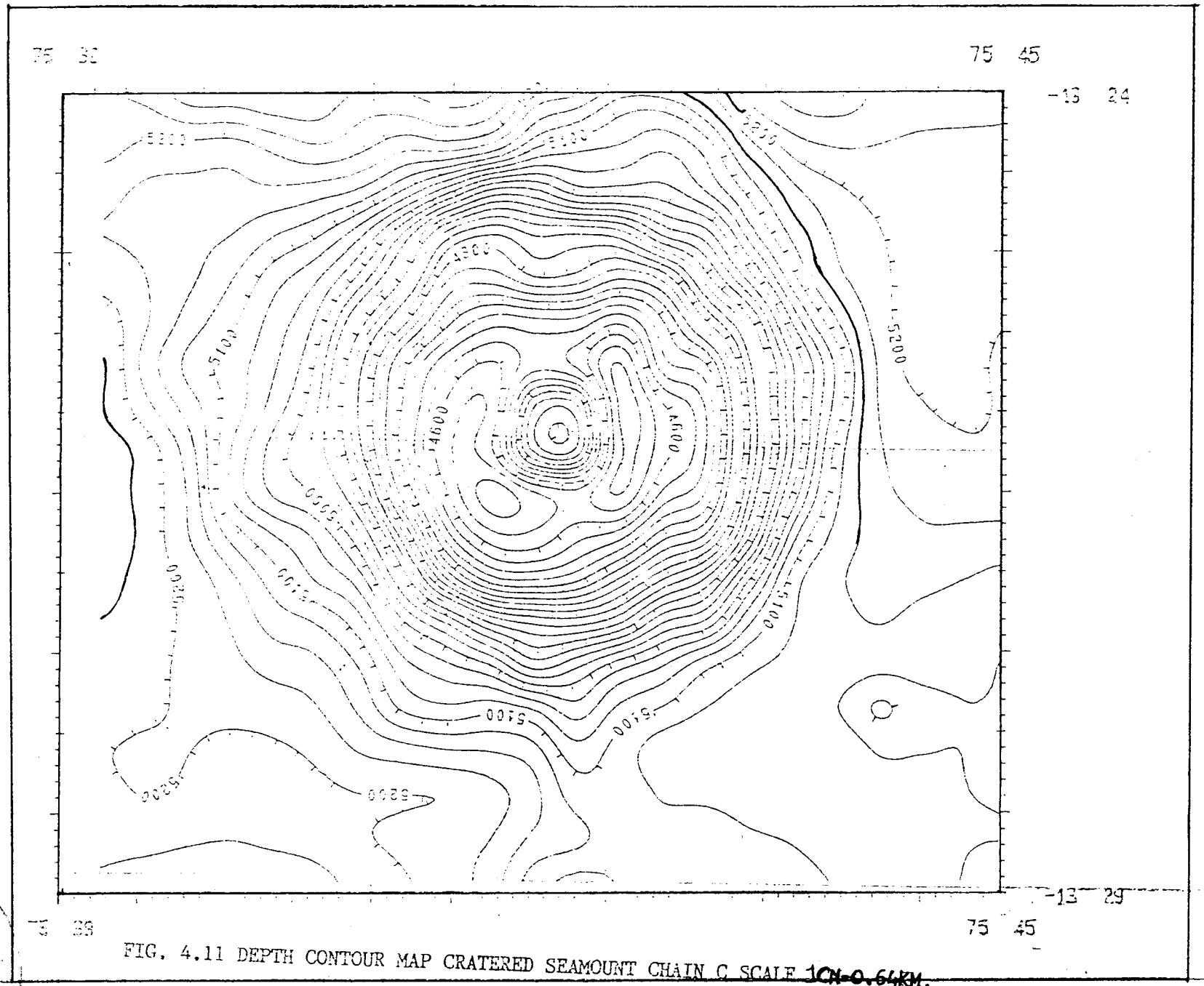

FIG. 4.11 DEPTH CONTOUR MAP CRATERED SEAMOUNT CHAIN C SCALE 1CM=0.64KM.

(r=0.76), but with height the inverse relation is insignificant here (r=0.4 only). Also, in this chain, one of the features has a cratered top. (S.No. 5, table 4.6, chain C). This occupied a smaller area(25 sq. km) and has a height of 650 m. Fig. 4.11 shows the depth contour map and fig.4.12, the E-W cross section across it's top. The depth of the crater is less, about 100 m only and which is about 0.8 km long. There is also a step like feature on the eastern flank. Cratered top represents the volcanic nature of the chains. Any geological process that involves effusion of materials from beneath the earth surface via some sort of vertical pipe of vent usually develops a cone, collar or ring of deposits around the exist, forming a crater.

4.5.3 Discussion:

Correlation matrix for 22 features involving all 3 chains A, B and C is presented in table 4.7. It is concluded with this that, for seamount and abyssal hills in Central Indian Basin, the flatness ratio 'f' has strong correlation with summit width (r=0.85) and inverse relation with summit height (r=-0.61). Sigma has good positive correlation with H-W ratio (r=0.86) and negative correlation with basal width (-.69) and area (-.57). Summit

height shows good correlation with area and basal width (0.64,0.65 respectively).

Table 4.7

Correlation matrix for different morphological parameters Chain B and C (number of points= 22)

Depth	1.00								
Height	-.94	1.00							
Area	-.60	0.64	1.00						
Length	-.63	0.65	0.94	1.00					
W(base)	-.62	0.64	0.97	0.96	1.00				
W(summit)	.29	-.34	-.04	0.08	0.01	1.00			
H-W	-.19	0.20	-.47	-.53	-.57	-.46	1.00		
Sigma	0.05	-.08	-.57	-.61	-.69	-.01	0.86	1.00	
Flatness	0.53	-.61	-.42	-.36	-.44	0.85	-.10	0.41	1.00
	Depth	Height	Area	Length	W(base)	W(sum)	H-W	Sigma	Flatness

Summit width to basal width correlation observed by **Mukhopadhyay and Khadge (1990)** is not seen here at all. Instead, 'f' and height are strongly inversely correlated here in contrast to poor positive correlation observed by them. However, their observations were based on single beam echosounding data.

The Central Indian Basin (CIB) is the result of seafloor spreading of Mid-Indian Ridge and the South East Indian Ridge (SEIR). The northward movement of the Indian Plate was set into motion by these two ridges at different velocities during the geological history. The age of the

crust in the present study area is lower Tertiary **(Patriat and Segoufin, 1988)**. The multibeam studies have shown that the seamount and abyssal hills in CIB not only occur as chains but also as localized isolated features. Morphologically, wide range is observed among the features ranging from pointed cones to flat topped seamounts. The seamounts north of 10^0S **(Mukhopadhyay and Khadge, 1990)** are larger and have more height compared to the seamounts in CIB studied here. The oceanic crust north of 10^0S is older (of Cretaceous age). According to **Morov (1966)**, the seamount heights are directly related to age of the lithosphere, area south of 10^0S being younger, seamounts are of less height. Seamounts especially, those occurring in chains are genetically related to existence of the fracture zone.

Sediment cover on the seamounts and abyssal hills of three chains is less. This observation is based on single beam echosounding records. On the top of the seamounts, the sediment cover is nil while gradually it increases on the flanks (<10 cm) and more than 10 cm at deep abyssal plains. Massive rock exposures are observed at the summits and slight exposure on the flanks **(based on photographic evidence, Iyer and Sharma, 1990)**. Numerous rock pieces, encrustations and pumices have been recovered from different sampling operations (dredging and free fall

grabs) carried out on the seamounts. Two principal rock types found are pumice and basalts. Basalts dredged are both fresh and weathered in some cases. 1-2 mm coating of ferromanganese is occasionally present. Mineral phases of these basalts are predominantly Plagioclase, olivine, rarely pyroxene (augite) and opaques **(Iyer and Sharma, 1990)**. Pumice samples show different shapes, sizes and vesicularity. Some of the pumices and broken rock fragments act as nuclei for the manganese nodules. Basalts are products of volcanism represent by seamount and abyssal hills here. The earlier eruption basalts have been weathered where as the newer eruption basalts are fresh. **Iyer and Karisiddiah (1989)** suggest that uprising magma was basic and highly fluid in nature ad underwent changes in it's composition due to varying pressure-temperature conditions. This has formed basalts dominant with plagioclase and olivine with less vesicles. Even for the pumice, submarine volcanoes are the source.

Geographically, chain A is located west of the 79^0 fracture zone and chain B and C near the $75^045'$ E fracture zone. In fact, B and C are on either side of the $75^045'$E fracture zone, though on the bathymetric map, no clear bathymetric trace of fracture zone exists. All these features might have formed by interaction of Reunion hotspot or Prince Edward hotspot with South East Indian

ridge (SEIR) and Central Indian Ridge (CIR). Prince Edward hotspot has most probably moved to it's present position from a original north easterly position in geological past **(Molnar and Stock, 1987)**. It is possible that fracture zone provided easy conduits for volcanoes **(Batiza, 1982)**. Although presence of fracture zone is not necessary for existence of a seamount in non ridge areas, there must be local zones of weakness to control location of majority of seamounts **(Epp and Smoot, 1989)**. Under normal spreading situation on the ridge, ridge system may have enough pressure to only lift magma to the top of the crust. An injection of plume material overpressurises plumbing system. Some of the excess pressure is released by formation of seamounts and some may be by formation of thick crust. **Epp and Smoot (1989)** based on studies on North Atlantic seamounts suggest that the excess pressure along the ridge system varied with distance and time. However, it is not clear how these variations are reflected in distribution of seamounts. Anyway, ridge system do not have steady state magma chamber. It is likely that small, discontinuous, transient magma chambers may be more likely on the slow spreading ridges (like SEIR and CIR). Factors such as volume of plume material, conduit geometry, location and offset of fracture zones, timing of plate

reorganizations and hotspot interaction will be responsible for seamount distribution and their varying morphology.

In conclusion, it can be stated that seamounts in CIB are comparatively less in number than in Pacific and Atlantic Oceans. They are also smaller in size and height. Wide range of shapes like sharp pointed cones to flat top mounts are present. Features like caldera and double peak, craters etc. are also noticed. Presence of seamounts in chains near the fracture zones is observed, especially south of the CIB. In the north (from 10^0 to $12^030'S$), the seamounts and abyssal hill are less concentrated. However, complete Multibeam surveys in CIB will throw more light on distribution and morphology of seamounts.

Chapter 5
Morphometric studies on a part of Central Indian Basin

5.1 Introduction

Modern geomorphologist relies heavily on the deductions based on measurements of landforms. Morphometry, the study of geometry of landscapes is an integral part of land gemorphology and can be effectively used for the marine data set also. Hypsometry (area-altitude relations), elevation- relief ratio, ruggedness factor and above all the slope angle studies are some of the aspects covered under morphometry.

Study of slopes and surface processes has been an important unit of geomorphological studies since the Second World War. Just as in the case of land surface, the deep sea floor is also punctuated by numerous hills and valleys etc. Infact, the abyssal hills are the largest physiographic units under the sea **(Rona et al. 1974)**. Slopes provide a basis on which by successive combination into larger units, general geomorphology of an area can be constructed. Quantifying and representing the seafloor ruggedness is a tougher task compared to that of land because of the inability to observe the processes involved and the topography first hand **(Leply, 1966)**. Study of morphometry of ocean floor is also important from economic point of view. It is essential to evaluate methods and to

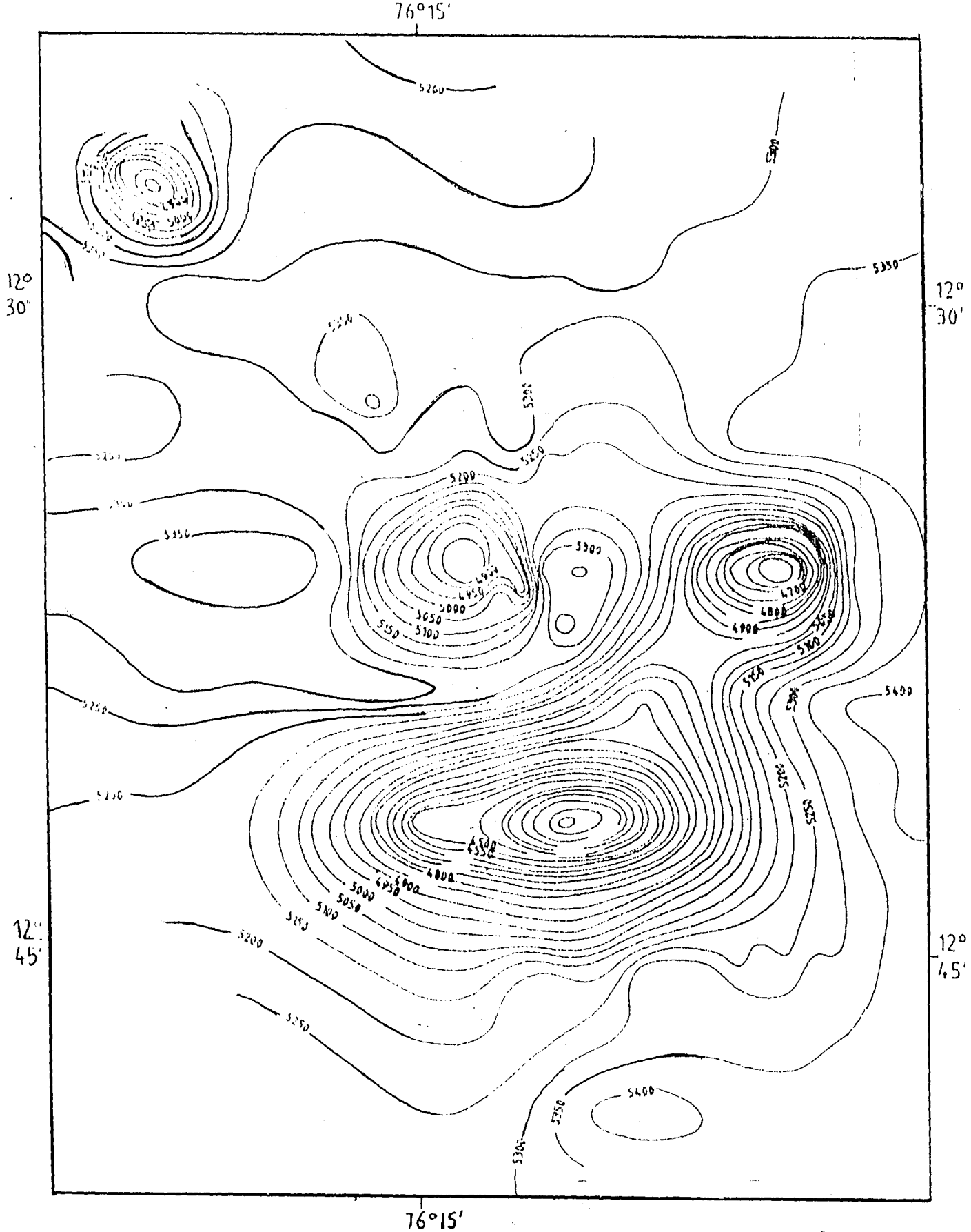

FIG. 4.1 DEPTH CONTOUR MAP OF UNCHARTED SEAMOUNT FROM ECHOSOUNDING DATA
SCALE 1 CM= 2.23 KM.

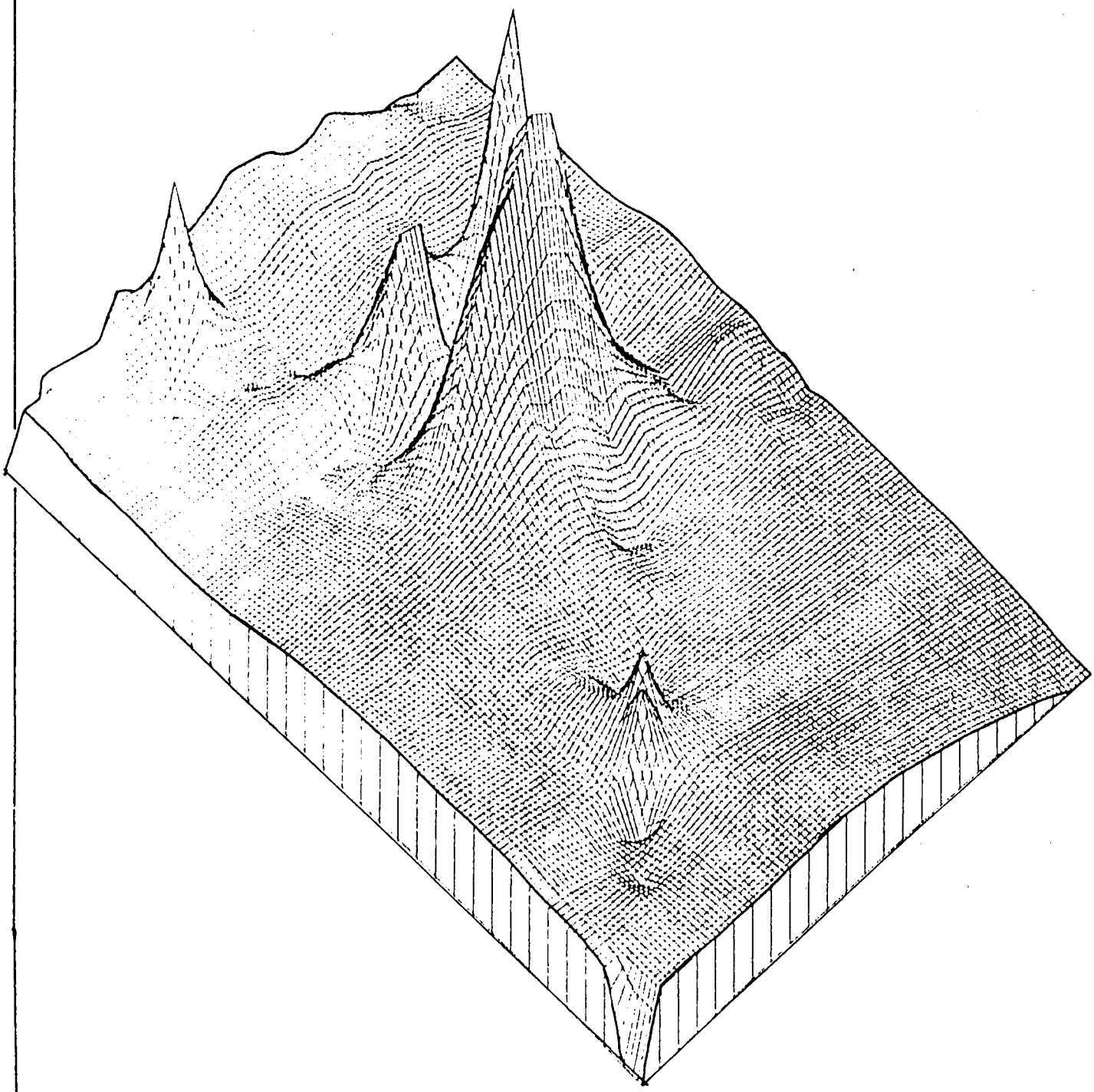

FIG. 4.2 ISOMETRIC VIEW OF THE SEAMOUNT.

analyse costs for exploitation of marine manganese deposits. Sea bed relief is an indicator of the underlayers and the conditions in which the soft superficial sediments have accumulated. Bottom relief will have very strong influence on movement and distribution of water masses and also on sediment transport, turbidity and chemical activity. Roughness of the bottom influences the flow at the boundary layer **(Paola, 1985)** which in turn influences the genesis of manganese nodules in the deep sea. Topographic configuration of ocean-floor plays an important role in many aspects of ocean dynamics **(Bell 1975)**. Quantitative study of depth data is essential as the particle size and sediment thickness is largely influenced by steepness. A study of slope angles and elevation-relief ratio can be used to characterise geomorphic provinces **(Agopova 1965)**. Surfaces with same slopes possess certain features in common in relation to relief-forming processes. Hence, it is essential that slope angle, morphometric and related studies are performed on deep sea floor data.

Morphometric studies carried out on a part of Central Indian Basin (CIB) using the single beam echosounding data is described here. For the multibeam swath bathymetric data, a technique has been developed to convert the depth grid into slope angle values grid. The technique with

results on three seamount areas in CIB has also been presented.

5.2 Morphometric studies using single beam echosounding data:

Area and methods:

Morphometric studies are carried out in area between longitude 75^0 E to 76^0 E and latitude 12^0 15′ S and $13^0$15′ S. (60 X 60 nautical miles, area 12,363 sq. km). Echosounding data collected along latitude wise tracks from different cruises conducted as part of project 'Surveys for Polymetallic Nodules' are used here. The Raytheon deep sea echosounder was used for echosounding and the Magnavox dual channel satellite navigator for the position fixing (details in Chapter.2). Echosounding records were digitised manually. These digitised values were used for preparation of bathymetric profiles (Fig. 5.1), depth contour maps (Fig.5.2) and slope angle map (Fig. 5.3). Bathymetric profiles which provide general information regarding the topography of the area are drawn along east-west tracks of survey lines with a vertical exaggeration of 1:27.5. A contour map was also prepared using manually digitised depth values. A computer programme was written and run on NORSK DATA (ND520) computer to calculate the slope angles from the depth values and a slope angle map is also presented.

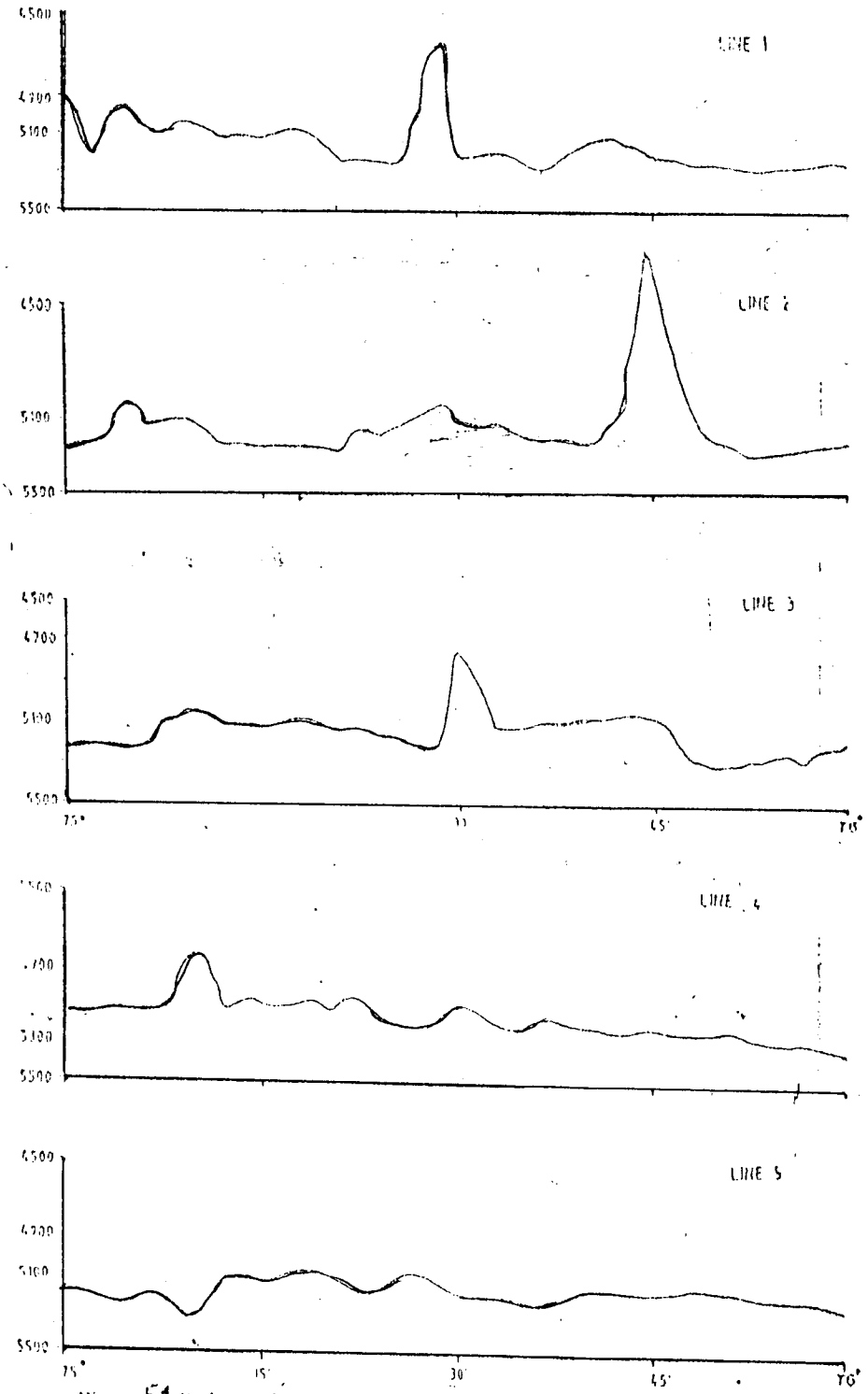

Figure 5.1 Bathymetric profile Lines 1, 2, 3, 4 and 5 (Vertical exaggeration 27.7).

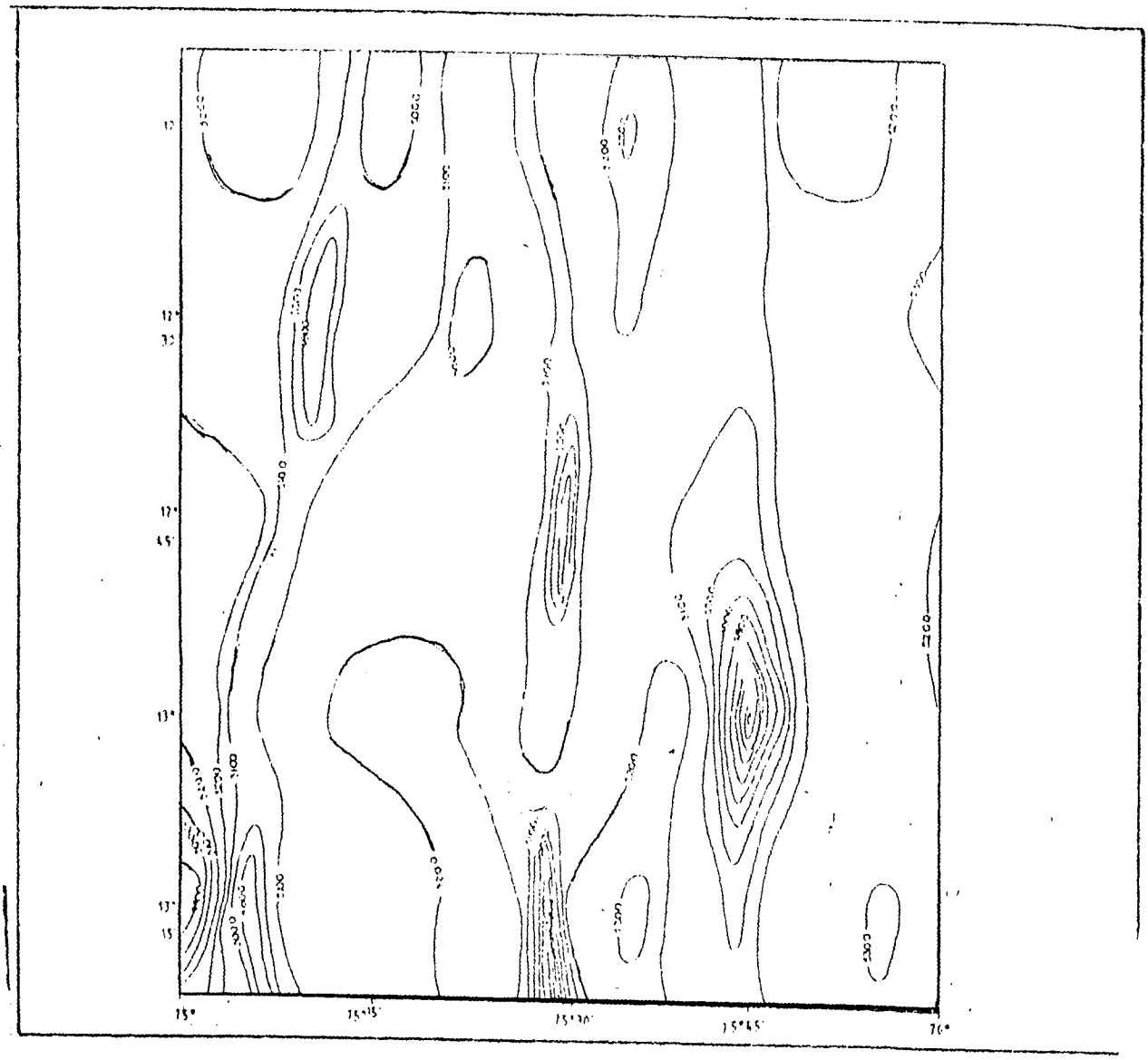

FIG. 5.2 DEPTH CONTOUR MAP OF THE AREA. SCALE 1 CM= 9.65 KM.

Results and Discussion:

Most prominent geomorphic feature encountered in the area is the seamount along 13^0 latitude (fig. 5.1, line 2). This seamount has a height of over 1000 m and has a basal width of 12 km. Extension of this feature is seen in profile along 13^0 15′ S also (Fig.5.1, line 1). Two abyssal hills are also observed in this area, one in line 1 and extending in lines 2 and 3 and having a height of 550-600 m. Another prominent hill of 250- 300 m height is seen in lines 1-4 (figure 5.1) at and around 75^0 04′ E. A valley 350m deep is observed at 75^o 1′ E in line 1.

Along lines 1, 2 and 3, which form the southern portion of the study area, seafloor is rougher whereas the northern portion (lines 4 and 5) is comparatively plain.

Slope Angles:

Slope angle map (fig.5.3) drawn using the slope angles calculated from the digitised depth values shows the prominence of gentler slopes (0-3 degrees). However, steeper slopes are concentrated in some patches. These areas of high slope angles correspond to the hilly regions as seen from the contour map (Fig. 5.2) and bathymetric profiles (Fig.5.1). Contours of slope angles 1, 3, 5 and 7 are closely spaced around 75^0 30′ and 75^0 0′ to 75^0 10′

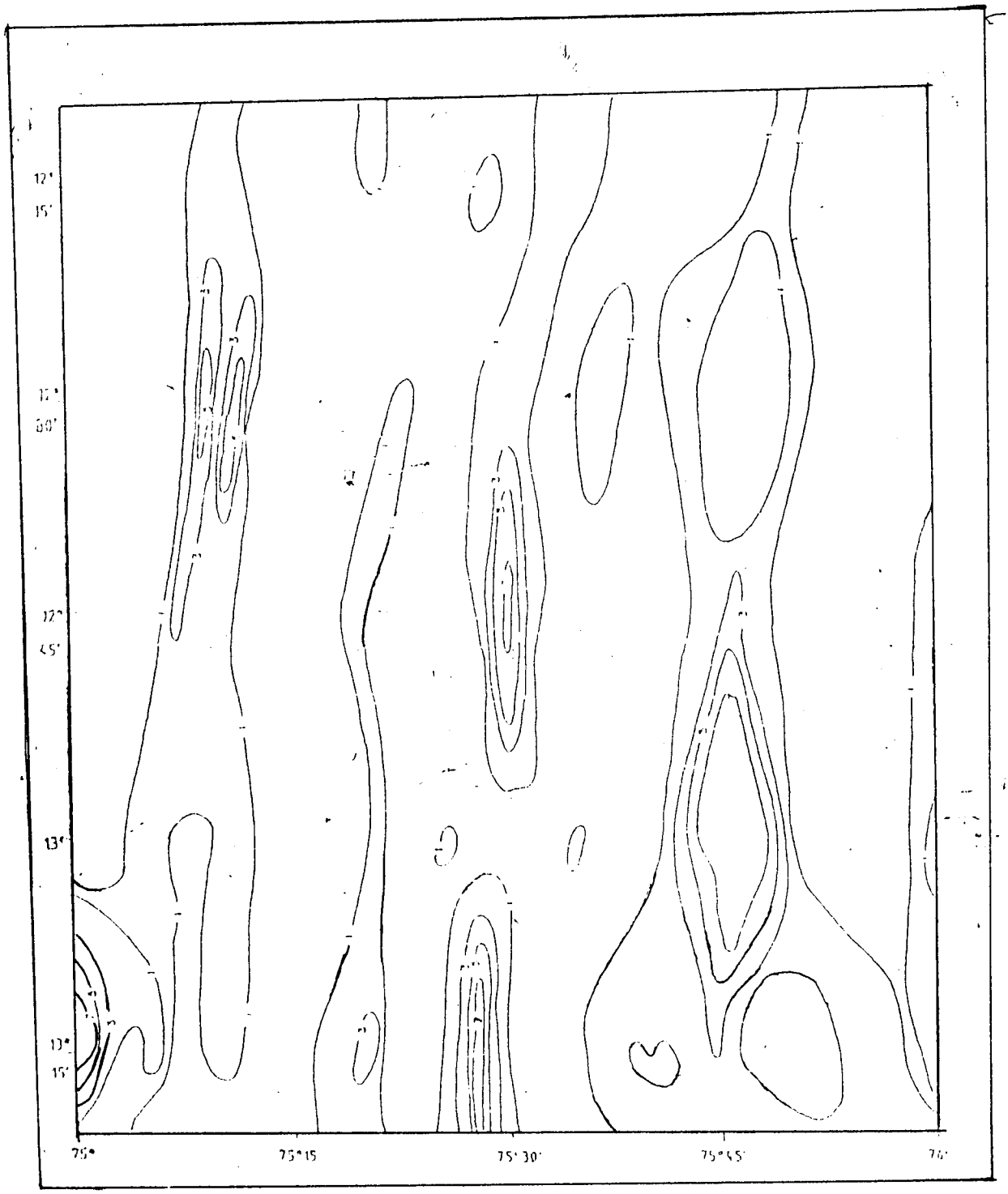

FIG. 5.3 SLOPE ANGLE MAP OF THE AREA. SCALE 1CM= 7.76 KM.

longitudes. The trend of closely spaced contours is almost north- south.

Along each line, slope angle values were calculated at intervals of 1.8 km. Of the 304 angles computed, 199 angle frequencies fall within the range of 0-1 degree (66.5% of the total). The frequency for steep angles is less in all the lines (5% for the entire area). The steep slopes are more rapidly altered than gentle slopes and hence the survival time for the gentle slopes is more **(Young 1972, p-167)**. Young's hypothesis for slope angle frequency as applicable to the terrestrial landforms was tested for the slope values calculated for the deep sea floor of Central Indian Basin. Young's hypothesis states that the angle frequency shows an approximately log-normal distribution irrespective of whether landscape is formed predominantly of steeper slopes or gentle slopes. Log-normal graph of angle frequency Vs slope angle ranges plotted for the entire area shows a linear regression between the two. The equation obtained for the regression line is

$$\log y = 2.44 - 0.1375\, x$$

where y= frequency of angles and x= slope angle ranges. The coefficient of correlation between the two variables is -.937.

The average slope in the whole area is 1.3056 degree, maximum being 15^0 observed in line 2. Average depth is 5116 m. Table 5.1 shows the line-wise break up of average slopes, standard deviation of slope angles and their skewness. It is observed that the standard deviation is more in lines 1, 2 and 3 and less in lines 4 and 5.

Table 5.1

Mean slope angle, standard deviation and skewness of slope angles for lines 1-5 and the whole area.

Line No.	Average slope (^{0})	Standard Deviation	Skewness
1	1.82	3.05	34.44
2	1.88	2.90	21.31
3	1.13	2.08	15.19
4	0.90	1.27	5.75
5	0.82	0.62	0.52
whole area	1.31	2.22	20.30

Table 5.2

Area enclosed in percent by different angle ranges

Slope angle range (^{0})	area enclosed in percent	cumulative % area enclosed
0-1	72.2	72.2
1-3	19.6	91.8
3-5	6.25	97.05
5-7	1.9	98.95
over 7	1.05	99.99

Table 5.2 shows the area enclosed in percent by different angle ranges. It is seen that 72.2% of the area has $0\text{-}1^0$ slope angles and 19.6 % area has 1-3 degree. Thus, 91.8% of area has angles in the range of $0\text{-}3^0$ and the rest 8.2% of the area has angles higher than 3^0. Gentler slopes predominate distinctly over steeper slopes.

Elevation-relief ratio and ruggedness.

Elevation relief ratio is one of the measures of seafloor ruggedness. It is often used as a substitute for tedious and time consuming hypsometric analysis of geomorphic data **(Pike and Wilson, 1971)**. Elevation-relief ratio is calculated by the formula:

$$E = \frac{\text{Mean Elevation-minimum elevation}}{\text{Maximum elevation-minimum elevation}}$$

Table 5.3 gives average depth, minimum and maximum depth and elevation-relief ratio for each of the 5 lines and for the entire area. Line 2 is quite rugged and has very high E of 0.82. E for line 5 is the least (.199). High E characterises broad, somewhat level surfaces occasionally broken by depressions and highs and low E indicates terrains with isolated relief features standing above extensive level surfaces. The elevation relief ratio

for the whole area is 0.788 which means the area has generally a fair number of depressions and highs.

Table 5.3

Mean, minimum and maximum depth and elevation-relief ratios, amplitude, REL, and ruggedness for five lines and whole area.

Line No.	Average Depth (m)	Minimum Depth (m)	Maximum Depth (m)	Elevation -relief ratio(E)	Maximum -Minimum (amp)	Rel sum of depth diff.	Rugged-ness (Rel-amp)
1	5121.1	4650	5350	0.67	700	3320	2620
2	5101.6	4245	5290	0.82	1045	3414	2369
3	5116.4	4730	5305	0.67	575	2145	1570
4	5103.3	4820	5320	0.58	510	1714	1204
5	5137.7	5085	5350	0.20	350	1575	1225
whole area	5116.0	4245	5350	0.79	636	2237	1601

The concept of ruggedness and REL (sum of depth differences along a profile) have recently emerged as factors for morphometric analyses of sea bed data (Froidefond and Berthosis, 1984).

REL is the sum of differences in elevation between different points on a line segment and ruggedness is the difference between REL and maximum amplitude for the segment. Table 5.3 gives REL, amplitude and ruggedness for different lines and the averages. Lines 1 and 2 have high value of ruggedness of 2620 and 2369. Though it was observed that line 2 has the highest elevation relief ratio (0.82), line 1 shows higher ruggedness. Lines 4 and 5 have less ruggedness values and the average ruggedness for the entire area is 1601.6. From the elevation- relief ratio, ruggedness and slope angle data it is confirmed that the southern portion of the study area is rougher compared to the northern portion.

Presence of a seamount and abyssal in the southern part make the area quite complex structurally. **Menard (1967)** suggested the high relief indicates slow spreading. Along 75^0 45′ presence of a fracture zone is suspected **(Kamesh Raju and Ramprasad, 1990)**. Motion can be non uniform across fracture zones in ocean basin and strike slip motion may occur along fractures. The differential movement in the crustal segments is taken up in the stress field of the fracture zones **(Andrews 1971)**. Secondary topographic features can result from these motions. Varying relief can also result from varying spreading rates. Segments of crust bounded by fracture zones (as in the

present area) may interact with each other because of varying and differential spreading rates and may, in turn, give rise to secondary topographic features.

Morphometric studies from single beam echosounding data on a part of Central Indian Basin show a varied seafloor consisting of abyssal hills, a prominent seamount and a valley. Structurally the area is quite complex. Geomorphic features have a nearly north-south trend. Though the average slope angle for the study area is 1.305, in patches, very high slope angles of over 15 degrees are noted. Dominance of gentler slopes (0-3 degrees making over 92% of total area) suggests a higher survival time for gentle slopes. The hypothesis of log-normal distribution of slope angles and their frequency of occurrence over the land areas is also found to be applicable for deep seafloor data. From elevation-relief ratio and ruggedness data, it is concluded that high E and high ruggedness corresponds to higher slope angles. Such studies have not been carried out extensively in world oceans and it is not possible to generalise based on this limited data. For that purpose, similar type of studies are essential in different provinces of World Oceans. Closer grid surveys and multibeam swath bathymetric surveys will elucidate topographic variations which could not be identified from the single beam

echosounding data. Especially for the slope angle studies, the multibeam data with full coverage of the seabed will be more precise and accurate. A technique has been developed for creating slope angle grid from the depth grid of the multibeam data which is described in the following paragraphs.

5.3 Slope angle studies using Multibeam swath bathymetric data.

Slope angle studies on seafloor data have evoked considerable interest in the last decade **(Smith and Shaw, 1989 and Kodagali, 1989a)**. Slope angle maps along with accurate depth contour map are essential for deep sea mining geologist to evaluate the resources and to eliminate unfavorable areas for mining. The path of the mine head has to be predetermined for which a detailed bathymetric and slope angle map of the area is a prerequisite. A technique has been developed for generating slope angle grid from the Multi beam sonar data.

5.3.1 Slope angle grid generation.

With the advent of multibeam system, the quality and the coverage of seafloor area have increased many fold. To generate a depth contour map from multibeam sonar data, the data from different survey lines is merged and a combined

grid of depth values is generated. All the depth values falling within the grid are added and arithmetic mean for the cell is calculated. The grid is assigned the depth value equal to this mean. If, there are no depth values existing within the cell, the value is interpolated or extrapolated using the surrounding values, thus creating a grid with one depth value for each grid cell. The technique developed for creating a slope angle grid from the depth values grid from HYDROSWEEP system. The slope angle grid generated from this program can be used for preparing a slope angle map of area or slope profile across the area. The program is developed on EPR 1300 computer but with necessary modifications, it can be used on any computer. The program can also be adopted for land altitude data to create slope angle grids **(Young 1972)**.

Input data:

The program uses two binary files as input files. File I is the grid parameter file which contains information as follows : (i) Latitude and longitude of lower left corner of the depth grid (in degrees), number of grid cells and grid cell size in seconds in first record and (ii) latitude and longitude of the upper right corner of the depth grid, cell width (in meters), lower left corner in degree and minutes- all as integers in second record.

Input file II is the grid depth values matrix file and it contains 128 depth values (real, in meters) per record . Matrix starts with first value of lower left corner continues in rows from west to east and south to north. The last record may not be filled completely.

Converting depth grid into slope angle values grid:

The grid parameter file is read to get the data on number of grid cells as grid points on x-axis, y-axis as well as and distance between them as well as distance between them in meters. Grid data file (input file II) is read to get the depth values. The depth values are stored in a matrix as integer values. Now for each cell starting from the south-west corner of the grid to the north-eastern corner, eight slope angles are calculated with respect to the depths in eight directions (four sides and four diagonals for cell IDE (4,4) as in Fig.5.4). However, for cells on the edges of the grid, angles are calculated only for sides and diagonals where the depth values are available. For example, for cell IDE (1,1) (Fig.5.4) angles are calculated for only three sides.

Each angle is computed as follows:

$$v1=(dep1-dep2)/d \qquad \ldots\ldots(1)$$

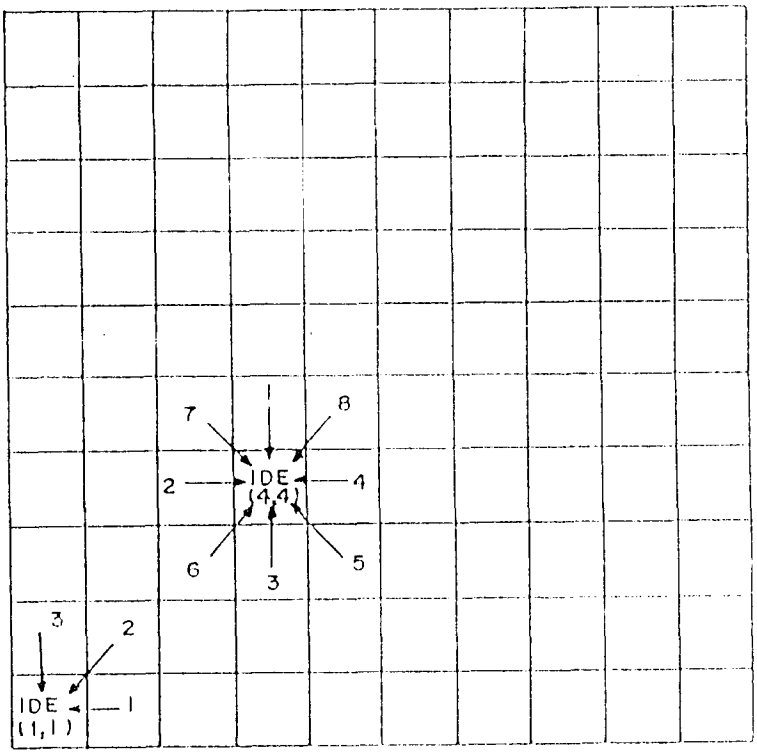

Fig. 5.4 Grid showing no. of angle values calculated – 8 for central cells and 3 for S-W. corner cell.

dep1-dep2 is the absolute difference in depth at two points,and d is the distance between them. For values on the sides, d is equal to grid distance while for diagonal values,

d= sqrt (2 X grid distance2)**

v1 in eqn. (1) is the tangent of slope angle. It is converted in to slope angle in degrees as follows.

angle= arctan(v1)X 180.0 X .3183 .....(2)

Each grid cell is now assigned an angle value equal to the mean of eight angles calculated for that cell (less than eight in case of cells on the wall of the grid) from eqn.. 2.

$$V_{ave} = \frac{\text{sum of theta}}{\text{No.of values per cell}} \quad \text{.....(3)}$$

in Eqn (3), V_{ave} is the average angle for the cell and sum of theta is the sum of angle values calculated for the grid cell.

All individual depth grid cells are thus converted to slope angle grid cells. These angles are stored in a binary output file- 128 values (real) in each record. A grid file of slope angle values is thus generated which can be used to create a slope angle map. This method of conversion of grid depths to grid slope angles is advantageous over the

method of calculating angles from individual survey lines. Here, the depth differences on all sides of a grid cell are considered and average angle for the grid cell is calculated which minimizes the ambiguity.

Results

Seamounts are the main physiographic features beneath the sea. Study of the seamounts in basinal areas where manganese nodule reserves are present is essential. Seamounts are suppliers of nodule nuclei **(Horn et al., 1973)**. Considerable areas around seamounts have very high abundance of nodules, but lesser elemental concentration **(Kodagali 1988)**. In spite of higher nodule abundances around them, they can be hazardous to future mining operations. Similarly. occurrence of manganese nodules of commercial interest is always associated with abyssal hills **(Frazer and Fisk 1981, Pattan and Kodagali, 1988)**.

Slope angle data generated from the above procedure using the MBS data on three seamount areas in CIB is described in the following paragraphs.

5.3.2 Slope angle studies- Seamount area I.

As seen from the depth contour map of the area (Fig. 4.5, chapter 3), there are three positive features in this area. Seamount at 12^0 35′ S and 76^0 18′ E has the height of

1350 m (depth at the top- 3950 m) with maximum basal width of 22.2 kms. Total area occupied by this seamount is about 330 sq. km. The shape and slope angle statistics of this large feature is tabulated in table 5.4. There are two abyssal hills north of this seamount which are comparatively small in size. The eastern abyssal hill appears as an extension of the seamount and has basal width of 11 km and height 850 m. Both the seamount and the eastern abyssal hill have gentler and lengthier western flank and short and steep eastern flank. Western abyssal hill has gentler flanks and is much smaller with basal width being 8 km and height about 500 m. Detailed morphology of this seamount area is described in chapter 3.

Slope angle map of this seamount area is given in Fig 4.8, chapter 3. Maximum slope angle is 38^0 (on the tallest feature). Average slope angle for this feature is 10.5^0 whereas for the two abyssal hills it is slightly higher- 13.5^0.

5.3.3 Slope angle studies- Seamount area II

Figure 5.5 shows the depth contour map of this area which has a tall abyssal hill. In this area also, there are three features. Southern feature at 73^0 32.5'E and 9^0 46' S is the largest of the three. It has a height of 800 m with

FIG. 5.5 DEPTH CONTOUR MAP OF SEAMOUNT AREA II.

Contour Interval 25m.

FIG. 5.6 SLOPE ANGLE MAP SEAMOUNT AREA II

CONTOUR INT. 5°

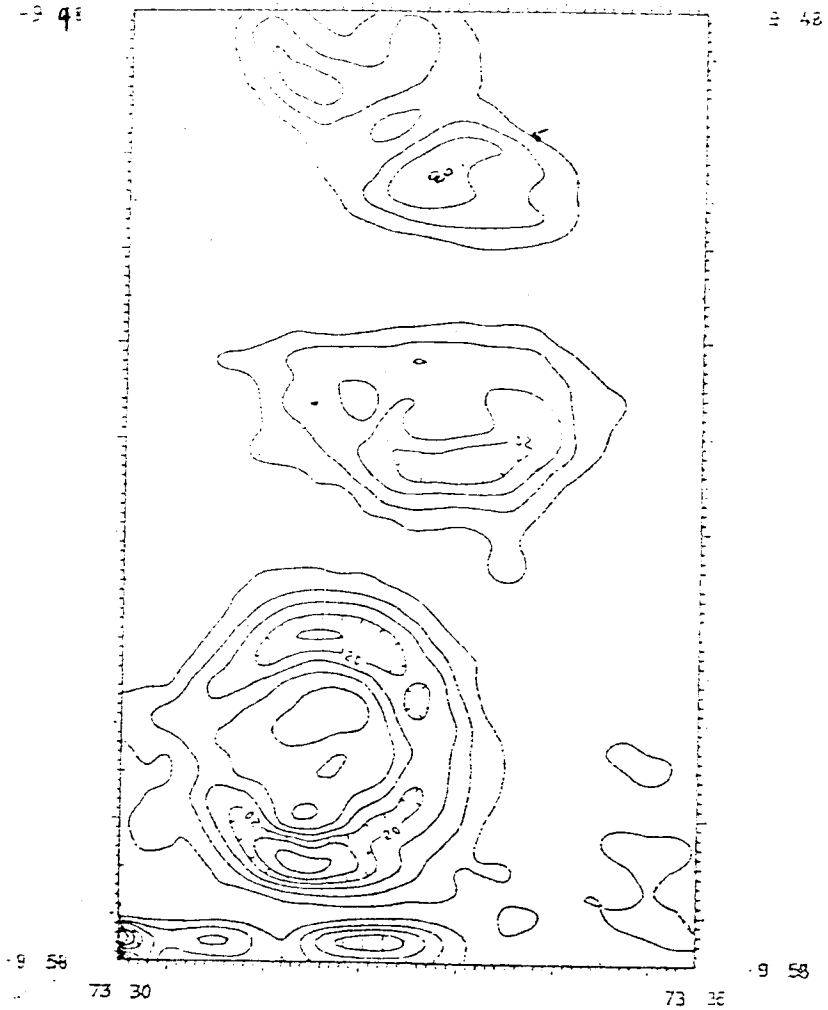

depth at the top being 4210 m. Area of this is about 40 sq. km. (Table 5.4). Other two features are comparatively small (Heights 500 m and 650 m) with basal widths being equal to the bigger feature.

Table 5.4
Depth, basal width, area and slope angle data of highest features in the three seamount areas.

Seamount area	Center position	Depth max. (m)	Depth min. (m)	Basal width (Km)	Area (Sq. Km)	Slope max (Degrees)	Slope mean (Degrees)
I	12^0 35′ S 76^0 16′ E	5100	3950	22.2	330	38	10
II	09^0 46′ S 72^0 32′ E	5150	4210	6	40	33	8
III	14^0 05′ S 79^0 19′ E	5100	3850	11	85	38	14

The slope angle map of this area (Fig. 5.6) shows that the highest angles are occurring at the tallest feature. Maximum angle for the Seamount is 33^0 where as for the two smaller features, the angles are in the range $5\text{-}21^0$. Slope angles surrounding the positive features is in the range of $0\text{-}4^0$.

FIG. 5.7 DEPTH CONTOUR MAP SEAMOUNT AREA III.

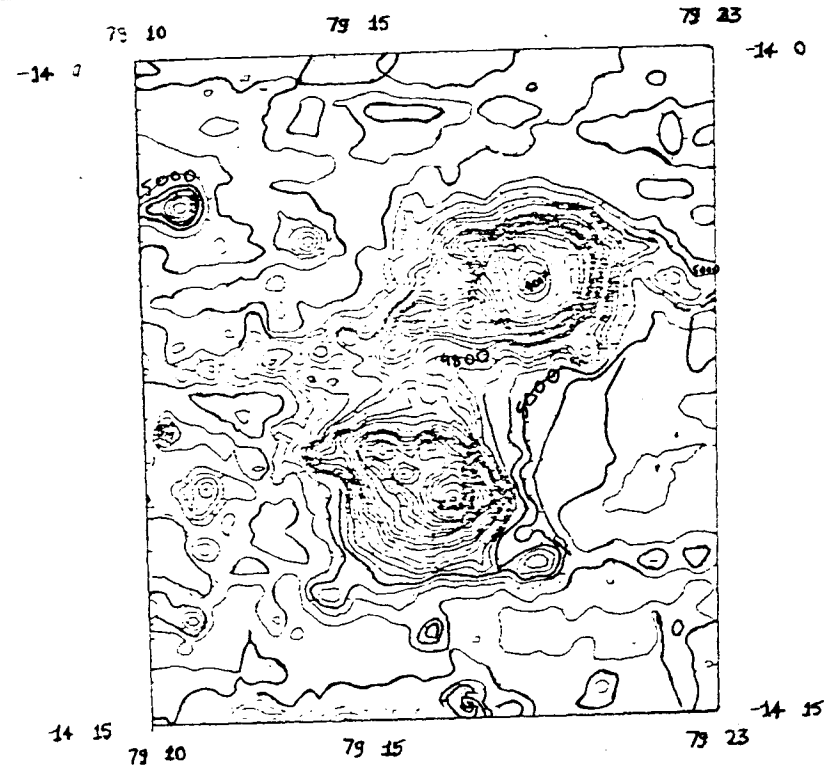

FIG. 5.8 SLOPE ANGLE MAP SEAMOUNT AREA III.

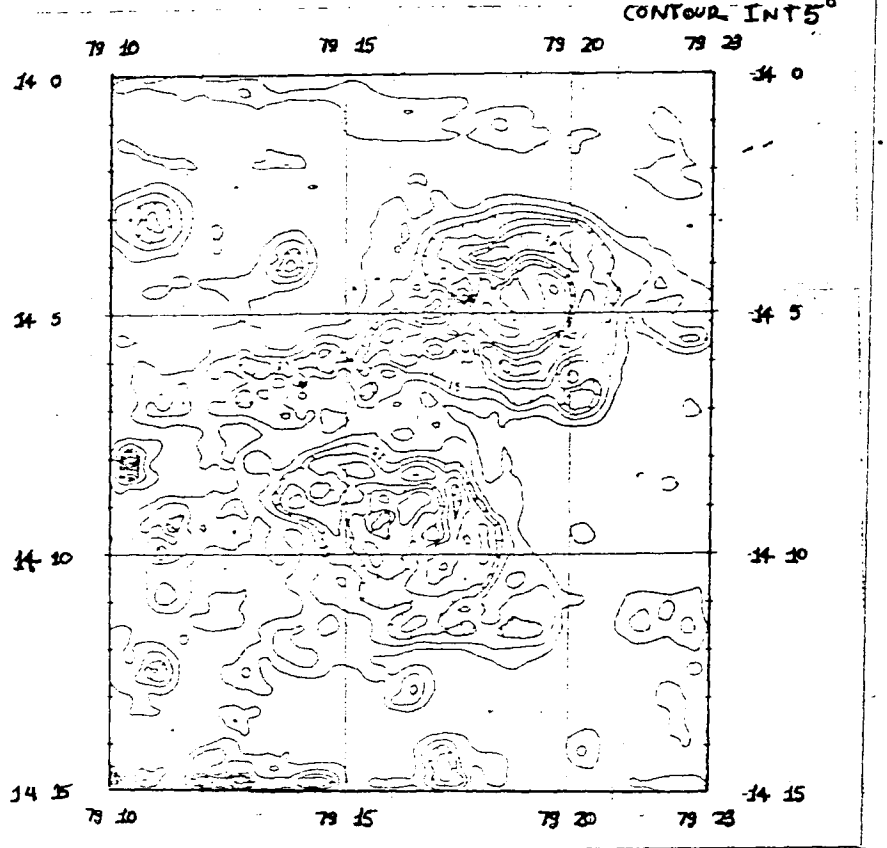

5.3.4 Slope angle studies: Seamount area III.

There are two seamounts in this area as seen in the depth contour map (Fig. 5.7). The average depth is about 5100 m. One seamount (center 79^0 16.5′ E, 14^0 10 S) has a basal extension of 11 kms and height of 1150 m depth at top being 3900 m (Table 5.4). Other seamount is situated north east of the first and has basal width of 11.5 kms and height of 1100 m. (79^0 19.5′ E and 14^0 05′ S) depth at the top of this feature is 3850 m. Area covered by the two seamounts is 76 and 85 sq km respectively. As seen from the depth contour map, the western sides of the two features are gentler while the eastern flanks are steeper.

Slope angle of this area (Fig. 5.8) indicates that the slope angles are higher on both these features. The maximum slope angle observed is 38.5^0, average being 14^0. Though the angles are higher at the seamounts, the area around seamount have slightly lower angles- in the range of $0\text{-}8^0$.

5.3.5 Discussion:

In all the three seamount areas, it is observed that the slope angle contours follow the trend of depth contour lines. Average slope angle for the seamount areas I, II and III is 10.5^0. Slope angle peaks correspond to the depth

peaks in all areas. Also, it is seen that the taller features have higher angles exception being seamount area II where the two abyssal hills have slightly higher average angle compared to the bigger seamount.

Though large areas with high abundance and grade are recognised in the Pacific and Central Indian Basin, favorable seafloor is not common. For deep sea mining, the generally accepted seafloor is the deep sea plain without seamounts, crevices, abyssal hills or other obstacles. Difference of surface elevation should be a maximum of 150 m and slope inclination should be less than 10^0. Which makes imperative that some area cannot be mined because of the topographical constraints. In the seamount areas in the present study, the average slope angle is upwards of 10^0 for over 80% of the areas. Hence, it can be safely assumed that about 80% of the area around the seamounts will be unmineable. Slope angle studies like this will help in demarcating unmineable areas.

Chapter 6
Polymetallic nodule distribution in different topographic domains.

6.1 Introduction and background.

India, after being accorded the 'Pioneer Investor' status in 1981 has been actively engaged in exploration for polymetallic nodules in the Central Indian Basin. With over four lakh sq.km of area surveyed with free fall grab sampling and echosounding, The National Institute of Oceanography, Goa has one of the largest data sets as far as nodules are concerned to carry out studies relating to distribution of nodules in different topographic domains. Areas of high abundance (up to 20 kg/m^2) of nodules with up to 2.5% of Ni+Cu+Co are present in the Central Indian Basin (CIB). Polymetallic nodules which are distributed in all the world oceans have been studied for over two decades now, the factors responsible for their varying abundance, chemistry etc. are not yet fully understood. Interest in the economic potential of nodules has intensified efforts in discovering the factors that control their abundance and distribution. For assessment of economic feasibility of the manganese nodule deposits, it is necessary to study the variations in their distribution and chemical composition. **Mero (1965)** pointed out that the most important requirement for nodule occurrence is the low sedimentation rate- typical of deep sea plains.

Sedimentation rates in the abyssal regions is around 1-3 mm/1000 years. Other factor is the availability of nucleating material **(Horn et al., 1973)** which is in turn controlled by topographic variations. Bathymetry is also one important factor in governing the distribution of nodules and mine site demarcation. The study of bathymetry will also unveil the small-scale geological processes responsible for the varying abundance of manganese nodules. Considerable work has been carried out on establishing the relation between bathymetry and distribution of nodules in Pacific Ocean **(Margolis and Burns 1976, Craig 1979, Frazer and Fisk 1981; Moore and Heath, 1966; Usui et al,1987)**. In Pacific Ocean, results indicate nodules are abundant in areas of high relief like the Clarion-Clipperton zone. Maximum abundance is reported at the steepest slopes and local topographic highs, hilltops and slopes. Regarding grade, inverse relationship with abundance is established **(Menard and Frazer 1978)**. Abundance increases with depth and is high on periphery and flanks of abyssal hills and is low in troughs **(Peutot and Melguen, 1979)**. In Atlantic Ocean, higher abundance of nodule is reported on rugged topographic terrain and distribution is patchy **(Ewing et al., 1973)**.

The Indian ocean is the most complicated and least studied ocean in the world. A number of seismic and

aseismic ridges, volcanic seamounts, volcanic islands, hotspots, and basins have rendered this ocean complex in structure and tectonics. This ocean is the product of historical separation of the Gondwana land from Pangaea and subsequent spreading of seafloor. Geomorphology and morphometry of the CIB have been described in the previous pages (chapters 2, 3 and 5). Influence of this structural and geomorphological barriers on the distribution, abundance and composition of manganese nodules have been described by **Pattan and Kodagali (1988), Kodagali (1988), Mukhopadhyay and Nagendernath (1988), Iyer and Sharma (1990).** It was found that both regional and local topography have direct bearing on nodule abundance and composition. In areas of high relief, for example, nodules occur abundantly but with patchy distribution and are of low chemical potential.

Regionally the Central Indian Basin includes four types of bottom sediments. Siliceous clay sediment type occurs at the central portion and occupies major part of the basin. It is bordered on the south by pelagic clay, on the north by terrigenous clay and on the west by calcareous ooze. However, the present study area entirely falls within the siliceous clay sediment region. The average water depth is around 5200m. Nodule abundances and

distribution in different topographic domains is discussed in this chapter.

6.2 Material and methods.

Bathymetry, and nodule sampling data have been collected onboard different chartered vessels viz., MV Skandi Surveyor, MV Farnell, MV GA Reay, DSV Nand Rachit and research vessel ORV Sagarkanya. Echosounding data was collected by Raytheon echosounder at 12.5 KHz and 3.5 KHz frequency on the chartered vessels and by Honeywell Elac Narrow beam sounder and deep sea echosounder on ORV Sagarkanya. During the survey the recorder was adjusted, sometimes to 4 seconds sweep rate with 4 seconds delay to obtain enhanced resolution of topography. The Magnavox dual channel satellite Navigation system was used for accurate position fixing. Sampling was carried out using free fall grabs (FFG) (make Preussag, Germany). At each station, 7 free fall grabs were deployed in a hexagonal pattern with one grab in the center. The grabs were spaced approximately 200 m. apart. Free fall grabs have distinct advantage over other sampling methods like Petersson grab and dredging in that they have rapid sinking rate (80 m per minute) which minimizes the effect of currents. Sample location can therefore be determined fairly accurately. The time spent on the operations is also less

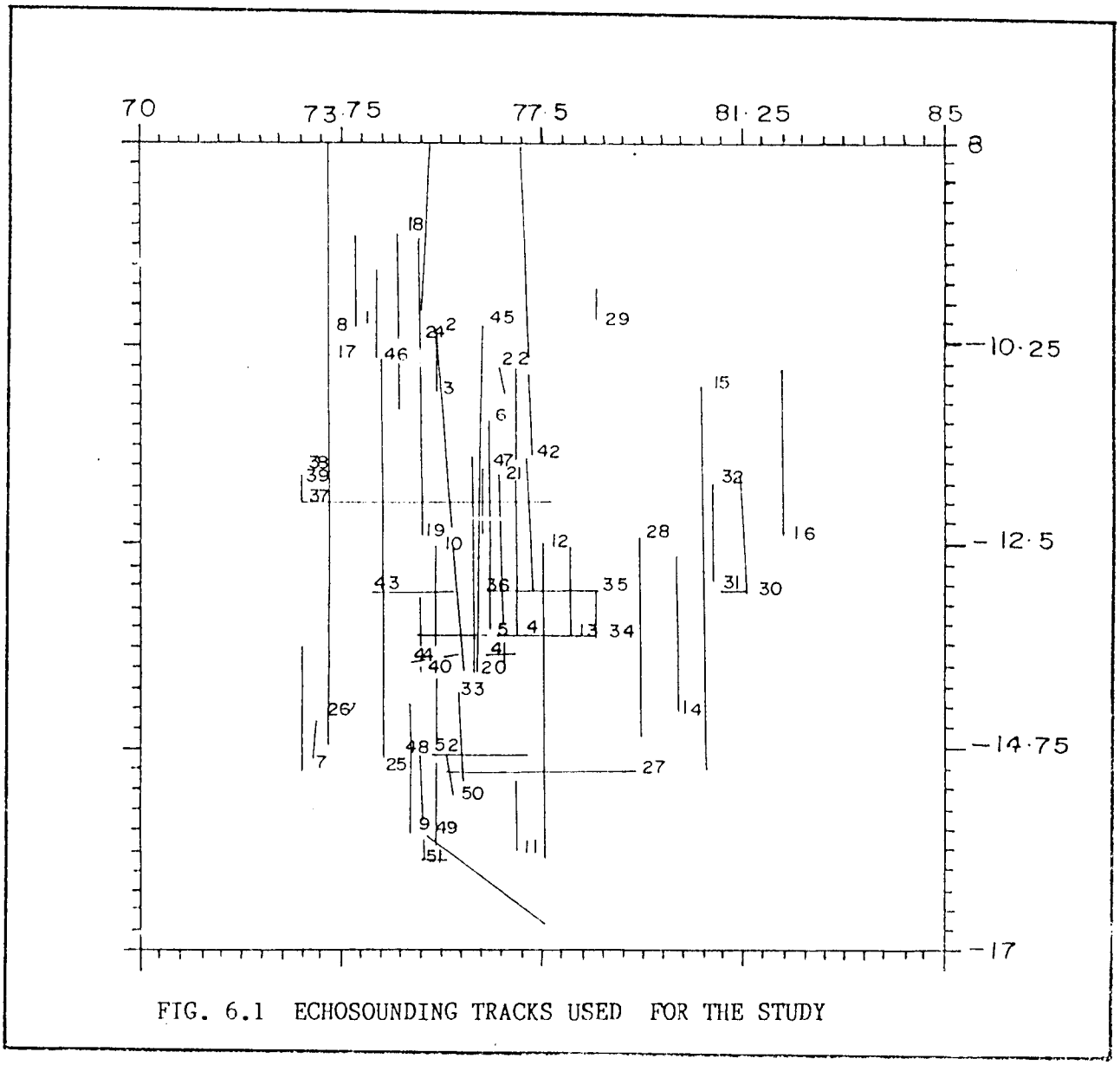

FIG. 6.1 ECHOSOUNDING TRACKS USED FOR THE STUDY

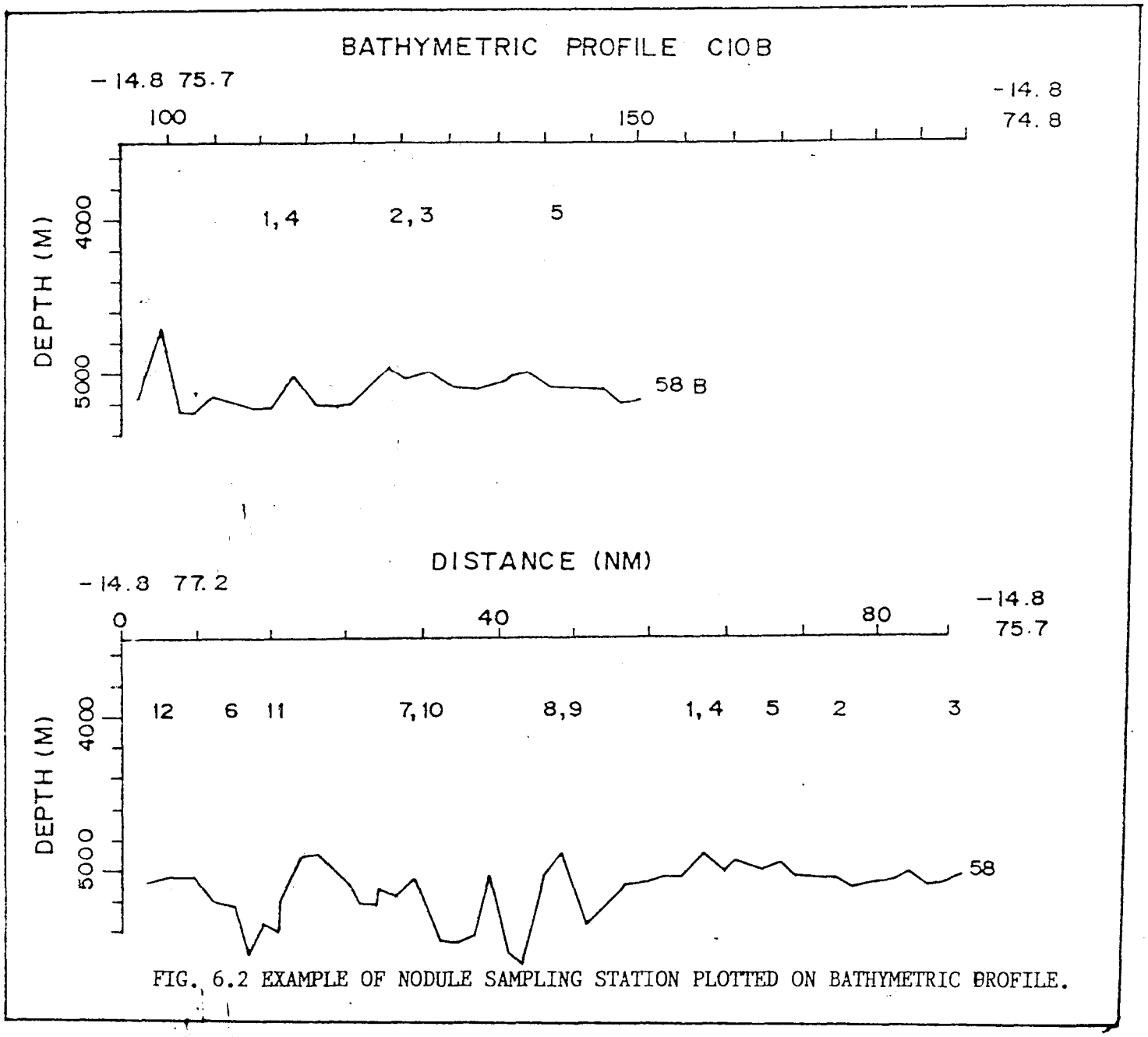

FIG. 6.2 EXAMPLE OF NODULE SAMPLING STATION PLOTTED ON BATHYMETRIC PROFILE.

as many grabs can be launched simultaneously. Nodule abundance (kg/m^2) was calculated from the total weight of nodules recovered from the grab divided by the area of the grab (0.13 m^2). Average abundance of the stations was calculated by averaging the abundance from different FFG lowered at the particular station. The echograms were digitized on the computer using the digitizer and interpolated one minute depth files were created. This file was merged with one minute position data file to obtain a master position depth data file (Procedure is described in detail in chapter 2). From this data file, around 66 latitudinal and longitudinal echosounding tracks were selected in the area. Fig.6.1 shows the tracks used for the study. A program was developed on the Norsk Data computer to draw the bathymetric profiles and to mark the location (using the CALCOMP plot routines) of the FFG sampling stations on the profile. 479 FFG sampling locations were plotted on the bathymetric profiles using this program (Example in Fig. 6.2). Each sampling station was assigned a appropriate topographic domain depending on it's location on the topographic profile. The stations located on the top of positive relief features like abyssal hills were classified as those belonging to ' Hill tops', those on negative relief as 'Valleys', remaining as 'Slopes' and ' Plains' depending on the inclination of the seafloor. Size

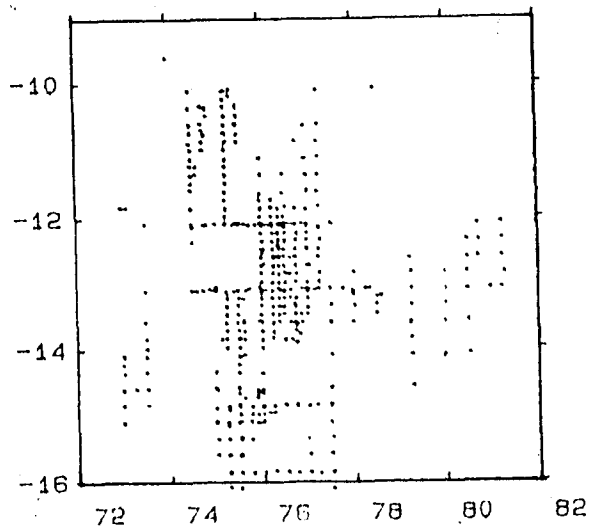

a). All Domains

b). Valleys

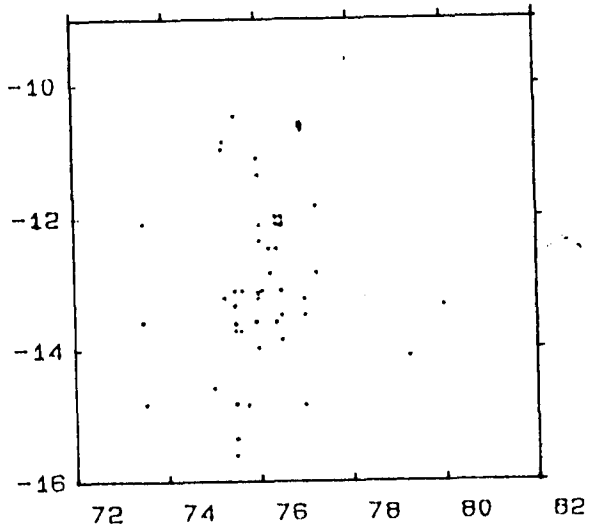

c). Hilltops

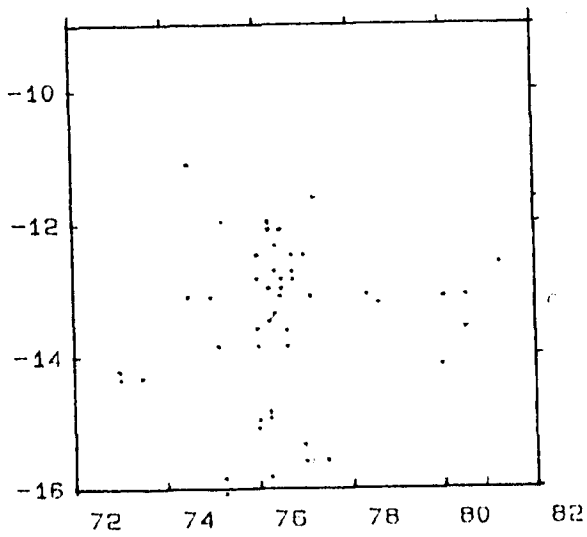

d). Plains

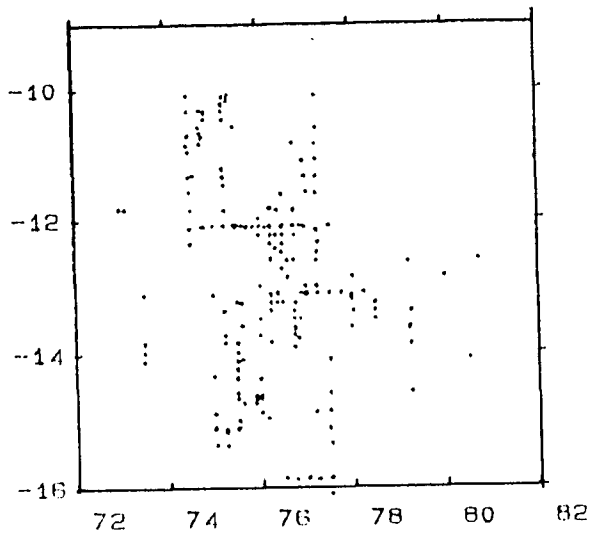

e). slope

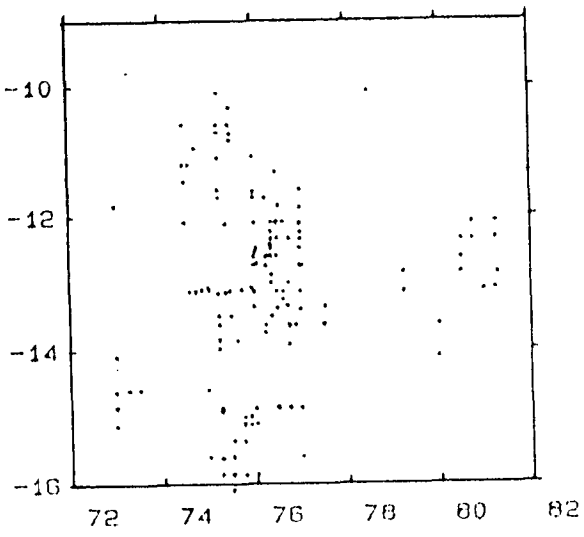

FIG. 6.3 (A-E) STATION PLOT COMBINED FOR ALL DOMAINS AND FOR DIFFERENT DOMAINS.

analyses of nodules were carried out with callipers and classified into <40, 40-60, 60- 80 and >80 mm size classes. Chemical data used in the study is obtained from the PMN data bank (Elemental concentrations in nodules were determined by AAS at different national laboratories).

6.3 Results and discussions:

479 ferromanganse nodule sampling locations in conjunction with echosounding profiles were divided into 4 topographic domains. The distribution and abundance of nodules and nodule sizes were studied for the four domains. The stations are spread over the Central Indian Basin (CIB) between 9^0 30′ S to 16^0 S latitudes and 72^0 30′ E and 82^0 E longitudes. Fig. 6.3 shows the station plot for different domains and combined plot showing the stations in all domains. As seen in Fig. 6.3, the selected stations are spread over the entire area though the concentration is more in the central region (10^0 S- 14^0 S and 74^0 E- 78^0 E). Infact, the selected tracks also are concentrated in the central region (Fig.6.1). Stations in plain and slope domain (Fig. 6.3 (c, d)) are also scattered everywhere. The stations for hill top domain are present mostly south of 11^0 S and stations from domain valleys are present west of 78^0 E longitude only.

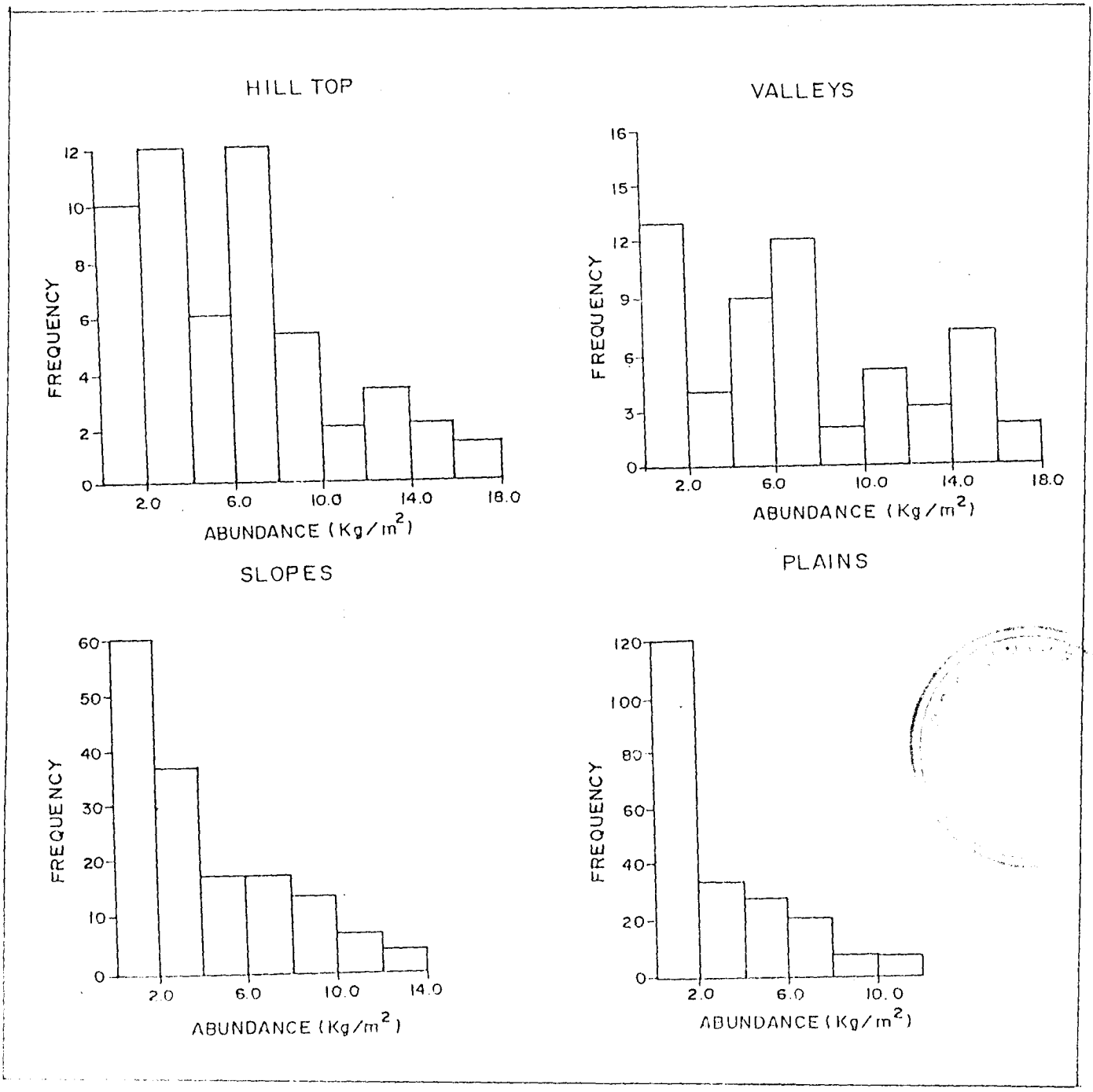

FIG. 6.4 HISTOGRAMS OF ABUNDANCE Vs. FREQUENCY OF OCCURRENCE IN DIFFERENT TOPOGRAPHIC DOMAINS.

Regions of rugged topography have yielded higher nodule abundances. Table 6.1 gives the mean, minimum, and maximum nodule abundance and statistical parameters like standard deviation, biased variance, skewness and kurtosis for different topographic domains. Highest mean abundance is obtained from stations from domain valleys (6.94 kg/m^2). Hill tops (5.81 kg/m^2) and slopes (4.303 kg/m^2) are next in line while stations from plains report the least abundance (2.72 kg/m^2). This sequence of decreasing nodule abundances in the order valleys, hill tops, slopes and plains confirms the earlier report from CIB **(Pattan and Kodagali, 1988 based on data from 54 locations only)**, though the data set used here is much larger. According to **Horn et al.,(1973)** more abundance of nodules on hill tops, slopes and valleys is an indication of availability of more nucleating material originating from volcanic activity around abyssal hills and seamounts or breaking down of basaltic rock fragments by weathering process. As seen from table 6.1, maximum to minimum nodule abundance is highest for valleys (0-17.8 kg/m^2) and least for plains (0-12.5 kg/m^2). Figure 6.4 shows the histogram of abundance Vs frequency of occurrence in different topographic domains. It is observed that the distribution is Gaussian in case of plains and slopes (fig 6.4 c, d) and Rayleigh type for hill tops and valleys (fig 6.4 a, b). Rayleigh type distribution

indicates that the abundances in the domains (Hill tops and valleys) shows large variations. Histogram shows two distinct peaks (2-4 and 6-8 kg/m^2) for hill tops and 3 peaks for valleys (0-2, 6-8 and 14-16 kg/m^2). For plains and slopes, the frequency in each range decreases with increasing abundances. This is particularly so domain plain whose histogram (fig 6.4, c) is negatively skewed. This fact is reflected on the standard deviation (SD) values also (Table 6.1). SD is least for plains (2.89) and maximum for valleys (5.17). SD increases from plains -slopes-hill tops- valleys. Biased variance is also maximum for valley and progressively reduces from valley to hill top to slope to least in plains. This confirms the fact that plains, though have less mean abundance of nodules, the deviations is less and distribution is regular **(Kodagali 1988, Pattan and Kodagali 1988)**. For valleys, maximum mean abundance is reported but the distribution is patchy. The values of skewness also shows the trend of gradual increase from valleys (0.41) to maximum for plains (1.13). Kurtosis however does not show any regular trend.

Table 6.1

Statistical parameters and abundance details for different topographic domains and combined for all domains.

Parameter	Domains				
	Valleys	Hill tops	Slopes	Plains	Combined
No. of cases	57	53	159	210	479
Abundance(kg/m^2)					
Minimum	0	0	0	0	0
Maximum	17.80	16.15	17.3	12.50	17.8
Mean	6.94	5.81	4.04	2.72	4.00
Standard Deviation	5.17	4.22	3.87	2.89	3.97
Biased Variance	26.30	17.54	14.86	8.30	15.76
Skewness	0.41	0.64	1.03	1.13	1.13
Kurtosis	-0.90	-0.29	-0.46	0.64	0.76

Table 6.2 gives the data on frequency distribution of nodule abundances with percentages in different topographic domains. For hill tops and valleys (showing Rayleigh distribution), several high frequencies occur (Hill tops 0, 2, 3 and 7 kg/m^2 and for valleys 0, 4, 6, 10 and 14 kg/m^2). But for slopes and plains frequency decreases with increasing abundances value- with maximum occurrence of nil abundance in both cases (27.7 and 39% respectively). The distribution for the combined data for all domains (table 6.2, e), abundance value zero was encountered for a total of 144 times (30.1%) while higher abundances of more than 10 kg/m^2 occur for a total of 44

Table 6.2

Frequency distribution of abundance in different domains and combined for all domains.

A) HILL TOPS

VALUE	FREQUENCY	PERCENT	
0	8	15.1	¦********
1	2	3.8	¦**
2	6	11.3	¦******
3	6	11.3	¦******
4	2	3.8	¦**
5	4	7.5	¦****
6	5	9.4	¦*****
7	7	13.2	¦*******
8	3	5.7	¦***
9	2	3.8	¦**
10	1	1.9	¦*
11	1	1.9	¦*
12	3	5.7	¦***
14	1	1.9	¦*
15	1	1.9	¦*
16	1	1.9	¦*
TOTAL	53	100.0	

B) VALLEYS

VALUE	FREQUENCY	PERCENT	
0	10	17.5	¦**********
1	3	5.3	¦***
2	3	5.3	¦***
3	1	1.8	¦*
4	5	8.8	¦*****
5	4	7.0	¦****
6	10	17.5	¦**********
7	2	3.5	¦**
9	2	3.5	¦**
10	5	8.8	¦*****
12	1	1.8	¦*
13	2	3.5	¦**
14	5	8.8	¦*****
15	2	3.5	¦**
17	2	3.5	¦**
TOTAL	57	100.0	

Table 6.2 continued.....

C) SLOPES

VALUE	FREQUENCY	PERCENT	
0	44	27.7	¦**********
1	16	10.1	¦********
2	14	8.8	¦*******
3	23	14.5	¦**********
4	15	9.4	¦********
5	3	1.9	¦**
6	8	5.0	¦****
7	9	5.7	¦****
8	7	4.4	¦****
9	5	3.1	¦**
10	6	3.8	¦***
11	2	1.3	¦*
12	1	0.6	¦
13	4	2.5	¦**
15	1	0.6	¦
17	1	0.6	¦
TOTAL	159	100.0	

D) PLAINS

VALUE	FREQUENCY	PERCENT	
0	82	39.0	¦**********
1	35	16.7	¦**********
2	14	6.7	¦*****
3	22	10.5	¦********
4	10	4.8	¦***
5	16	7.6	¦*****
6	11	5.2	¦****
7	6	2.9	¦**
8	5	2.4	¦**
9	3	1.4	¦*
10	2	1.0	¦*
11	2	1.0	¦*
12	2	1.0	¦*
TOTAL	210	100.0	

E) ALL DOMAINS

VALUE	FREQUENCY	PERCENT	
0	144	30.1	¦**********
1	56	11.7	¦**********
2	37	7.7	¦*********
3	52	10.9	¦**********
4	32	6.7	¦********
5	27	5.6	¦*******
6	34	7.1	¦********
7	24	5.0	¦******
8	15	3.1	¦****
9	12	2.5	¦***
10	14	2.9	¦****
11	5	1.0	¦*
12	7	1.5	¦**
13	6	1.3	¦**
14	6	1.3	¦**
15	4	0.8	¦*
16	1	0.2	¦
17	3	0.6	¦*
TOTAL	479	100.0	

times only. The combined data also shows Gaussian type negatively skewed distribution of nodule abundance.

Results of size analyses on nodules in CIB indicate that the smaller size nodules (<40 mm) are more in all the environments **(Pattan and Kodagali 1988)**. Number of larger size nodules is much less. On top of abyssal hills, the number of <40mm nodules was relatively more (84.3%). It is observed that the in all domains there is a trend of decreasing number with increasing size which may be due to slumping or may be burial or fragmentation of some large size nodules **(Margolis and Burns 1976)**. In contrast to observation in Pacific Ocean **(Margolis and Burns 1976)**, Smaller nodules are more on hill tops than in valleys in Indian Ocean. **Heye (1978)** also reported less number of smaller nodules on the plains than the seamounts in Central Pacific Ocean.

For the genesis of manganese nodules, geological processes responsible for the production of the nuclei, supply of transition elements to the abyssal environment, maintenance of nodules in the sediment-water interface are the important factors. Generation of fracture zones, differential spreading rates, localised volcanism and other tectonic activity are responsible for the secondary bathymetric features to develop. Accretion of nodules is

initially dependent on existence of solid substrate (seed) in an oxidised environment **(Cronan, 1972)**. In areas around the seamounts and abyssal hills (domains hill tops, valleys and slopes in the present case) are likely to contain many basaltic material and fragmented nodule nuclei, resulting in higher nodule abundances in these regions. **Glasby (1973) and Horn et al.(1973)** used the production and dispersion of volcanogenic material from seamounts and fracture zones to explain the higher abundances in rough terrains. Exposure of fresh basaltic rock as well as volcanic flows could produce new supply of nodule nuclei associated with each tectonic episode. Rolling down of nodules from slopes and hilltops into nearby low lying areas like valleys also increases nodule abundances in valleys. Wide range of nodule sizes and morphologies typical of such areas can also be explained by multiple episodes generating different nuclei **(Craig, 1979)**.

Sedimentation is another controlling factor in nodule abundances. Rapid sediment accumulation inhibits nodule growth as this buries nodules and also potential nodule nuclei below the sediment-water boundary layer. The burial leads to reduction in supply of necessary transition elements and nodules are isolated from geochemical conditions existing on the seafloor. Winnowing of a thin sediment cover would combine previously buried and exposed

nodules which will result in a mixture of nodules of diverse size in same area. **Johnson (1972), Moore and Heath (1966)** have shown that the sediment thicknesses vary over even short distances and is strongly related to bathymetry of the region. The hill tops, flanks have very less sediment cover while the plains may have a very thick sediment cover which will result in more uniform nodules.

6.4 Metal content in nodules:

Table 6.3 gives the bulk chemical composition (mean and Standard deviation) of manganese nodules from different domains and combined for all domains. The analyses were carried out using standard Atomic Absorption Spectrophotometer (AAS) techniques in different national laboratories (NML Jamshedpur, RRL Bhubneshwar and HZL Udaipur) and stored in NIOPMN data bank. Nodules for analyses were chosen as representative in shape, size and morphology for particular free fall grab sample. The bulk chemical compositions represent the compositional trends, but variations in chemistry for internal chemical layers and size and morphology could not be studied. Some known correlations exist between transition elements composition nodules in world Oceans. There is a direct relationship between Manganese and Copper and nickel content. Fe shows

positive correlation with cobalt and inverse correlation with Mn, Cu and Ni (Cronan, 1972).

Table 6.3

Mean and standard deviation of elemental concentrations for different domains and combined data.

	Domains				
	Valleys	Hill tops	Slopes	Plains	combined
Results from Stations	39	36	92	118	285
Iron					
Mean	8.71	8.9	8.25	6.96	7.86
S.D.	3.14	3.23	2.79	2.26	2.8
Manganese					
Mean	24.53	24.55	24.51	25.6	24.95
S.D.	3.47	4.06	3.68	3.5	3.65
Cobalt					
Mean	0.15	0.17	0.14	0.12	0.14
S.D.	0.05	0.07	0.05	0.04	0.05
Copper					
Mean	1.12	1.07	1.16	1.27	1.19
S.D.	0.32	0.28	0.31	0.27	0.3
Nickel					
Mean	1.07	1.05	1.12	1.32	1.19
S.D.	0.38	0.40	0.4	0.35	0.39
Cu+Co+Ni					
Mean	2.34	2.36	2.42	2.71	2.52
S.D.	0.65	0.69	0.66	0.56	0.64
Fe/Mn ratio					
Mean	2.81	2.75	3.37	4.11	3.70
S.D.	1.66	1.42	1.31	1.24	1.38

As seen in Table 6.3, the Fe content is highest in nodules from hill tops (8.9%) and least on plains (6.96%). Conversely, Mn content is highest on plains (25.6%) and least on valleys (24.53%). Cobalt content doesn't show much variation in nodules from different domains (0.12 to

0.15%), though is high at valleys (0.15). Volcanic edifices, seamounts or ridges are the major source of cobalt for nodules and crusts. Co can be incorporated in any of the iron hydroxide or manganate phases that form nodules and crusts. Thus, the supply of cobalt is only less and consequently its concentration is less in all environments. Also, Co content in seawater is much less than Co and Ni, Co enrichment entirely depends on local sources such as volcanic seamounts **(Frazer and Fisk, 1981)**. Copper and Nickel like Mn are maximum on plains (1.27 and 1.32% respectively) and minimum on valleys and hill tops (1.07 and 1.05%). For Hill tops, valleys and slopes, the Cu content is more than the Ni content marginally but for plains the Ni content is more than the Cu content. Even for Clarion-Clipperton nodules, nodules contain slightly more Cu than Ni **(Frazer and Fisk, 1981)**. Total metal content (Ni+Cu+Co) is also highest in nodules from plains and least at valleys. Ranges of metal concentrations in nodules from different domains are comparable to ranges reported from similar domains in other basins of world oceans **(Frazer and Fisk, 1981)**. Standard deviation values for different metals (Table 6.3) shows the variability of metal contents within the domains. Generally it is observed that all elements show higher deviations in case of hill tops and valleys and less deviations for plains. Since bulk chemical composition

actually represents a time average of both primary accretion and secondary diagenetic conditions experienced by a nodule deposit, Standard deviation of any component could best indicate the heterogeneity of environmental conditions affecting them **(Craig, 1979)**.

Mn/Fe ratio is an important indicator of chemical variability of nodules. Also, Mn/Fe is a pointer on the origin of nodules. **Bonnati et al., (1972)** described a genetic classification of ferromanganese deposits based on Mn/Fe ratio and total metal content (Cu+Co+Ni). Hydrogenous deposits which cover most of the seafloor are produced by slow precipitation of constituents of seawater in an oxidised environment and are characterised by Mn/Fe ratios of .5 to 5 and high Cu+Ni+Co contents. Adjacent to submarine volcanoes, hydrothermal deposits result from more rapid precipitation from solutions generated by volcanism and /or high heatflow have Mn/Fe ratios less than 0.5 and low Cu+Co+Ni contents. All nodules in the present data set lie in the hydrogenous range of **Bonnati et al, (1972)**. According to **Halbach et al, (1981)** lower Mn/Fe ratio is characteristic of hydrogenous origin. In this case, valleys and hill top nodules have Mn/Fe ratio of about 2.75 which lies on the hydrogenous field of three component diagram of **Bonnati et al, (1972)**. The hydrogenous accumulation is caused by direct precipitation of colloidal compounds fro

near bottom seawater. It is commonly agreed that nodules on elevations represent a hydrogenous end member where no sediment interactions are involved **(Halbach et al. 1981)**. Reasons for low Mn/Fe ratio are lack of sediment cover at the top of hills or with outcropping volcanic rocks limiting diagenetic supply Mn and excess supply of iron containing solution by weathering of volcanic rocks or by submarine volcanism. Plains have highest Mn/Fe ratio of around 4.11 which indicates a diagenetic origin **(Bonnati et al,1972)**. This diagenetic origin is the result of mobilisation of metals and subsequent precipitation in the peneliquid layer, which makes nodules rich in Mn, Ni and Cu. These diagenetic reactions causing changes in Mn/Fe ratios take place in the sediment with which nodules are associated. The fact that Mn and Fe are involved in the post depositional chemical reactions and are recycled between dissolved and solid forms during diagenesis is established by **Calvert and Piper (1984)**. In the Pacific Ocean Mn/Fe ratios decrease upwards the slopes **(Halbach et al. 1981)** - 1.5 for slopes of seamounts, 2-2.5 for base of seamount and up to 4 for the nodules from the basin. **Stackelberg (1982)** also reports low Mn/Fe for nodules from slopes and more from the plains. The trends are similar here in CIB, though the Mn/Fe ratios themselves are slightly higher for all domains. However, ratios obtained

for a smaller set of data from CIB **(Pattan and Kodagali, 1988)** were much smaller for Hill tops (2.17) and slightly higher for plains (4.39).

6.5 Inter element relations.

Table 6.4 shows correlation coefficients between pairs elemental concentration in nodules from different topographic domains and for the total data set. The values of r(correlation coefficient) are at confidence level of 99.9%. The relationships established are along the expected lines. Between different domains, the coefficient of correlation varies only marginally. For plains, all the correlation values are mostly insignificant. For hill tops, slopes and valleys, strong positive correlations among Mn, Ni and Cu are found. However these positive correlations are not so significant for the plains (Mn:Cu= .25, Mn:Ni=.35 only). Fe and Mn are negatively correlated in all the domains, particularly strong in case of hill tops. Cobalt is also negatively related in all environments with Ni and Cu. Inverse relation between Ni and Co is in contrast to that observed by **Frazer and Fisk (1981)** who reported direct correlation for Ni:Co on hill tops. Co and Fe have good positive correlations for nodules of all domains. Mn and Co have negative correlations (r= -.2 to -.42) which is almost same as that reported by **Halbach and**

Ozakara (1979) though in contrast to this **Frazer and Fisk (1981)** reported from Mid Pacific seamounts positive correlations between Mn and Co.

Table 6.4

Correlation coefficients between element pairs and between nodule abundance and Mn/Fe ratio in different domains and for combined data set.

element pairs	Domains: Valley	Hill tops	Slopes	Plains	Combined
Mn:Fe	-.56	-.64	-.50	-.36	-.49
Mn:Co	-.31	-.42	-.36	-.20	-.33
Mn:Cu	.60	.64	.50	.25	.45
Mn:Ni	.72	.76	.65	.35	.57
Fe:Co	.72	.47	.74	.65	.68
Fe:Cu	-.75	-.72	-.76	-.50	-.69
Fe:Ni	-.84	-.81	-.84	-.67	-.80
Co:Ni	-.53	-.62	-.64	-.54	-.61
Co:Cu	-.43	-.40	-.57	-.40	-.49
Ni:Cu	.92	.90	.90	.75	.86
Mn:(Ni+Cu+Co)	.68	.62	.60	.32	.53
Fe:(Ni+Cu+Co)	-.79	-.76	-.81	-.61	-.75
Abundance: (Ni+Cu+Co)	-.62	-.13	-.44	-.20	-.40
Abundance: Mn/Fe	-.58	-.24	-.42	-.40	-.46

Co and Fe in nodules precipitate from seawater whereas other metals accrete from sediment pore waters. Most of Mn is also supplied by seawater. The concentrations of Ni, Cu show strong direct relationship (r= over 0.9) in all domains. Similarly, Mn and total metal content (Ni+Cu+Co) show direct relations (r= 0.32 to .8) while Fe and total metal content show strong inverse relationship (r=-.61 to -

.81). Direct relationship between Mn and total metal content is probably related to todorokite mineralogy.

Cluster analyses on nodule abundance and chemical data in different topographic domains was also carried out. It is observed that abundance, Fe and Co typically form one group in all domains, though with varying coefficients of correlations (Table 6.5 a-d gives the dendograms of cluster analyses). All other elements are grouped as one. In this cluster Cu, Ni and Cu+Co+Ni are in one cluster in all domains. In nodules from hills and plains, Mn, Mn/Fe form one cluster. Cluster I (containing abundance, Fe, Co) and cluster II (containing Mn, Cu, Ni, Cu+Co+Ni and Mn/Fe) are negatively correlated. This negative correlation between clusters I and II is maximum in valleys (Table 6.5, a, -0.6 while in three other domains, it is less significant (-.4 to -.45).

Table 6.5

Dendograms produced from cluster analyses on abundance and chemical data in all four domains.

a.Domain-----valleys no. of points 39

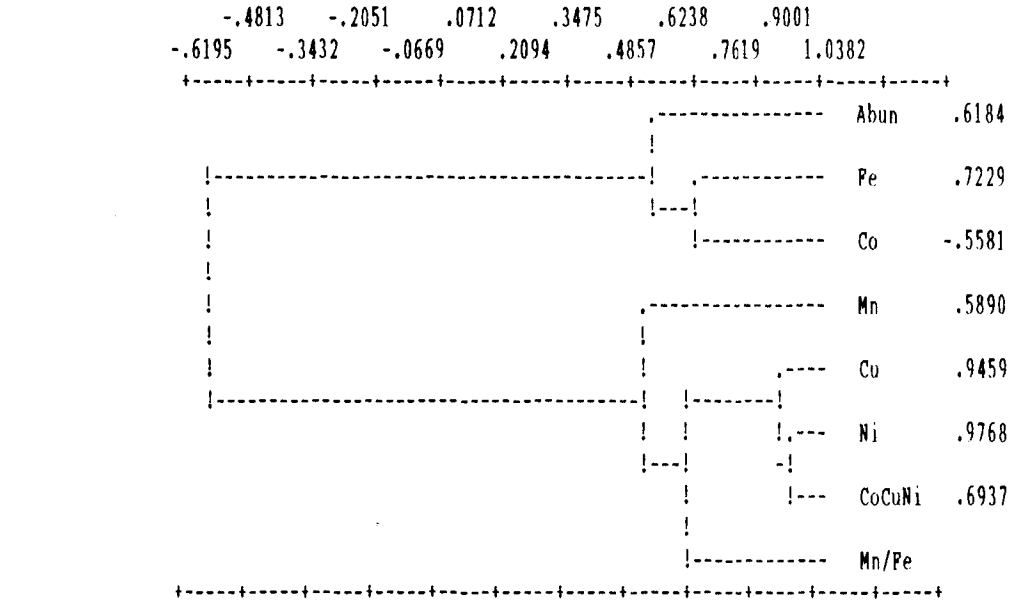

b. Domain hills, no of points-36

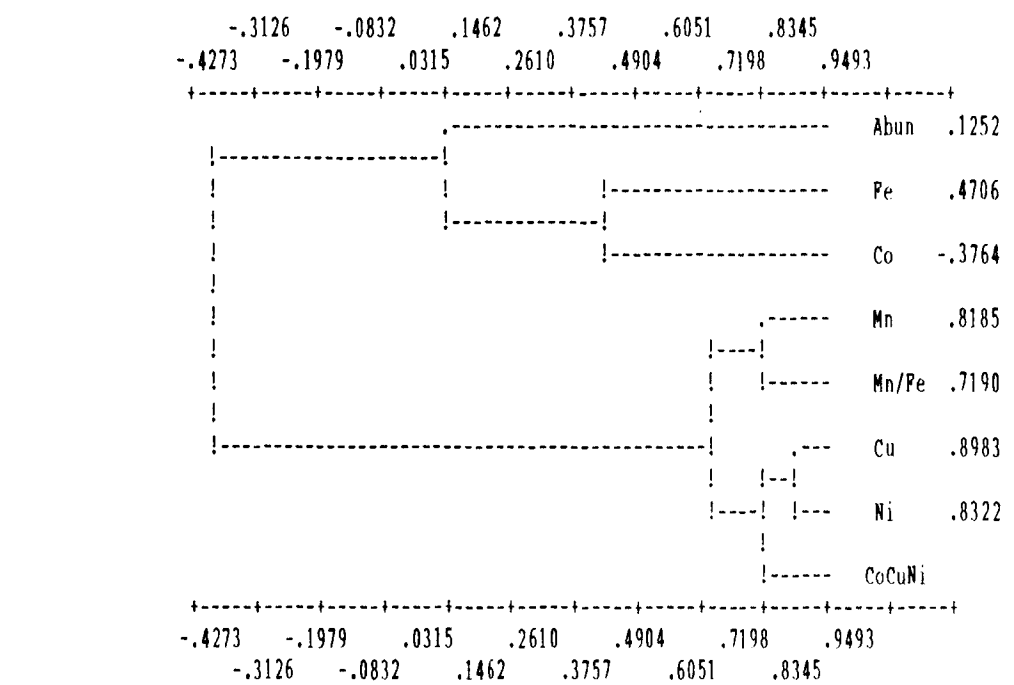

Table 6.5 continued.....

c. Domain---- slopes no of points 92

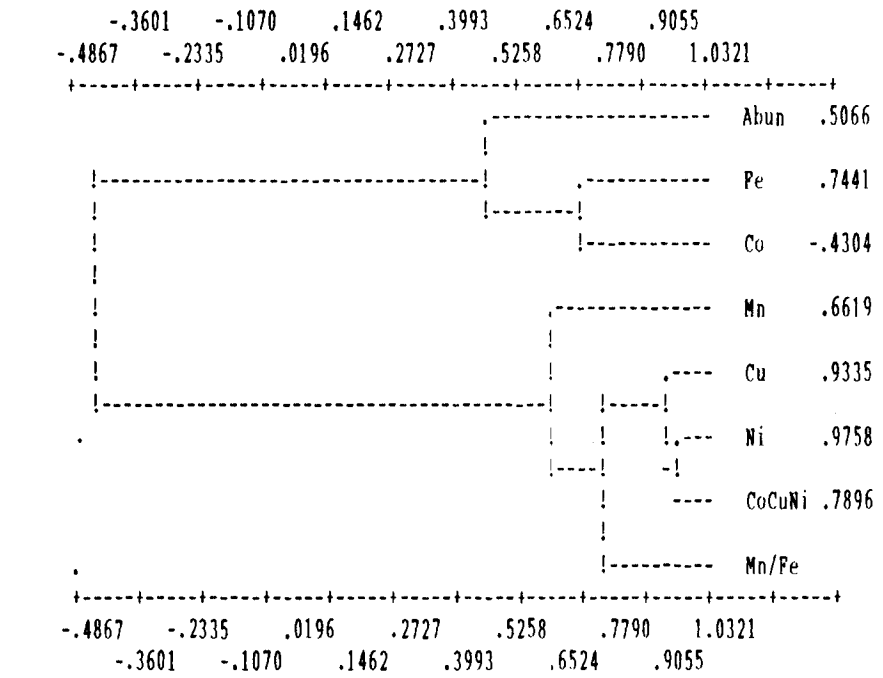

d. Domain--plains.

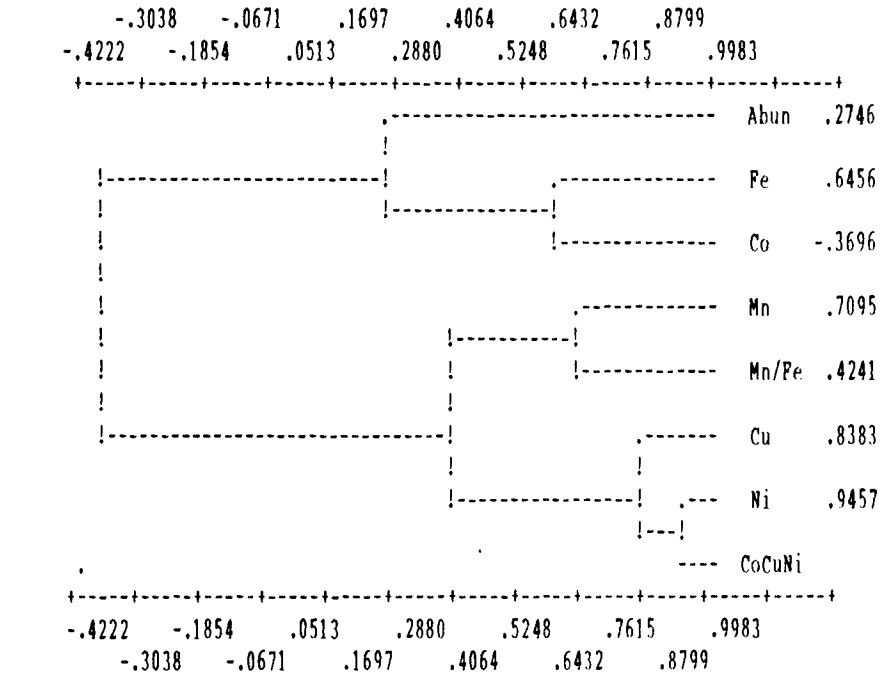

6.6 Nodule abundance and composition:

Previous reports have indicated the inverse correlation existing between nodule grade (Ni+Cu+Co) and nodule abundance (Menard and Frazer, 1978,r=0.40). For few patches of about 500 sq.kms. area in the Pacific ocean, a more significant negative correlation of r=-0.84 was reported **(Skornyakova and Andrushchenko, 1974). Mizuno and Moritani (1977)** have also reported significant inverse relation (r=-.75) in the Pacific.

Present data base of 479 nodule sampling stations (285 stations have both abundance and chemical data), also shows a inverse relation between nodule abundance and total metal content (r=-.4, table 6.4). This value is nearly same as that reported by **Frazer and Fisk (1981)** from Pacific (r=.43). In the CIB, **Sudhakar (1988)** confirmed inverse correlation between grade (Ni+Cu) and abundance based on data from 435 locations (r=-.52). However, at the valleys, the inverse relation is more significant for the present data set (r=-.62) and is low for plains (r=-.2) and for hill tops (r=-.13). Mean abundances in all domains were plotted against mean total metal content and the inverse

relation is more significant with r=-.86 and the straight line fit obtained has the equation y=-.078x+2.84.

Similarly, relation between abundance and Mn/Fe ratio were calculated (Table 6.4). In all the domains, the two parameters are negatively correlated. For valleys, the inverse relation is most significant (r=-.58) while for hill tops it is very less (r=-.24). Combined for all domains, abundance and Mn/Fe are negatively correlated at r=-.46, which compares well with the earlier report from CIB **(Sudhakar, 1988, r= -.54)**. Mean abundances in all domains were also plotted against mean Mn/Fe ratio. The inverse relation for the mean values is r=-.84 and the straight line fit has the equation y=-2.79x +4.48.

To conclude it can be stated that nodule abundances in all topographic domains has inverse relationship with total metal content (Ni+Cu+Co) and Mn/Fe ratio. Higher the nodule abundance, total metal content will be less. Such an inverse relation is due to the fact that some environmental factors seem to affect both grade and abundance. One of these is the local topography. Seamount tops, slopes and valleys are the domains where the nodules are most abundant where as the nodules richest in Ni and Cu are associated with smooth plain terrains where the nodule abundance is less.

Chapter 7.
Influence of regional and local topography on distribution of polymetallic nodules.

7.1 Introduction:

In the previous chapter, nodule distribution in different topographic domains was discussed. The nodule abundance data for each sampling station used for that study was the average abundance from five or seven free fall grabs (FFG) lowered at each station. The detaile topography at the lowering position of FFGs was not considered. It is proved beyond doubt that topography is the important factor in controlling the distribution of polymetallic nodules. World wide, despite the high seafloor coverage and enrichment of valuable metals in the regional deposits, variability of nodule distribution and chemical composition complicates localised seafloor trends **(Bonnati and Nayudu, 1965, Meyer 1973 and Craig 1975)**. Recognition of causes of the local variability as well as small scale bathymetric obstacles to the deep sea mining systems is important for assessment of economic feasibility of nodule mining.

In the present study, data from detailed echosounding and nodule sampling survey conducted by MV Farnella, a chartered vessel from United Kingdom are used. Bathymetric relief is variable throughout the region. Effect of

localised tectonism on abyssal topography, sedimentation patterns and volcanic activity during structural development of the area can be related to the observed variability of nodule distribution within distances of few kilometers. Nodule sampling from different bathymetric settings both regionally (bathymetry of the area surrounding the station) and locally (bathymetry at the lowering position of individual FFG) is discussed here.

7.2 Bathymetry and sampling.

Sixteen free fall grab (FFG) stations at intervals of 15 nautical miles were selected. This data base was used to study the influence of regional topography on the abundance of polymetallic nodules. Between four to seven FFG were launched at each station in a hexagonal or square pattern with one grab being at the center. The samplers were lowered about 200 m apart.

The free fall grab sampling is advantageous over the conventional dredging and other sampling methods because of a more accurate determination of sample location and also possibility of calculating exact abundance of nodules. The time spent on the operations is also less as many grabs can be launched simultaneously. Also, additional tools like a small sediment collector and a photographic device can be added to the FFG. The rapid rate of sinking of FFG (about

FIG. 7.1 FIGURE SHOWING THE LAUNCHING OF A FREE FALL GRAB.

80 m/min) also minimises the effect of currents. The FFG descend to the seafloor, release their ballast weight, sample nodules and pop up to the surface within 2-4 hours. Fig. 7.1 shows one of the FFG being lowered. The Preussag FFG used in the present study has a gripping surface of .13 m^2. Recovered samples can be converted to the exact estimate of nodule abundance in terms of Kg/m^2 by multiplying the sample weight by the factor 7.692. The echosounding was carried out during the survey by Raytheon echosounders (12 KHz) and recorded on the line scan recorder.

Profiles drawn along the sampling stations show the topography of the area (Fig.7.2 A-D). Three of these profiles are parallel to latitudes whereas the fourth one is parallel to longitude. These profiles are drawn with vertical exaggeration of 1:20. The position of the FFG launches are shown by a downward arrow on the detailed bathymetric profiles (Figs. 7.3 to 7.6) that are presented at true scale to give correct picture of the local topography. These profiles and the sampling data are used to study the influence of regional and local topography on the abundance of nodules.

The average abundance at a station is calculated by dividing the total weight of the nodules collected at a station by the number of FFG that recovered the nodules.

7.3 Results and Discussion:

Though the data used for this study is from 16 stations, a host of bathymetric settings are observed in the region. The topographic profiles drawn (Fig.7.2 A-d) illustrate the regional bathymetric character of the survey sites. Average abundance of manganese nodules, recovery efficiency of FFG at each station are tabulated in table 7.1.

The average weight divided by the area of coverage of the grab (0.13 m^2) gives the average abundance of the nodules per station. The recovery efficiency of for each station is also calculated (table 7.1). Recovery efficiency is the ratio of the number of free fall grabs lowered at a station to the number that successfully brought the nodules. The average efficiency is 65.8% and average abundance is 7.84 kg/m^2.

Stations V1, V2 and V3 are set in an area of moderate bathymetric relief. Average depth in these sites is 5200 m. The profile (Fig.7.2 A) shows the nature of the seafloor on a regional scale around these sites. This is a North-South

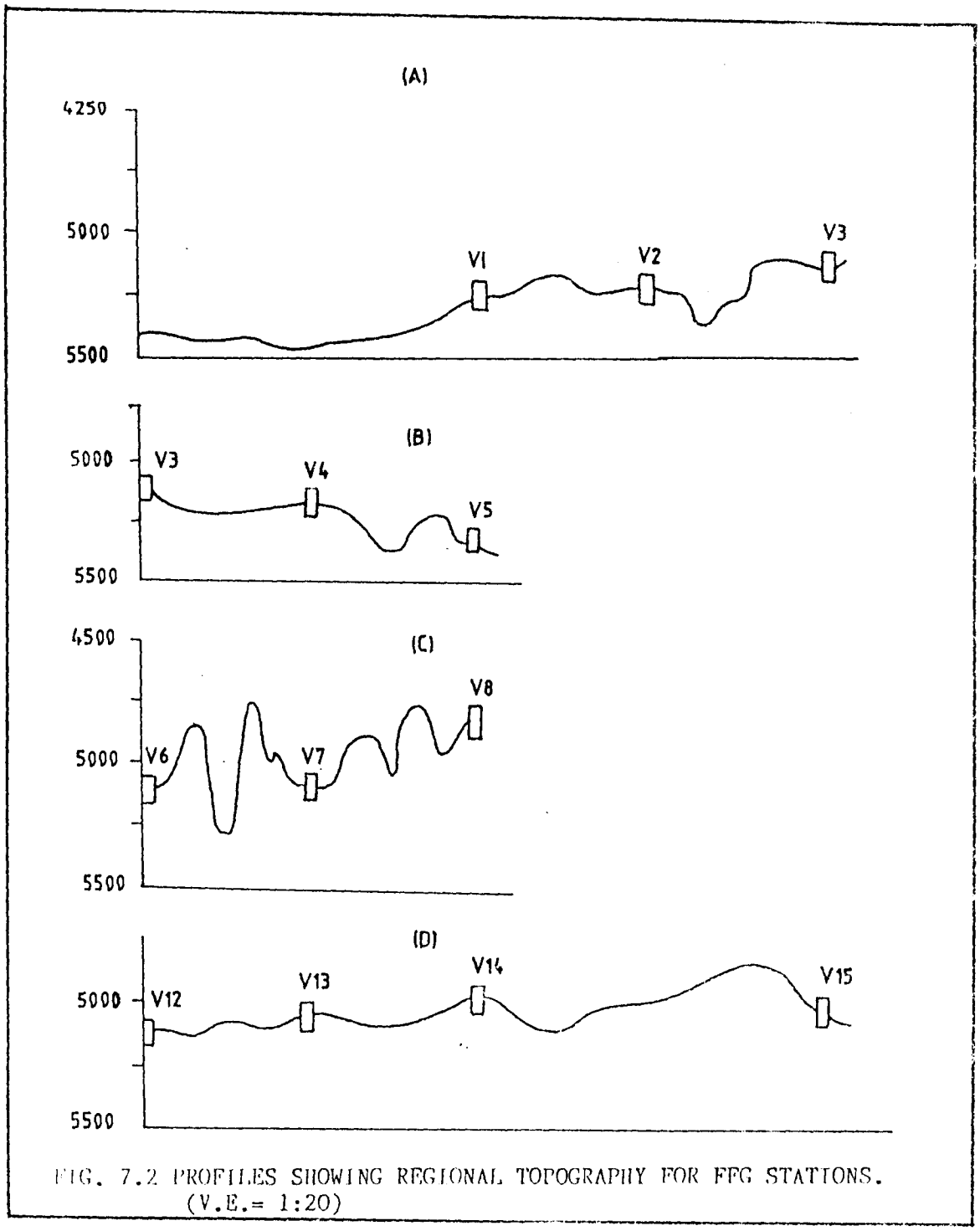

FIG. 7.2 PROFILES SHOWING REGIONAL TOPOGRAPHY FOR FFG STATIONS.
(V.E.= 1:20)

Table 7.1

Nodule recovery, abundance and chemical analyses at different stations

Station No	Recovery Efficiency (%)	Nodule Abundance (Kg/m^2)	Average (No. of Assays)	Mn (%)	Fe (%)	Co (%)	Ni (%)	Cu (%)	Ni+Cu+Co (%)	Mn/Fe
V1	71	9.85	7	27.98	7.37	.13	.97	1.11	2.21	3.96
V2	80	6.35	8	28.32	7.42	.14	1.02	1.17	2.33	4.05
V3	100	6.31	7	21.97	10.37	.17	.78	.66	1.61	2.18
V4	71	1.85	3	32.81	5.69	.11	1.09	1.38	2.08	6.01
V5	00	00	----------no sample----------							
V6	57.14	9.42	6	21.91	13.22	.21	.68	.49	1.39	1.67
V7	80	8.65	8	25.51	9.61	.17	.95	.89	2.01	2.80
V8	75	14.55	6	20.32	10.89	.17	.72	.51	1.40	1.87
V9	100	7.50	8	25.74	8.52	.15	.90	.95	2.00	3.36
V10	85.7	8.14	10	21.79	10.15	.15	.76	.70	1.61	2.49
V11	00	00	----------no sample----------							
V12	50	3.85	3	25.41	8.93	.15	.94	1.16	2.25	2.91
V13	75	1.00	2	29.77	6.85	.14	1.00	1.14	2.28	4.45
V14	75	2.30	5	29.27	7.29	.13	.96	1.18	2.28	4.10
V15	71	15.84	8	20.68	16.14	.21	.45	.32	1.02	1.27
V16	42.85	3.85	6	23.60	8.50	.14	.85	.80	1.79	3.05

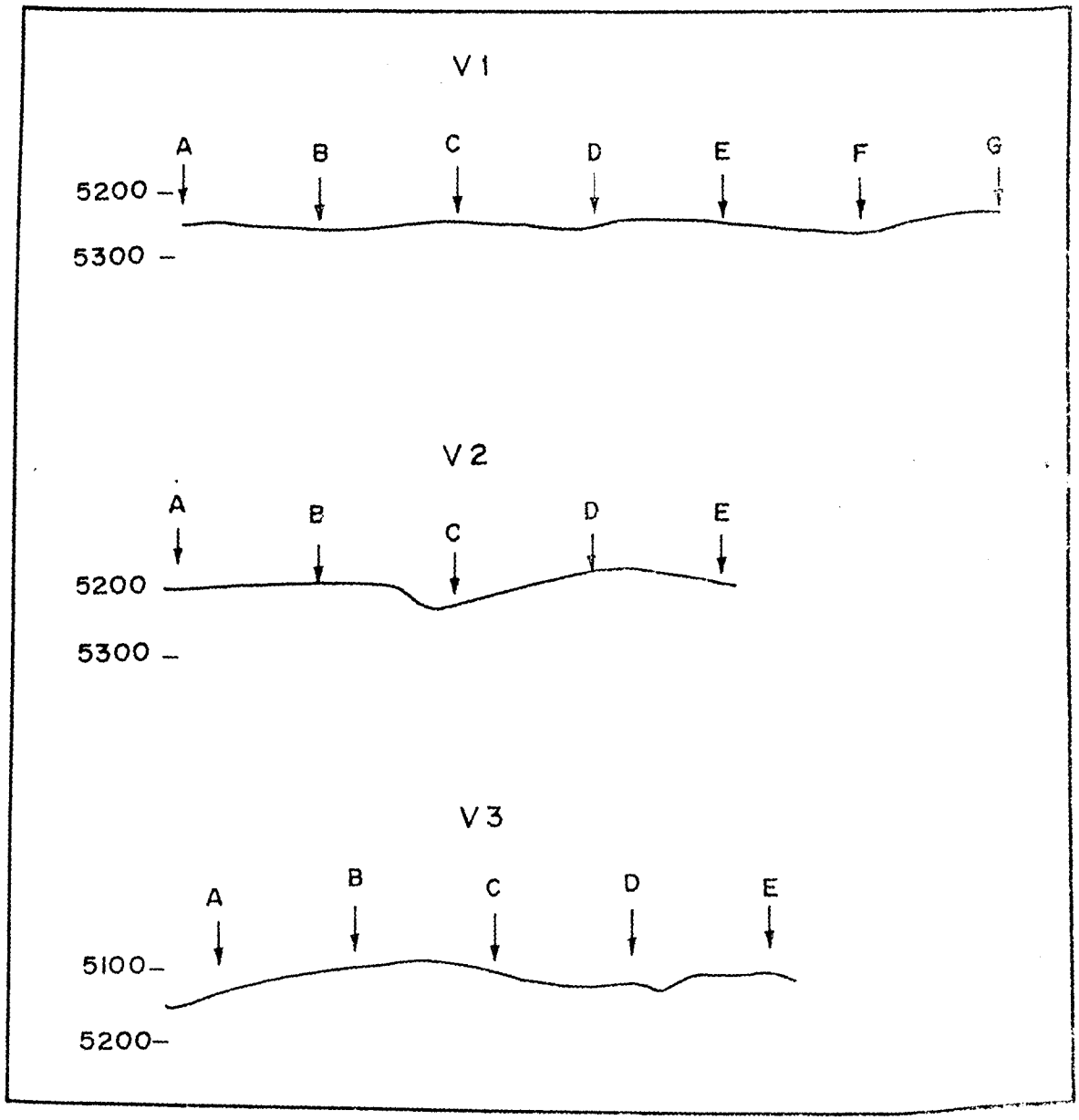

FIG. 7.3 DETAILED BATHYMETRIC PROFILES AND FFG LAUNCHING SITES FOR STATIONS V1, V2 AND V3.

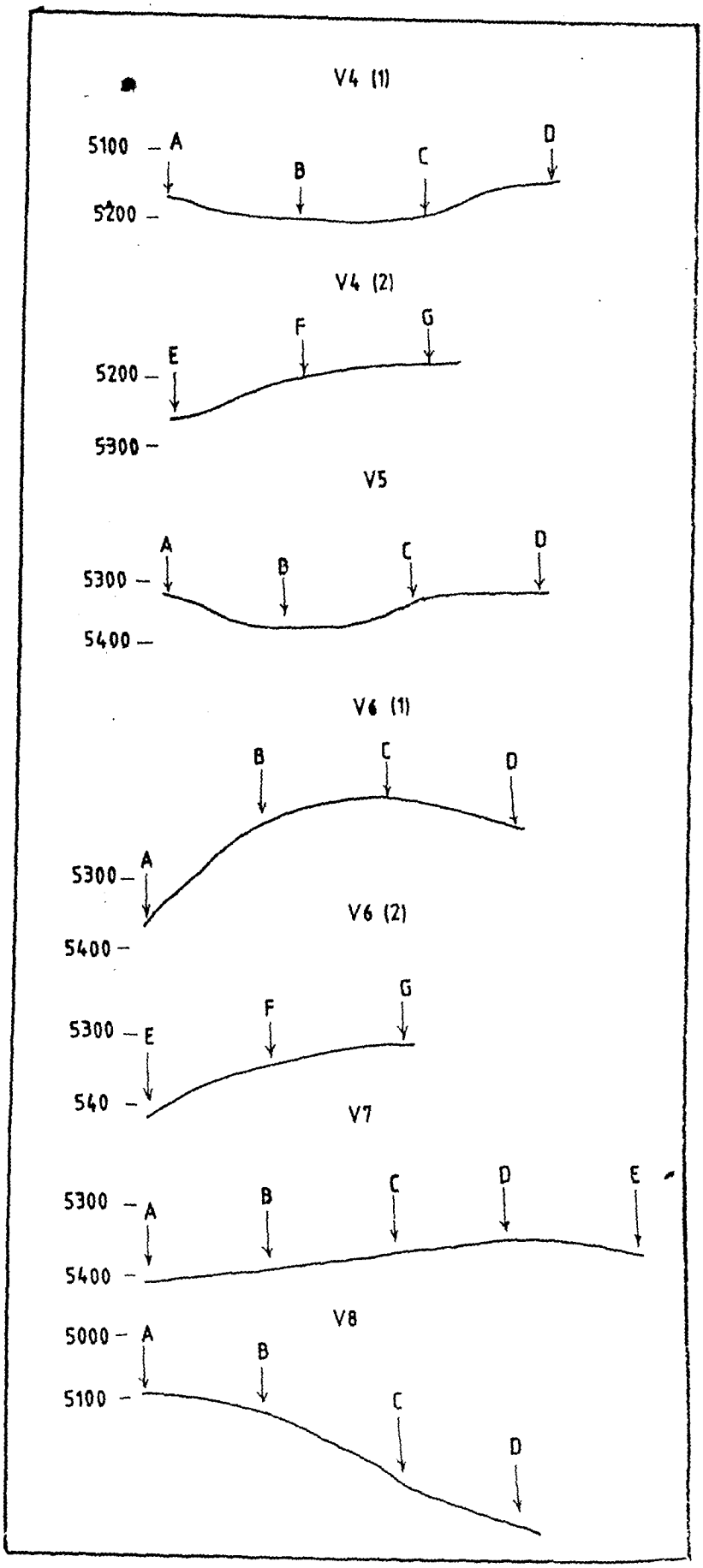

FIG. 7.4 DETAILED BATHYMETRIC PROFILES AND FFG LAUNCHING SITES FOR STATIONS V4,V5,V6,V7 AND

profile (longitudinal). Site V1 is on the flanks of a broad valley the deepest point of which is 5500 m. At site V2 the relief is about 75 m whereas site V3 is at shallowest depth (5100 m). The local topography around these sites is shown in profiles drawn to true scale in Fig. 7.3. It is observed in station V1 depth is uniform locally but regionally the site is on a valley slope and abundance here is high, average 9.85 kg/m^2. In site V2 the local relief was up to 50 m and 5 FFG were operated here. 3 of these FFG were from greater depths and two from shallower depths. FFG from deep depths reported higher abundance than those launched at shallower depth in this station. This shows that distribution of nodules is patchy at sites having some local relief.

Site V4 is located near the top of a valley (250 m) deep and recovery is low (1.85 kg/m^2). Nodules might have rolled down the valley by gravity. The sediment cover as evidenced from the echosounding records is very thin. Site V5 is along the same latitude and on the slope of adjoining valley (Fig.7.2 B). This valley is very steep and recovery of nodules is nil possibly because the nodules rolled down the valley. In these two sites the regional topography seem to have played an important role in influencing nodule characters rendering the local topography inconsequential (Fig. 7.4).

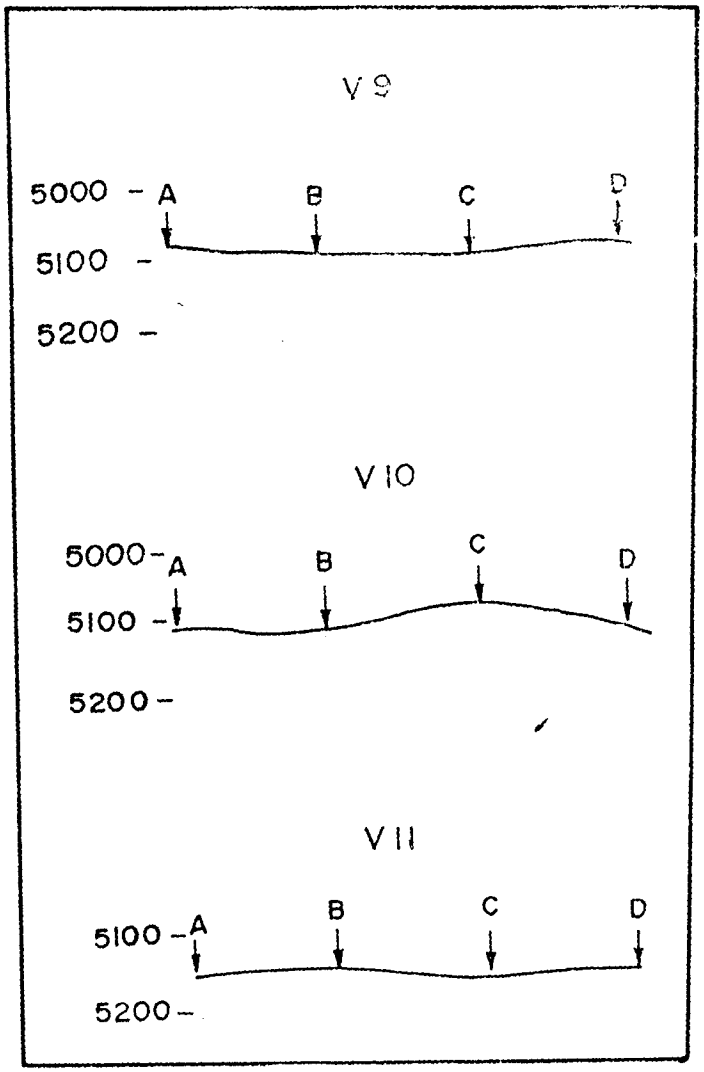

FIG. 7.5 DETAILED BATHYMETRIC PROFILES AND FFG LAUNCHING SITES FOR STATIONS V9, V10, V11.

Sites V6, V7 and V8 are along the same latitude (Fig.7.2 C). They are set in the very rough topographic terrains. Two unchartered abyssal hills with peaks reaching to over 350 m are observed. The structures as observed in the figure may illustrate the trend of intermediate lineation zones. Lines on the profile indicate the possible faults. These faults which might have originated at bottom and extended to the top are perpendicular to the south east Indian ridge. Site V7 set in a broad valley shows local variations in depth up to 50 m. Seafloor abundance of nodules is average 8.65 kg/m^2 . Site V8 is on the shallow part of the valley but the local depth variation (Fig. 7.4) is considerable (up to 250 m). The recovery in each grab lowered in this station is shown in Table 7.2. Abundance in this highly rugged terrain is more, average being 14.55 kg/m^2. But the distribution is patchy with two grabs showing negligible recovery. This phenomenon of higher abundance in places of high relief is also reported from North Equatorial Pacific Ocean **(Craig 1979)**.

Stations V9, V10 and V11 are from plain regions. Individual launching sites of FFG (Fig. 7.5) are also from plain terrains and the abundance of nodules in these stations is comparatively low (7.5, 8.1 and 0 Kg/m^2). All

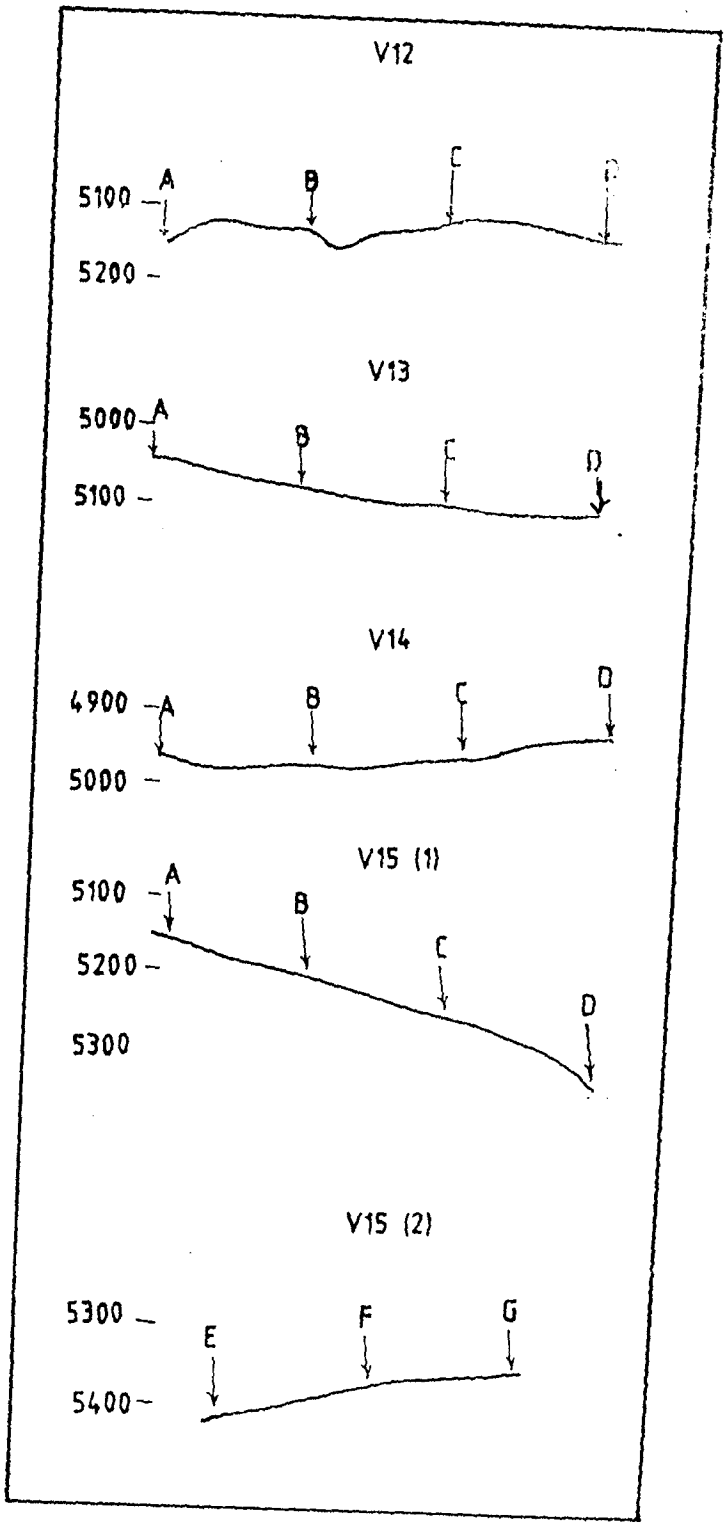

FIG. 7.6 DETAILED BATHYMETRIC PROFILES AND FFG LAUNCHING SITES FOR STATIONS V12, V13, V14 AND V15.

the 4 FFG at station V11 are dropped at perfectly plain area and no sample was recovered from any of these FFGs.

Stations V12, V13, V14 and V15 are set in areas of comparatively low bathymetric relief (Fig.7.2 D). At site V12, depth is 5,150 m with very less local relief. Recovery is also very low (3.85 kg/m^2). In sites V13 and V14 also recovery is less (1.0 and 2.3 kg/m^2 respectively) as they lie on higher altitude on the peaks of the sides of a valley. As there is no micro relief (Fig. 7.6) in these sites nodules might have rolled down the valley. Site V15 on the other hand, situated on the same latitude is at the bottom of a depression which 175 m deep. The local topography as seen from detailed profiles (Fig. 7.6) is also quite rugged. This site also, like V8 reports high abundance of 15.84 kg/m^2. The distribution is patchy in this site also. Two out of seven FFG didn't bring any nodules.

The recovery in each grab lowered at stations V3, V8 and V15 is shown in Table 7.2. It shows the sporadic distribution of nodules in these regions of rugged topography. In contrast to this, the data of grabs from sites V4, V9 and V13 show uniform distribution of nodules. The local and regional topography at these station is much less rugged in comparison to sites V3, V8 and V15. This

Table 7.2

Nodule abundance from different grabs lowered at stations from rugged and plain terrains.

Regions of rugged topography			Regions of plain topography		
Station No.	FFG	Abundance (Kg/m²)	Station No.	FFG	Abundance (Kg/m²)
V3	A	10.0	V4	A	3.87
	B	15.38		B	0.0
	C	15.38		C	0.92
	D	0.77		D	4.62
	E	0.62		E	0.77
V8	A	16.0		F	0.92
	B	16.0		G	4.62
	C	0.0	V9	A	3.85
	D	11.54		B	3.85
V15	A	16.7		C	4.0
	B	0.0		D	9.7
	C	27.69	V13	A	1.55
	D	0.0		B	2.46
	E	24.23		C	2.46
	F	8.46		D	0.0
		G 1.08			

shows that the distribution of nodules is patchy with higher nodule abundance in areas of rugged topography. Areas with little or no relief have lesser abundance but more uniform distribution. (tab.7.2)

Nodule abundance was found to be in direct relation with the local relief. The regional topography in which the station is set also plays a key in the distribution and coverage of nodules. It is also observed that distribution is patchy in areas where the abundance is high and relief is more. In plains, although the abundance is less, the distribution is uniform.

The bathymetric profiles parallel to the latitudes were found to indicate more ruggedness of the seafloor in comparison Fig 7.2 B-D) with profiles parallel to the longitude (Fig 7.2 A). such areas may be associated with some structural trend and may also indicate irregular micro topographic character. The nodule coverage in such areas is variable.

The nodule formation is dependent primarily on the availability of solid substrate (seed) in an oxidised environment. Nodules accrete around nuclei composed of rock fragments, palagonite, fragmented nodules, sediment clasts, shark tooth etc. Abyssal sedimentation also

influences nodule development. Rapid sedimentation reduces growth by burying sediments and potential nuclei. Sediment thickness which varies over short distances is also dependent on bathymetric relief **(Johnson, 1972)**. Sediment transport from abyssal hill to adjacent lows increases sedimentation rates, thus hindering rate of nodule development in low lying areas. Slow deposition rates bring forth rapid nodule development in and around hill flanks and crests which explains higher abundances in these regions.

7.4 Metal content in nodules

Table 7.1 gives the bulk chemical compositions of nodules from the stations discussed in previous paragraphs. Some known correlations exist between transition elements composition nodules in world Oceans. There exists a direct relationship between Manganese and Cu+Ni content. Fe shows positive correlation with cobalt content and inverse correlation with Mn,Cu and Ni. Mn/Fe ratio is also an indicator of chemical variability of nodules **(Kodagali 1988; Mukhopadhyay and Nagendernath 1988 and chapter 6)**.

In spite of stations being close to each other, chemical analyses of nodules shows great variability. Mn-Ni, Fe- Co have direct relationship and Mn/Fe ratio ranges from 1.2 to 4.45 with one station reporting as high as

6.01 ratio. **Bonnati et al. (1972)** put the nodules with Mn/Fe ratio between 2.5-5.1 and high Cu+Co+Ni content as belonging to 'hydrogenous' origin. At places such as the spreading centers and near the submarine volcanoes resulting deposits are 'hydrothermal'. Hydrothermal deposits have Mn/Fe ratio less than 0.5 and low Cu+Co+Ni levels. All samples collected and analysed during the present study fall within the hydrogenous class.

Varying chemical composition is related to nodule size and/or morphology . Here it is observed that diversity in chemistry can also be due to the combination of geochemical processes acting in different bathymetric settings. The Mn/Fe ratio is comparatively higher in stations set in a plain topographic terrain (Stations V4, V9, V13). Among these, Ratio at station V4 is 6.01. Stations V3, V8, V15 lie on regions of rugged topography and report low Mn/Fe ratio of 2.18, 1.87 and 1.27 respectively which is much less than the values from sites set in plain terrain. Cobalt content in these stations is also high (.17, .17 and .25) as also the Fe content. Direct relationship between Mn and Cu+Ni+Co and Fe-Co content as established by **Fuestenau (1966) and Cronan (1972)** is also confirmed from this study.

Chapter 8.
Influence of seabed topography on the distribution of polymetallic nodules and associated features. : A study based on photographic observations

8.1 Introduction:

In the previous chapters, manganese nodule distribution in different topographic domains (chapter 6) and influence of regional and local topography on the distribution of nodules (chapter 7) was discussed to show that topography is one major factor governing the nodule distribution. Here, influence of seafloor morphology on distribution of nodules and features associated with them is studied based on the underwater photographic data.

8.2 Data acquisition and processing

The data was acquired with two of the underwater remote- sensing techniques, namely the underwater photography and the echosounding. The underwater photography was carried out with cameras mounted on deep-towed vehicles as well as on the sampling devices. The computations of nodule coverage and abundance from the seabed photographs were carried out as described by **Sharma and Kodagali (1990)**. An attempt was also made to interpret the type of substrate (like rock / Fe-Mn encrustation, sediment cover etc.) and the thickness of the sedimentary layer, from the impact of the camera counterweight as

observed in the photographs. The relative abundance (RA), i.e. the extent of agreement between nodule abundance from the photographs and the grabs at the same location was estimated, which gives an idea of the possible burial of nodules.

The single beam echosounding data was collected using hull- mounted transducers, operated at 3.5 and 12 KHz. The position data was obtained from the dual channel satellite navigation system. The echosounding data was processed as per the procedure described in chapter 1. Around 60 E-W and N-S trending echosounding profiles were selected across the survey area. 213 Sampling locations with photography data were plotted on these profiles. Each station was assigned a corresponding topographic domain, depending upon its location on the topographic-profile. The stations located on the positive relief features were classified into 'hill tops', and those on negative relief as 'valleys', and the remaining as 'slopes' and 'plains' depending on the inclination of the seafloor topography in these areas.

8.3 Results

8.3.1 Regional bathymetry and distribution of nodules

The regional bathymetry of the area **(Fig. 2.6, chapter 2, after Kodagali et al., 1992)**. comprises of a large

observed in the photographs. The relative abundance (RA), i.e. the extent of agreement between nodule abundance from the photographs and the grabs at the same location was estimated, which gives an idea of the possible burial of nodules.

The single beam echosounding data was collected using hull- mounted transducers, operated at 3.5 and 12 KHz. The position data was obtained from the dual channel satellite navigation system. The echosounding data was processed as per the procedure described in chapter 1. Around 60 E-W and N-S trending echosounding profiles were selected across the survey area. 213 Sampling locations with photography data were plotted on these profiles. Each station was assigned a corresponding topographic domain, depending upon its location on the topographic-profile. The stations located on the positive relief features were classified into 'hill tops', and those on negative relief as 'valleys', and the remaining as 'slopes' and 'plains' depending on the inclination of the seafloor topography in these areas.

8.3 Results

8.3.1 Regional bathymetry and distribution of nodules

The regional bathymetry of the area **(Fig. 2.6, chapter 2, after Kodagali et al., 1992)**. comprises of a large

number of seamounts and abyssal hills in the southern and the southeastern parts which have flanks with variable slopes (2^0- 25^0) followed by the abyssal plains as well as the intervening valleys.

Photographic data from 1034 locations between 10^0 - 16^0 S, 72^0-80^0 E in the CIB were evaluated for distribution of nodules and their coverage and abundance. Since, the nodule distribution is known to be patchy and heterogeneous **(Glasby, 1976)**, the data from all the locations sampled in each 1^0 grid were averaged. It is observed that the higher nodule concentration (20- 40, 40-60 and > 60 %) lies in the southern and south eastern part of the survey area, whereas lower nodule coverage (< 20 %) is in the remaining areas. Correspondingly, the distribution of nodule abundance will also be similar, as the abundance is a function of the coverage and the average diameter of the nodules.

Comparison of bathymetry with nodule coverage shows that the areas of rugged topography (like seamounts and abyssal hills) have higher nodule concentrations than the flat abyssal plains. This data was confirmed by relating the data on water depth with nodule parameters at individual locations in different topographic domains (Table 8.1). The minimum depth recorded for the hill tops

Table 8.1

Details of nodule parameters in different morphological domains as observed from photographic data

Domain	Nodule Coverage (%)	Photo Abundance (kg/m^2)	Relative Abundance (%)
Hill tops	60.00	15.40	231.00
	00.00	00.00	00.00
	12.34*a	3.48	47.45
Slopes and Flanks	75.00	16.32	275.00
	00.00	00.00	00.00
	15.32*b	3.96	60.21
Valleys	03.00*c	1.00	227.00
	00.00	0.00	00.00
	00.25	0.20	44.91
Plains	19.00	4.10	140.00
	00.00	0.00	00.00
	1.36	0.83	32.57

*Excluding locations with only Fe-Mn encrustations (?) and no nodules, as follows :

(a) 2 locations with 100 % and 1 with 60 % coverage, on the hill tops.
(b) 1 location with 60 % coverage on the slopes.
(c) 1 location with 50 % coverage in the valleys.

is 4180 m, the valleys are noticed in depths varying from 4850 to 5550 m and the intervening depths show the presence of the slopes (depth range 4425 to 5500 m) and the plains (depth range 4708 to 5500 m). The nodule concentrations are the highest along the slopes (average = 15.32 % coverage, 3.96 kg/sq m abundance in photo and 6.65 kg/sq m in grabs); followed by the hill tops (average =

12.34 % coverage, 3.48 kg/sq m abundance in photo and 5.53 kg/sq m in the grabs); the abyssal plains (1.36 %, 0.83 kg/sq m and 3.56 kg/sq m) and the least in the valleys (0.25 %, 0.20 kg/sq m and 2.03 kg/sq m). However, due to patchy nature of distribution of nodules, areas without nodules occur in all the domains.

The results from photographs and the grabs have a better agreement along the slopes (average RA = 60%) and the hill tops (av. RA = 47%) as compared to the valleys (av. RA = 44%) and the plains (av. RA = 33%), which indicates that there are less number of nodules buried at the hill tops and slopes than in the valleys and plains.

8.3.2 Distribution of various parameters in different topographic domains.

The frequency distribution of nodule coverage, the nodule abundance from the photographs as well as the relative abundance were plotted for various classes in each of the domains. The distribution of these parameters with respect to morphological units, is described in the following paragraphs.

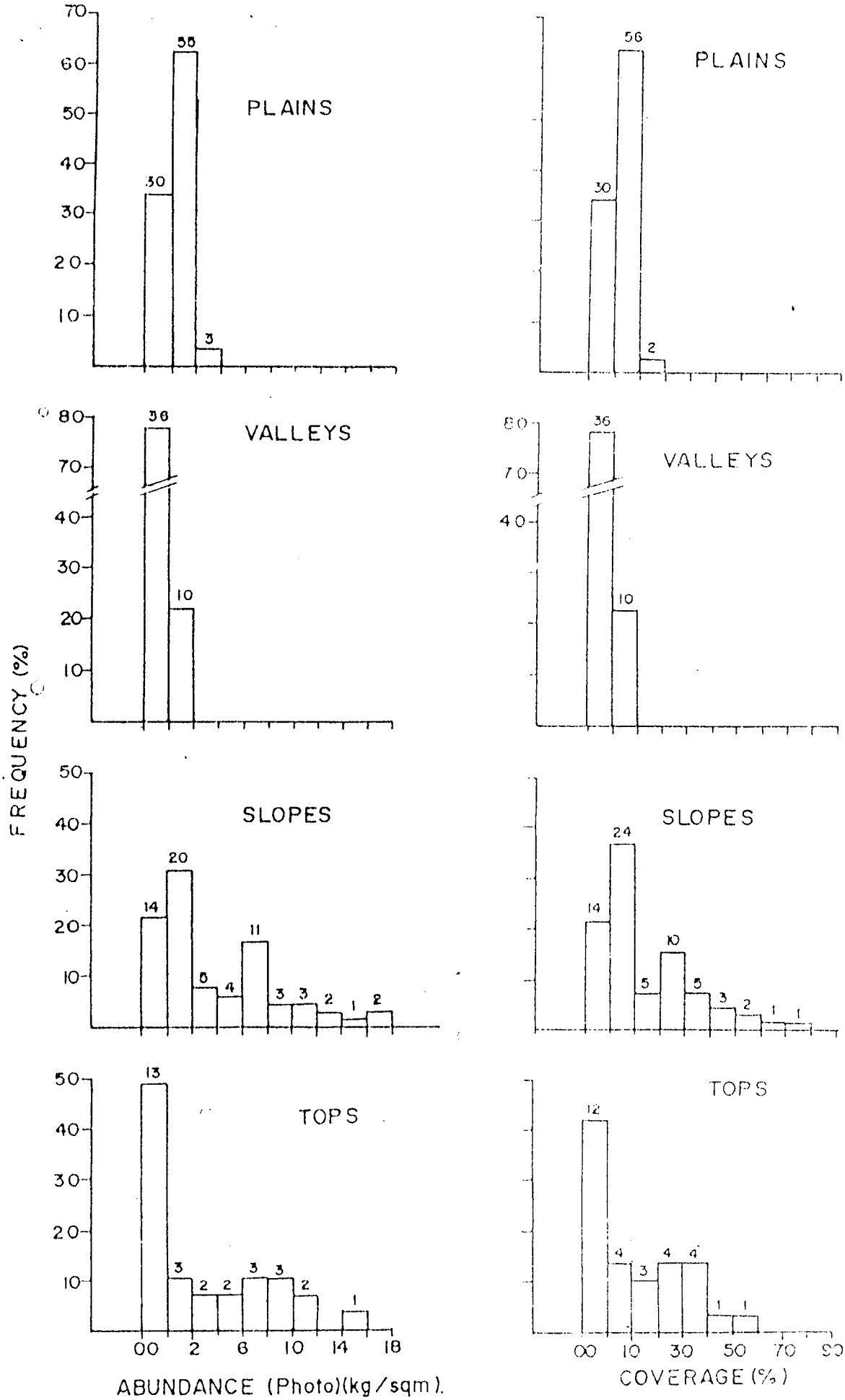

FIG. 8.1 FREQUENCY DISTRIBUTION OF NODULE ABUNDANCE IN PHOTOGRAPHS AND NODULE COVERAGE IN DIFFERENT TOPOGRAPHIC DOMAINS.

a) Nodule coverage:

Very few locations on the hill tops have a high nodule coverage and many of them (35%) have nil coverage, followed by coverages upto 40% on seabed (Fig. 8.1). The two locations with 100% coverage have entire photograph area covered with Fe-Mn encrustations (and no nodules), which are observed as hard dark coloured substrata. On the other hand, the slopes have some locations (22%) with no nodule coverage, and the coverage of nodules varies from less than 10% to as high as 70-80%. Most of the locations in the valleys appear to be devoid of exposed nodules, as more than 75% locations have no nodule coverage and more than 22% locations have less than 10% nodule cover. The only location with 50% coverage is a Fe-Mn pavement on the seabed. Whereas in the abyssal plains, there are more number of locations (67%) with at least some nodules (<10% coverage) exposed on the seafloor.

b) Nodule abundance (in photographs):

The abundances estimated from photographs are generally very low in all the domains (Fig.8.1). Most of the locations on the hill tops (46%) and in the valleys (78%) and many locations along the slopes (23%) and the plains (31%) have no nodules at all, whereas frequency of nodule abundance upto 2 kg/m^2. is lower for the hill tops

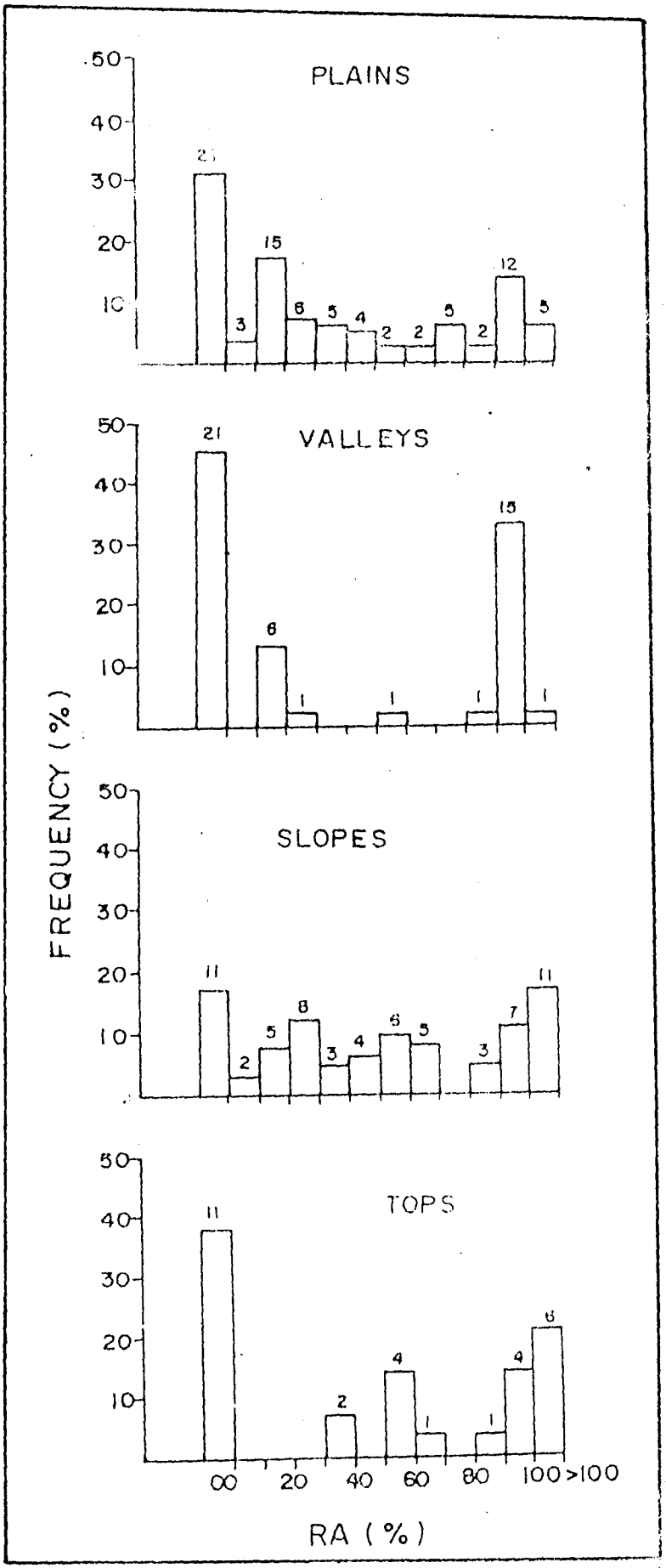

FIG. 8.2 FREQUENCY DISTRIBUTION OF RELATIVE ABUNDANCE IN DIFFERENT TOPOGRAPHIC DOMAINS.

(11%) and the valleys (22%) and higher for the slopes (32%) and the plains (66%). Nodule abundances above 4 kg/m^2. are recorded in some of the locations, which are situated on the hill tops (upto 16 kg/m^2) or the slopes (upto 18 kg/m^2) only.

c) **Relative Abundance:**

Along the hill tops, in many cases (35%) there is a very good agreement (RA > 90%), as also no agreement at all (38% cases with RA = 0%) and for the remaining (27%), it varies from 30 to 70%, majority of them between 50 - 60% of RA (which means a 50-50 agreement). Along the slopes, there is a variable agreement (0 to 100%), depending upon the position on the slope and other influencing factors like exposure of nodules due to sediment cover and their concentration in the area.

In the valleys, majority of the locations (44%) have no agreement at all, because the grabs have recovered some nodules whereas they are not seen in the photographs (Fig 8.2). Another large number of cases (38%), show a very good agreement (RA > 80%), which is because at many of the locations in the valleys, there are no nodules recorded either in grabs or in the photographs. There are a few locations, (18%) where RA varies from 10 to 60%. The abyssal plains, also have a high number of cases (27%)

with no agreement at all, but at the remaining locations the relative abundance is highly variable (< 10 to > 100%) depending upon local environmental conditions and nodule populations. Those locations where photographs have recorded more nodules than the grabs, have RA values above 100%. This is because of high nodule density, and the grabs have failed to recover all the nodules.

8.3.3 Distribution of substrata in different topographic domains.

Substrata like rock exposures and sediments occur in varying proportions on the seabed. Frequency of occurrence of rock exposures (with or without sediments) is higher on the hill tops or the slopes than in the valleys and in the plains (Table 8.2). Rock exposures are observed in about 40 locations in the entire CIB. These exposures vary in their areal extent from 6 to 100 % coverage and range in depth from 4200 m to as deep as 5400 m, but a large number of them (21/40) are located at depths less than 5000 m.

Occurrence of only rock as a substrate is very rare and generally it is associated with a thin layer of sediments. The thickness of the sediment cover increases towards the abyssal plains and the valleys, with no or very few rock exposures in these regions. Thinner

Table 8.2

Frequency of occurrence of substrata in different morphological domains (figures in parenthesis indicate frequency percentage).

Domain (n)	Rock+V.Thin/ Thin sed.	Thin sed.	Int.thick sed.	V.Thick sed.
Hill tops (26)	5 (19.20)	5 (19.20)	3 (11.5)	13 (50)
Slopes and Flanks (60)	3 (5)	4 (6.66)	21 (35)	32 (53.33)
Valleys (44)	1 (2.27)	-	2 (4.5)	41 (93.18)
Plains (83)	1 (1.2)	-	7 (8.43)	75 (90.36)

sedimentary layers are generally restricted to the hill tops and the slopes, and the thicker ones in the negative relief features. There is a tendency for the sediment to get transported downslope from the positive relief such as the abyssal hills and seamounts, exposing the rock outcrops (with less sediment cover) in these regions, and the sediments get accumulated in the basinal areas of the valleys and the flat plains.

The sediment cover plays an important role in the exposure of nodules. The mixed layer or the sediment-water

interface boundary (SWIB) layer obscures the nodules from the camera view **(Cronan and Tooms, 1967)**. The nodules get partially or fully buried, resulting in lower abundance estimates from the photographs than the grabs. If the SWIB layer is thin , there is a high ratio of agreement because more number of nodules are exposed; whereas in case of a thick SWIB layer, there is low agreement **(Sharma, 1989)**. Hence, many locations on the hill tops have a better agreement (i.e. higher RA), whereas the slopes and plains have a variable RA, and the valleys have very low RA values.

However, the presence of thick sedimentary layers is also observed in many of the photographs taken on the hill tops and slopes. Similarly, at a few locations in the valleys and plains, rock exposures and thin sediment layer are observed, indicating that besides the major topographic features, the local topography also influences the presence of certain substrata. Hence, the sediments may accumulate in the microrelief on the hill tops and similarly rock exposures can be found along gently sloping abyssal plains or sides of the valleys. These local topographic variations and the existing substrata also influence the occurrence and concentration of the nodules at these locations **(Kodagali, 1988)**.

Relation of seafloor features with seabed topography

Distribution of nodule coverage and abundance show a preferential occurrence in certain morphological domains. The average as well as maximum nodule populations recorded on the and the slopes are much higher than those recorded in the valleys and the plains (Table 8.1). High nodule coverages (average= 12% and 15%), as well as nodule abundances in the photographs (average = 3.48 and 3.96 kg./m^2.) and the grabs (av. = 5.53 and 6.65 kg/ m^2.) are observed along the hill tops and slopes, respectively. Nodule concentrations are much less in the valleys (av. = 0.25 % coverage, 0.20 and 2.03 kg/m^2 abundance) and the plains (av. = 1.36 % coverage, 0.83 and 3.56 kg/sqm. abundance). The slopes appear to have higher concentrations of nodules than the hill tops and crests, as at many locations the hill tops have Fe-Mn encrustations (or rock outcrops) which cannot be recovered by the grabs. Similarly, the plains have a higher nodule population than the valleys, as also many locations in the valleys have no nodules at all. However, locations with no nodules are also common in all the domains, which confirms the patchy distribution of these deposits in all the morphological settings of the seabed. It has also been observed that the distribution is less patchy in the plains than the other domains **(Kodagali, 1988)**.

A very good agreement between photography data and the grab data is observed along the slopes (average RA = 60%) which suggests that the remaining (< 40%) nodules are buried in these areas, and hence not recorded in the photographs, but were collected in the grabs. This agreement decreases on hill tops (average RA = 47%), probably due to some sediment patches on them; and it further reduces in the valleys (average RA = 44%) and the plains (33%), as the nodules are more likely to be buried in these areas.

Since, many of the hill tops are situated at the depths between 4800 and 5400m, along with slopes, valleys and plains, the presence (or absence) of the rocks and sediments also depends on the morphological variations of the seabed. Most of the rock exposures (with or without sediment cover) and the locations with thin sediment are found either on the hill tops (10/19) or the slopes (7/19), and the occurrence of thick and very thick sediment cover is much higher in the valleys (44/181) and the plains (82/181) as compared to those on the hill tops (14/181) and along the slopes (41/181) (Table 8.2). The rock outcrops are generally found at lower depths and also have a few nodules associated with them. Of the 40 locations, where the rock exposures were observed, no

nodules were associated at 23 locations (57 %), and less than 5 kg/sq m abundance observed at 12 locations (30 %) and only 4 locations had nodules more than 5 kg/ sq m.

8.4 Factors influencing the distribution of nodules in the CIB.

8.4.1 Seabed topography

The results show that there is nil or very less sediment cover on the hill tops of the seamounts and abyssal hills, as well as on their slopes, which gradually increases towards the abyssal plains and deep valleys. Dredging operations have shown the presence of massive rock outcrops on the hill tops, on which thick layer of Fe-Mn encrustations are observed. Broken fragments of these rocks are carried downslope by gradient and currents and these act as nucleating agents to various sources of metals, forming thick nodule fields along the slopes and flanks. The nodule abundance is found to be very low and the distribution is patchy in the abyssal plains and the valleys, where the rock fragments as well as the nodules which roll downwards get buried under thick sediment cover. Observations in other oceans also show sparse population of nodules in the abyssal plains and valleys **(Cronan and Tooms, 1967; Glasby, 1976)**.

8.4.2 Availability of nucleating material from rock outcrops.

Most of the rock exposures are observed at locations in lower depths, and associated with the elevated areas of the seafloor, such as the hill tops and the slopes. These outcrops are either the locations for formation of the Fe-Mn encrustations, or when subjected to submarine erosion act as sources of nucleating material for the formation of polymetallic nodules.

The broken fragments of these rock outcrops, which are transported along the slopes and flanks, act as nuclei for the accretion of the oxides from the hydrogenous as well as diagenetic sources of metals, thereby resulting in large concentrations of nodules in these areas. The distribution (and morphology) of nodules are controlled by availability of potential nucleating agents on which oxide minerals can accrete **(Glasby, 1973)**. According to the 'seed' hypothesis **(Horn et al., 1973)**, the nodule population is controlled by the distribution of the 'seeds' or the rock fragments which act as nuclei for nodules. Two principle types of rocks - basalts and pumice, as the nuclei of manganese nodules are observed **(Iyer and Sharma, 1990)**. The basalts are derived from the

local seamounts and the pumice may be transported from the distant submarine volcanism **(Iyer and Karisiddaiah, 1988)**.

8.4.3 Effect of Sediment cover

The thickness of the sediment cover increases from the hill tops towards the slopes, valleys and plains, which not only affects the exposure **(Fewkes et al., 1979; Felix, 1980;)** of nodules, but the nature of the nodule substrate (sediment type) also seems to affect the nodule population **(Sorem et al., 1979)**.

Siliceous ooze is the dominant sediment in the study area, with a thin strip of calcareous ooze in the west and red clays to the south **(Udinstev, 1975)** and higher nodule abundances are associated with the siliceous ooze in this area **(Rao, 1987)**. Because of the loose porous nature and high interstitial water content of this sediment, Ni and Cu may be able to diffuse through the interstitial waters to remain enriched at the sediment surface where they could be incorporated into forming Fe-Mn oxides **(Horn et al, 1972)**. These elements could be supplied to the nodules not only by the dissolution of calcareous organisms at or near the sediment surface, but also by dissolution of siliceous organisms after burial. The nodule occurrence in the Indian Ocean is associated with areas of

low sedimentation rates, which are also away from influx of the continental detritus **(Glasby and Read, 1976)**.

The above observations suggest that, although, the presence (or absence) as well as the quantity of nodules depend upon factors such as the rock exposures, availability of nucleating material as well as the sediment thickness and sedimentation rates **(Glasby, 1973; Horn et al.,1973; Frazer et al.; 1978)**, these factors are in turn controlled by the regional bathymetry. Hence., the bathymetry is the overall controlling factor for the occurrence and distribution of nodules.

Chapter 9.
79^0 E fracture zone and polymetallic nodule distribution.

9.1 Introduction:

Multibeam swath bathymetric surveys have helped in identifying the southern extension of the 79^0 E fracture zone (Chapter 3, area I). Prior to the MBS mapping of this area, extensive nodule sampling had been carried out. The nodule distribution on two sides of the fracture zone- the eastern down thrown side and the western side are discussed here briefly.

9.2 Methods:

Nodule sampling was carried out in the area (12^0 S to 14^0 30'S and longitudes 78^0 50'E to 79^0 17'E) using the free fall grabs (FFG, manufactured by Preussag, Germany) on four ships ORV Sagarkanya, MV Skandi Surveyor, MV Farnella and DSV Nand Rachit. Fig. 9.1 shows the trend of the fracture zone and the nodule sampling locations on it's two sides. A total of 67 stations were occupied on the west of the fracture zone while 42 stations on the east. At each sampling location, 4 to 7 FFG were lowered. The average abundance for the station was calculated by averaging the nodule abundances from all the grabs launched at the station.

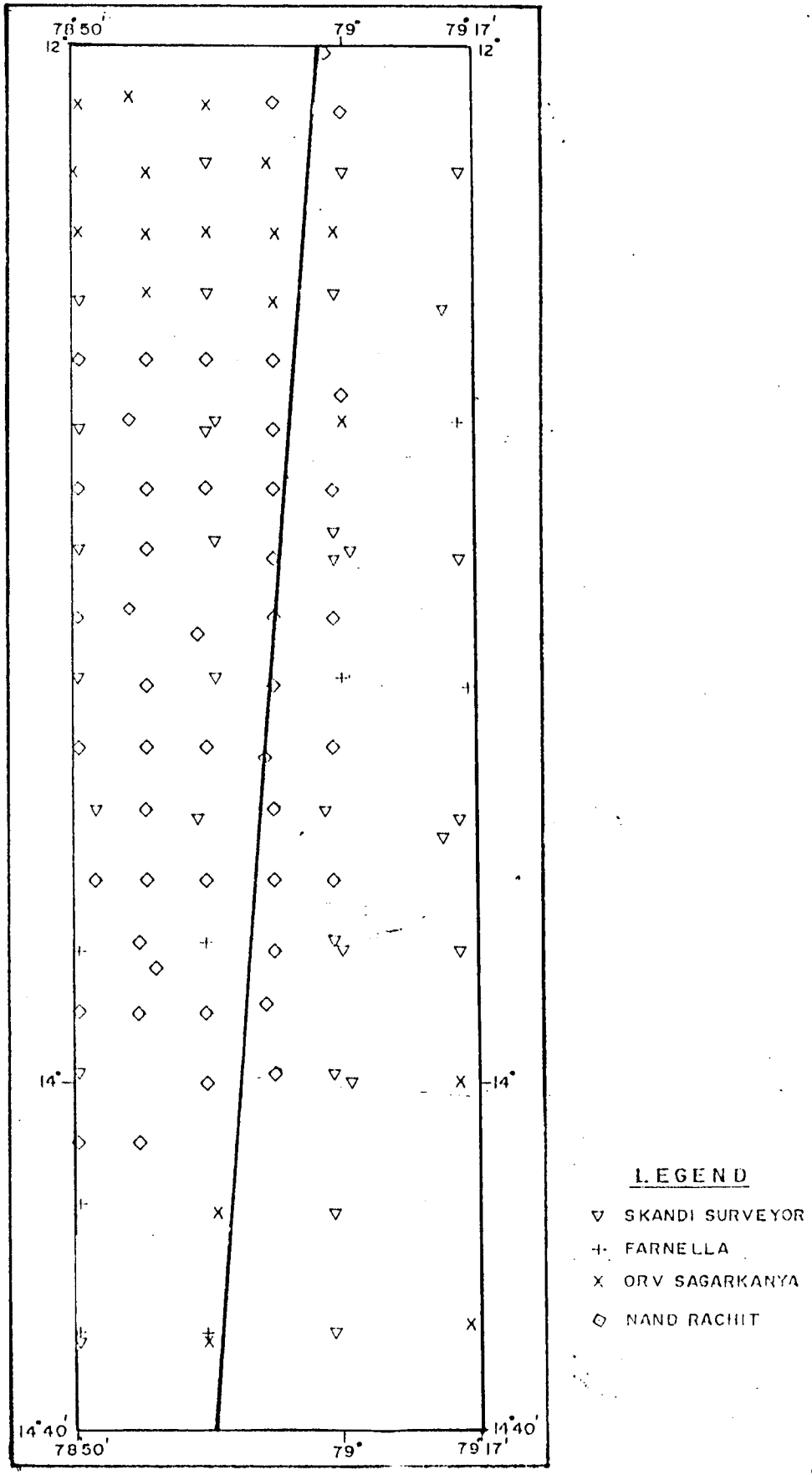

FIG. 9.1 TREND OF FZ AND NODULE SAMPLING LOCATIONS ON EITHER SIDES OF THE FZ.

The depth data was collected by Hydrosweep- Multibeam swath bathymetric survey system. The topography of the area, nature of the fracture zone is described in **chapter 3, area I**. Fig. 3.4 (chapter 3) shows the depth contour map of the fracture zone region. The eastern side is the downthrown side with a varying downthrow of 150 to 400 m.

9.3 Results and Discussions:

9.3.1 Nodule abundances.

Details of nodule abundances on the east and western side of the fracture zone are tabulated in table 9.1. There is striking difference in nodule abundances on the two sides. Mean abundance on the east is 3.56 kg/m^2 and to the west it is 5.45 kg/m^2, though the minimum and maximum abundances observed are same. The standard deviation also are comparable (4.29 and 4.76). Frequency distribution of nodule abundances shows (table 9.2) occurrence of nil abundances for maximum cases on both the sides (17 cases on the west out of 67 and 15 cases on the east out of 42). Though the distribution is Gaussian in both the cases, the frequency distribution is perfectly skewed negatively on the east of fracture zone. West of the fracture zone, abundance value of 2 kg/m^2 appears 7 times, 5 kg/m^2 for 8 times and 8 kg/m^2 for 6 times. East of fracture zone,

Table 9.1

Details of nodule abundances on two sides of the fracture zone.

	No. of Stations	Nodule abundance Maximum (kg/m^2)	Minimum	Mean	Standard Deviation	Biased Variance
East of fracture zone	42	17.5	0	3.56	4.29	17.95
West of fracture zone	67	17.5	0	5.45	4.76	22.34

Table 9.2

Frequency distribution of nodule abundances on two sides of the fracture zone.

Abundance value	East of fracture zone		West of Fracture zone	
(Kg/m^2)	Frequency	percent	Frequency	percent
0	15	35.7	17	25.4
1	9	21.4	5	7.5
2	2	4.8	7	10.4
3	2	4.8	2	3.0
4	2	4.8	2	3.0
5	3	7.1	8	11.0
6	2	4.8	2	3.0
7	1	2.4	3	4.5
8	0	0	6	9.0
9	0	0	4	6.0
10	3	7.1	1	1.5
11	0	0	3	4.5
12	1	2.4	2	3.0
13	1	2.4	0	0.0
14	0	0	2	3.0
16	0	0	2	3.0
17	1	2.4	1	1.5
Total	42	100.0	67	100.0

about 57% of cases have abundances in the range 0-1 kg/m^2, bringing down the average for the area to 3.56 kg/m^2 only.

Fracture zones are linear features which originate as transform faults offsetting ridge crest. The fracture zone are reported to have higher nodule abundances- the famous being the Clarion-Clipperton fracture zone belt in the Pacific Ocean considered to be the most promising nodule deposits in the world. The nodule growth rates are higher especially near volcanic islands, seamounts and fracture zones **(Lalou et al., 1973 and Morgenstein 1973)**. Nodules from the vicinity of Mendocino Fracture zone have a growth rate of 40-81 $mm/10^6$ years **(Andrews, 1976)**. It is hence assumed that volcanic influences and fracture zone may enhance growth of nodules- especially having higher growth rates intermittently and instantaneously bringing the average higher **(Andrews, 1976)**. Fracture zones regions show rugged topography and marked changes in depth of seafloor across the zone. It is observed in the present case that the depth difference across the zone is up to 400 m. The eastern side is the downthrown side and this side is less rugged. The western side is more rugged generally and also, more seamounts and hills are present compared to the eastern side. The higher nodule abundance on the western side of the fracture zone may be because of the higher

ruggedness of the seafloor there. Seamounts and abyssal hills on the western side have distinctive high relief have had periods of volcanic activity even after the generation of the seafloor in the region. These areas present unique environment for nodule development due to the depth variations, availability of volcanic materials etc.

In contrast, the eastern side of fracture zone is comparatively plain having less ruggedness of the seafloor. The reason for the eastern region being plain can also be that the sedimentation rates here are high. At the DSDP site 215 which is also on the eastern side of the 79^0 E fracture zone, the sedimentation rates are high. It is also speculated that the terrigenous input from the Ganga and Brahmaputra may reach up to this site. **(Based on initial reports of Deep Sea Drilling Project)**. Now the question arises that why the sedimentation rates are high on the east and just few kms on the west of the fracture zone, they are less. It is quite likely that the downthrow of a couple of hundreds of meters **(as seen in Fig.3.5., chapter 3 showing the cross section profiles across the fracture zone)** has acted as a barrier for the sediments, thus increasing the sediment input on the eastern side. The downthrow is sharp and sudden and it may act as a barrier preventing the sediments to be deposited on the west of the fracture zone. Because of this barrier of fracture zone,

seafloor is plain on east and also there is thick layer of sediments, and consequently less nodule abundance. That is why we have a case where a few kilometers apart, there is striking variation in nodule abundances.

9.3.2 Metal content of nodules

Table 9.3.

i. Chemical data for nodules from eastern side of Fracture zone.
(Results from 24 stations)

ELEMENT	MINIMUM	MAXIMUM	MEAN	STD.DEVIATION
Cu	.376	1.72	.94	.390
Ni	.58	1.51	1.01	.263
Co	.091	.22	.137	.028
Ni+Co+Cu	1.081	3.18	2.097	.631
Fe	4.03	13	7.898	2.468
Mn	17.4	30.33	24.648	3.363
Mn/Fe	1.45	7.78	3.453	1.339

ii. Chemical data for nodules from western side of Fracture zone.
(Results from 38 stations)

ELEMENT	MINIMUM	MAXIMUM	MEAN	STD.DEVIATION
Cu	.276	1.52	.897	.366
Ni	.39	1.55	.942	.276
Co	.091	.29	.156	.047
Ni+Co+Cu	.907	3.18	2.002	.600
Fe	4.18	16.96	8.039	2.896
Mn	15.64	33.51	24.201	3.997
Mn/Fe	1.02	7.49	3.515	1.508

Results of bulk chemical analyses on nodules from both sides of the fracture zone are presented in table 9.3. The chemical data used here is from **Banakar et al., 1989.** Though there is contrasting nature for nodule abundances, the metal content does not have any surprises. Metal content of nodules on both sides of the fracture zones are similar. Mean nickel content, copper content, total metal content and manganese content are higher on the eastern side of the fracture zone. The iron content, cobalt content and Mn/Fe ratio are higher on the western side. However, the difference is marginal. Elsewhere in the world oceans it is observed that the cobalt content is higher around the fracture zones, more so on the downthrown side **(Andrews, 1971)**. On this fracture zone, the cobalt content is high-up to 0.29% but, the mean cobalt content is higher on the western side (0.156) which is not the down thrown side. The mean cobalt content on the downthrown side is 0.138. The eastern side has lesser abundance and higher total metal content (inverse relation between grade and abundance). The cobalt content is inversely related to total metal content and hence on the western side, Co is higher while the total metal content is less. Hence, it may be concluded that the higher cobalt content is not related to the downthrown side of the fracture zone but is related to iron content and the lesser total metal content (Ni+Cu+Co). The inter element

relations are also on the predicted lines on the two sides of the fracture zones. On the eastern side, Mn and Ni+Cu+Co are strongly correlated (r=0.64) and also Mn and Ni (r=0.68) and Mn and Cu (r=0.59). On the western side Co and Fe and Mn and total metal content are positively correlated (r= 0.63 and r=0.54 respectively). Mn and Co are weakly inversely related on both sides (r=-0.3). Fe has strong negative correlation with Cu, Ni and Mn on the western side while the negative correlation are weaker on the eastern side.

Thus, the presence of the 79^0 E fracture zone has strong influence on the distribution of nodules. The downthrown side has less abundance. The metal contents do not show much variation. However, the cobalt content is more in the area around fracture zones and it is slightly less on the downthrown side and more on the normal side.

Chapter 10.
Topography and nodule mining.

10.1 Introduction

Deep ocean floor is the store house of vast quantities of mineral resources. They have not been exploited till today only because of the technological constraints. Two major mineral deposits of the deep ocean floor are the hydrothermal deposits associated with the ridge system and the manganese nodules spread over the floor.

Nodule mining inspite of uncertain state of technology as of today offers many advantages which are not possible with land mining. Firstly these deposits do not have any overburden, hence material can be removed without use of explosives etc. **(Pearson, 1975)**. Secondly, using cameras, TV etc., complete exploration prior to mining is possible.

Although, manganese nodules are distributed world wide, all the known reserves can not become future mine sites. Once the resources have been identified, more intensive investigations are made to determine the extent of reserves. Additional criterion are applied and seafloor areas are identified that may eventually become mine sites. Minesite concept brings together information in a way that

recognises the interplay among a number of dynamic factors which must satisfy a set of technical and economic conditions **(Anon., 1987)**. Defining a mine site is thus accounting for these factors. There are several factors which are to be studied to delineate a mineable deposit of polymetallic nodules. These factors have to be considered vis a vis the mining system which is proposed to be employed.

Important factors in minesite selection are,

a. Bathymetry-seafloor topography and water depth.
b. Abundance, Distribution of polymetallic nodules.
c. The metal content (grade)
d. Mining system- i. Dredge and sweep efficiency
   ii. Limitations of the system
e. Environmental and economic factors.

Apart from these, the other factors which influence the finding and defining of a minesite are the quality of sediments, currents and number of safeworking days (seastate less than 5) in the area etc. To select the mining equipment, knowledge of seafloor sediment, maximum water depth, features of seafloor topography, maximum and minimum elevations and slopes is essential.

10.2 Ocean Mining Site:

Ocean mine site is defined an area with 100 m. tonnes of nodules with an average abundance of 5-7.5 kg/Sq.m with recoverable content of 1.2% nickel, 1% copper, 0.2% cobalt and 22 % manganese **(Amann 1975)**. In addition to this, the topography should be generally good and over 250 days of fair weather conditions should prevail in a year. The area should be able to sustain recovery for 20 years with annual recovery of $3 * 10^6$ dry metric tonnes **(Anon., 1987)**.

It is generally observed that the conditions of abundance and metal content in nodules and weather conditions are met with in large areas of North Equatorial, Central Pacific Ocean and Central Indian Basin. The scarce results available from Atlantic Ocean and some other basins from Indian Ocean are not encouraging. However the basic conditions of favorable basement floor is hard to find and hence the topographic factor plays a vital role in selection and sizing of mine site.

For deep sea mining, the generally accepted seafloor is the smooth deep sea plain without seamounts, crevices, abyssal hills or other obstacles **(Pressaug, Germany report 1985 based on Pacific Ocean Experience)**. The depth should not exceed 6000 m. and difference of

surface elevation should be to a maximum of 150 m. The slope inclination should be less than 10^0.

Manganese nodules of commercial interest are always associated with abyssal hills **(Frazer and Fisk 1981, Pattan and Kodagali 1988 , Kodagali 1988, chapters 6,7 and 8).** Favorable areas are the one with generally undulating topography. Hills may be sporadic or may have certain trend. Along with these hills, there are numerous other obstacles like the escarpments (few to 100s of feet), outcrops of boulders and pillow basalts and encrustations up to few meters in diameter.

It is apparent that some portion of the mine site cannot be dredged or mined because of the topographic constraints. Some such areas which have to be dispensed with are the areas with tectonic faults, volcanic flows, erosion channels, seamounts, large abyssal hills etc. Also portions of seabed which is too weak to sustain mining equipment will have to be left out. Endeavors during exploration stages should be to get more data on bottom topography and minimize the unmineable area in the mine site. One must also know the degree of local relief at which operation of the mining equipment becomes impossible.

Bathymetry: Water depth will influence the minimum concentration capable of being recovered at deeper depths

larger and larger tracks will be required. Bathymetric studies will be extremely important in deciding about pipe length of mining system. The general depth differences in the area will determine area exploitable with given pipe length.

From geological point of view, conditions under which the nodules have (and are being) formed mainly derive from plate tectonic considerations **(Andrews 1971)**. Proximity to volcanic centers, depth of seafloor, sedimentation rates, rates of deposition and evolution of structures beneath the deposits like abyssal hills, fracture zones, volcanic features are all related to movement of material outwards from mid oceanic ridge crest. This motion exposes the nodule region to a variety of oceanic environments. Thus bathymetry, will play major role in distribution of polymetallic nodules and in turn on their mining.

Macrotopography: (regional topography) This is important to determine the areas within the minesite which are actually accessible to mining. Macrotopography contributes to collector control requirements, especially side slope and operational speed variations. Abrupt changes in the seafloor make it difficult if not impossible to operate the mining system expected to be used.

Microtopography: Microtopography has significant contribution in defining the mine site. The study is essential to establish the collector dynamics which influences the collection rate. It is also important in running gear and collector control parameters.

Obstacles: Obstacles are also significant in defining mineable area. Obstacles are in fact a part of microtopograhic features. These influence in the collector survivability and efficiency.

Subbottom: Sub bottom may not be of direct concern in mining system design and operation, nevertheless its importance cannot be underestimated in initial reconnaissance phases of exploration. Acoustic properties of surface sediments can be correlated with nodule abundance by subbottom studies. Depth to acoustic basement from seafloor can be found which may help in minimizing hazards to mining equipment.

Topographic studies and their relation to occurrence and distribution of manganese nodules have been in progress concurrently with exploration activities. The data available on topography and subbottom are sufficient to have an exact estimate of these factors.

10.3 Mineable area and mine sizing formula:

As discussed earlier, only a part of the total mine site is actually going to be mined. Mining engineers have arrived at a sizing formula considering different factors which influence in sizing **(Siapno, 1975, Kaufman, 1974 and Pasho, 1979)**. The mine sizing formula suggested by different authors are essentially same except for the unmineable area to total area ratio which mainly depends on the bathymetric data available.

$$As = \frac{Ar * D}{C * E * M}$$

where As= size of the mine site
Ar= Annual recovery
D= Duration of mining
C= Abundance (dmt/sq.km)
E= Overall mining efficiency (%)
M= Proportion of area which is mineable.

M (proportion of area which is mineable) which appears on the denominator of above formula can be further expanded as under

$$M = \frac{\text{Unmineable area}}{\text{Total area.}}$$

Unmineable area= (area below cutoff abundance+ area below cutoff grade+ area topographically inaccessible)

10.4 Bathymetric data collection:

Collection of Bathymetric data for exploration and detailed survey leading to mine site selection are necessary. Large areas will have to be prospected and evaluated with equipments that will increase the amount of information and accuracy step by step. As discussed in earlier pages, morphology of the seafloor being one of the major factors which influence the mineability of nodules, precise bathymetric mapping through all stages of exploration with closer and closer grids is essential requisite.

Conventional echosounders with frequencies 3.5-30 kHz have been in use for the bathymetric studies. Enhanced resolution is obtained by using narrow beam (less than 3^0) sounders with gyrostabilised transducers. Use of CESP (correlation echosounder processor) is also helpful in providing noise free records.

in the echosounders of lower frequencies, probability of penetrating the upper layers of sediment will increase. 3.5 kHz records can indicate stratification of upper 50 m. or so of sediments. It can also indicate intrusions or extrusions of volcanic rocks and such other obstacles which will be hazardous to mining. Echosounder within a

deep tow package will have higher accuracy and sensitivity.

FADS (finite Amplitude Depth Sounder) : this is a modified narrow beam bathymetric survey system with high power output and a beam width of 3 degrees. System provides enhanced resolution under extreme weather conditions also. FADS operates similar to all other sounders but method of generating acoustic signal is different. In normal sounders, transmitted signal when it arrives back at the transducer is greatly decreased in signal strength due to spreading losses, alpha losses and bottom losses. Transducer converts attenuated acoustic signal back into an electrical signal. Throughout it's entire trip, the signal remains of same frequency. Greatest loss in such cases is due to spreading loss. FADS uses high frequency transducer which permits narrow beamwidth. Frequency is 70 kHz and primary beam width being 2.4^0. This frequency is modulated at an FM sweep of 6-8 kHz. Non linearity of water acting on signal effects it in such a way that 70 kHz is attenuated and only 6-8 kHz signal is propagated through the water. For depth sounders Narrow beam width, ships roll and pitch become a problem. This problem is overcome by using stabilized platform for transducer. FADS system incorporates the towfish to act as the stabilized platform.

Swath bathymetry survey system: This is essential for contouring of the seabed in a short time. For any mine site to be identified, it is necessary that the bottom contour map with good precision be drawn first. These system are basically multinarrow beam echosounders and are capable of measuring depths simultaneously from a series of beams pointing at discrete angles of incidence in the athwartship direction. India, realizing the importance of such a system for delimiting mine site has acquired one such system (Hydrosweep manufacturers M/S Krupp Atlas Elektronik, Germany). This particular system is an improvement on the SEABEAM system (Manufacturers General Instruments Corporation, U.S.A.) in having a swath of twice the water depth with 59 beams. The system and the data obtained from the system are described in chapters 2, 3 and 4. Hydrosweep uses two identical arrays mounted at right angles to each other, one of them being parallel to the ship's keel. Each array is made up of three modules of 96 elements arranged in a planar configuration with 4 rows of 24 elements. Because they are identical, these arrays can be used either in transmit mode by driving each element separately or in receive mode by combining the elements in groups of 4 to form 72 receive channels which are used to form 59 beams spaced 1.5^0 apart with beam widths ranging from approximately 1.9^0 in the center to

2.7^0 for the outer beams. Transmitted beam is stabilized against roll or pitch. The system is capable of determining the mean sound speed through the water column which by interchanging the transmit and receive functions between two arrays. By comparing the depth measurements made of the center beam in the athwartship mode over a number of successive pings with those obtained on the 59 beams in the fore aft mode, the system performs an approximate raybending inversion to determine the mean sound velocity. A contoured depth data is displayed on-line and is as well stored by the data logger. The logged data can further be used for post-processing **(other details of the system are presented in Chapter 3).**

Bathymetric side scan sonars: Side scan sonars are conceptually cheaper and less complicated than swath bathymetric system. They also offer wider swath coverage, sometimes up to 7 times the depth. Side scan sonar system like SeaMARC, Bathyscan, GLORIA can be used from any ship adding flexibility and cost effectiveness to a bathymetric plan.

It is necessary to decrease profile distances to increase accuracy. This will necessitate using accurate and special navigation systems. The Global Positioning System (GPS) will be more useful than the traditional

satellite navigation methods. More detailed survey which will be confined to smaller areas (to study features like seamount, abyssal hill etc.) will have to be carried out using acoustic navigation system (ATNAV).

Use of deep tow system (with instruments like echosounder, side scan sonars, underwater cameras and television) can be effectively used for the detailed study of bottom features, obstacles and evaluate the nodule coverage also. Deep tow package is thus an integrated exploration system with extended range of vision albeit with decreased operational speed.

Use of Remotely operated vehicles (ROVs) may also be necessary for a near first hand knowledge of the seabed. However to use system like Deep tow packages and ROVs it is mandatory that the detailed bathymetric map of the study area is available.

10.5 Echosounding survey strategy

Bottom morphology is a prerequisite for mineability of manganese nodules. Exact topographic map of the bottom is hence essential. Area must be topographically mapped to determine initial path for the miner. During exploration stage only, a mining plan should be established capable of guiding mining operations.

Surveys should be phase wise narrowed down beginning from 1 degree interval grids to as less as possible-upto 5 nautical miles **(Fellerer, 1975)**. The survey from swath bathymetric system should be carried out in the entire area with sufficient overlap. This task has to be performed before the deep tow and ROVs are used in specific areas like abyssal hills, seamounts, valleys, escarpments, etc. An accurate Navigation should be employed with the above surveys.

10.6 Identifying less productive areas :

India, in 1987 was allotted an area of 1,50000 sq kms for detailed exploration by International Seabed Authority. It was also stipulated that, 50% of this area (75,000 sq. km) will have to be surrendered back to the authority phase wise. The strategy for identifying less productive and unmineable area for surrender of areas will have to be based on the nodule abundance, grade and topographic data. One of the many possible approaches for identifying less productive and unmineable blocks is described here.

Of the three main data sets, abundance and grade can be quantified easily. The whole area can be divided in to blocks of 1/4 degree (about 760 sq.kms area). Krigged averages of the abundance and grade can be calculated for each of the blocks. It is necessary that the detailed

bathymetric map of the area- encompassing all the quarter degree blocks is prepared. If the multibeam data is available for the blocks, then more weightage can be given to the bathymetric data. As discussed in chapter 4, areas around the seamounts and abyssal hills will have to be marked first as these areas are most likely to be inaccessible for the mining equipment. The number of contours in a block is one factor which will directly reflect the roughness of the seafloor. Larger the number of contours in the block, rougher will be the seafloor in the block. So, from the bathymetric data, for each block the number of contours in one section, number of seamounts and the area occupied by the seamounts have to be calculated. So, with this the data available for each block will be 5- number of seamounts, area of seamounts and number of contours from the bathymetric data, and average abundance and grade data.

The minimum, maximum and mean for all the five parameters for all the blocks is calculated. For each parameter, (maximum-mean) is divided in to five (division 0-1 corresponding to factor 0, division 1-3 corresponding factor -1 and division 3-5 corresponding to factor -2) and (mean-minimum) is divided in to five (division 0-1 corresponding to factor 0, division 1-3 corresponding

factor 1 and division 3-5 corresponding to factor 2). For example take the case of factor area of seamounts:

for area of seamounts say --- maximum is 172 sq.km
minimum is 0
and mean is 26 sq.km

a) Maximum-minimum = 172-26 divided by 5 is 29.2

In the block is seamount area is 26-55.2, factor is 0
55.2-113.6, factor is -1
113.6-172, factor is -2

b) Mean-minimum = 26-0 divided by 5 is 5.2

In the block if seamount area is 26-20.8 factor is 0
20.8-10.4 factor is 1
10.4-0 factor is 2

Similarly factors are calculated for each block for all the five parameters. Then weightages are given for each factor as follows.

Abundance and grade ----	250 each
Seamount area and no. of contours----	200 each
No. of seamounts	100

That is, the grade and abundance are given weightage of 500 while topography (3 factors derived from it) is given 500. Now each factor for each block is multiplied by the corresponding weightage and is summed.

For example, for block no. 10,

Abundance----	factor	2 * weightage 250	500
Grade	factor	-1* weightage 250	-250
No.of seamounts	factor	-1*weightage 100	-100
Area of seamounts	factor	-2* weightage 250	-500
No. of contours	factor	-2* weightage 250	-500
Total			-850.

This way, the factor multiplied by weightage summation for all the blocks in the area is calculated and listed in ascending order of summation value. That is, highest negative value (the worst block) is first and highest positive value (the best block) is last.

This is one of the ways of arriving at the worst blocks for the area in terms of topography, abundance and grade. As an modification, the areas of seamounts can be straight away picked irrespective of the block boundaries and marked as unmineable areas or data on slope angles can be used as a criterion to identify the unmineable blocks. Also, depending on the reliability of the data, weightages for different parameters can be altered and above procedure repeated.

10.7 Conclusion:

For delineating a deep sea manganese nodule mine site, the critical factor will be the topography. The macro, micro topography knowledge is essential for locating discontinuities and obstacles to mining system. A good portion of mine site (up to 20%) or more will be ultimately unmineable because of topographic constraints. The unmineable portion will be much higher, some times up to 80% in areas around the seamount, abyssal hills etc. Data from conventional echosounders which have been employed to study bathymetry of seabed will not be sufficient to decide the mineability of the area. Detailed survey has to be carried out using Finite Amplitude Depth Sounders (FADS), swath bathymetric system, side scan sonars, deep tow system (with side scan sonars, underwater camera and television, echosounding transducers etc.) and Remotely operated vehicles (ROVs). For identifying unmineable blocks in the mine site, data on abundance, grade and bathymetry will be the key factors. By quantifying and providing suitable weightages to different parameters, the unfavorable areas can be identified.

Chapter 11.
Conclusions.

2.1 Indian ocean, the most complex of world oceans consists of a number of isolated ocean basin having low relief.

2.2 In Indian ocean, there are 3 active ridge system and several fracture zones.

2.3 Over 4,20000 line kilometers of single beam echosounding data is used to construct a detailed depth contour map of the area, which is first of it's kind.

2.4 Central Indian Basin (CIB) can be divided into 3 zones as plain, medium relief and rugged areas. The average depth is 5200 m. and several seamounts and abyssal hills are identified from single beam echosounding data.

3.1 Multi beam swath sounding (MBS) has distinct advantages over single beam echosounding in that larger area can be covered in lesser time and more accurately.

3.2 For the first time, southern extension of the 79^0 Fracture zone is identified with the help of MBS data. The fracture zone clearly shows the crest-trough topography. The eastern side is the downthrown side and the downthrow varies from 150-450 m. Southern portion of this area has a number of seamounts and abyssal hills.

3.3 East-west lineaments are prominent in the CIB. These lineaments are narrow and long, 10-15 nm in length. The depth difference is about 100-140 m. Lineaments along the north south direction exhibit alternating high and low patterns. Lineaments flexure at the fracture zones and are more prominent in plain areas than on the rougher terrains.

3.4 A deep sea graben is recognised from MBS surveys at the northern part of CIB. Two parallel faults have resulted in a graben. The eastern fault is long and has higher down throw of 220-360 m. The western fault is about 35 km long with downthrow of 200 m. The basal width of the graben is around 12 kms.

4.1 Seamounts are important physiographic features beneath the sea. Numerous seamounts have come to light from the CIB.

4.2 Uncharted seamount at $12^{0}35'S$ and 76^{0} 16′ E was surveyed in detail by narrow beam echosounding has a height of 1250 m with gentle western flank and steeper eastern flank. There is a step like feature on the western flank.

4.3 The seamount was also surveyed by MBS. The comparison of Narrowbeam echosounding and MBS data shows that for accurate mapping of the feature, MBS mapping is essential. The area of the seamount obtained from MBS data is much larger and a small caldera is also recognised. However, the

nature of the flanks and the step like features are recognised from both the studies.

4.4 Three distinct chains of seamounts are recognised from the MBS surveys. Most of the seamounts in chain A (near 79^0E fracture zone) are having sharp conical peaks. There are two cratered volcanoes each in chain B and C, with craters of depth 100-180 m. Correlation between different morphological parameters like flatness ratio to summit width, summit height to area and basal width are established. Inverse correlation between flatness ratio and height is established.

4.5 Seamount chains are located near the fracture zones and there trend is parallel to that of the fracture zones. Origin of seamounts is related to that of the fracture zones. Basalts with varying amount of alteration are dredged from these seamounts. The sediment cover on the seamounts is negligible.

5.1 Morphometric studies on 60 x 60 nautical miles area shows predominance of lower slope angles ($0-1^0$). About 72% of the area is covered by angles in 0-1 degree range.

5.2 Young's hypothesis of log-normal distribution of slope angles is applicable to deep sea floor data also.

5.3 High ruggedness value and elevation-relief ratio corresponds to high slope angles.

5.4 A technique developed for converting depth grid of multibeam data to slope angle grid can be effectively used for generating slope angle maps of any area. Slope angle data on three seamount areas shows predominance of higher slope angles, average being 14^0 and maximum being 38^0.

5.5 Over 80% of area of the seamounts will be unmineable because of inaccessible terrains.

6.1 A computer program developed to superimpose nodule sampling locations on bathymetric profiles can be used to divide the nodule sampling stations in to different domains.

6.2 From 479 nodule sampling station data it is concluded that highest mean abundance is at the valleys (6.94 kg/m^2) followed by hill tops and slopes and least on plains (2.72 kg/m^2).

6.3 Frequency distribution of nodule abundances is Gaussian on plains and Rayleigh (irregular) type on valleys and hill tops.

6.4 Fe and Co content is highest on nodules from hill tops and least on plains. Conversely, Mn, Ni and Cu are highest on plains and least on hill tops.

6.5 Fe:Mn and Co:Mn are negatively correlated in all domains while Mn and total metal content (Ni+Cu+Co) show direct relation ship. Inverse relation between nodule abundance and total metal content is also established.

6.6 Cluster analysis on chemical and abundance data shows that abundance, Fe and Co content form one group while other elements form one group in all topographic settings.

7.1 Nodule abundance is directly related to the relief. Higher the relief, higher is the abundance. Both regional and local topography has direct bearing on the nodule distribution.

7.2 Distribution of nodules is patchy in areas of high relief and uniform on plains.

7.3 Availability of nuclei, sedimentation rate, sediment thickness are important factors in nodule distribution.

7.4 Nodule from less relief areas have high Mn/Fe ration, Mn and Ni content and those from rugged regions have high Fe, Co but low Mn, Ni and Mn/Fe ratio.

8.1 The factors which influence the occurrence of nodules, such as the rock outcrops and sediment cover, also are controlled by bathymetry for their localization and extent.

8.2 Fe-Mn encrustations (and rock exposures) are always located on the crests or the (upper) slopes of the abyssal hills and seamounts, whereas the slopes have a variable sediment cover and the plains and valleys invariably have a thick sedimentary layer.

8.3 The burial of nodules is nil or much less on the crests and slopes as compared to that in the valleys and plains.

8.4 The areas of thicker sediment cover have lower nodule abundances, as compared to the areas of thinner sediment cover.

8.5 The information on influence of bathymetry on distribution of nodules and its associated features can be used as important tool for planning the nodule exploration and mining activities.

9.1 Comparison of nodule abundances on two sides of the 79^0 E fracture zone shows that the western side has higher average abundance (5.45 kg/m^2) compared to the eastern side(3.56 kg/m^2).

9.2 Western side of the FZ is more rugged compared to the eastern downthrown side and hence the abundance is more on west.

9.3 Sediment thickness on the downthrown- eastern side of FZ is high. The downthrow has acted as a barrier for the sediments coming from North eastern region and the sediments are dumped on the eastern side.

9.4 The chemical composition of nodules from two sides does not show any noticeable variation.

10.1 Topography is an important factor in mine site selection and sizing.

10.2 State of art bathymetric survey equipments have to be used in a planned manner during exploration stage itself.

10.3 Information on microtopography, macro topography and obstacles is essential prior to nodule mining.

10.4 Bathymetric information clubbed with average abundance and grade data can be used to identify unmineable and less productive areas.

References.

AGOPOVA, C P (1965). Quantitative characteristics of bottom slope angles in seas and oceans. Oceanology, V 5, No.4, 135-138.

ALLMENDINGER R AND RIIS F (1979). Galapagos rift at 86^0 W: Morphological and structural analysis. Journal of Geophysical Research, V 84, No. B(10), 5379-5389.

AMANN H M (1975). Definition of an ocean mining site. Offshore Technology conference proceedings. Houstan, Texas, USA. V I. OTC-2238, 891-908.

ANDREWS J E (1971). Abyssal hills as evidence of transcurrent faulting on north Pacific fracture zones. Bulletin Geological Society of America. V 82, 463-470.

ANDREWS J E (1976). Aspects of geologic setting of manganese nodule deposits. In: Technical Bulletin No.2 paper presented at IDOE workshop Sova, Fuji, Septermber 1975- CCOP/SOPAC. 713-725.

ANONYMOUS (1987). Delineation of mine site and potentials in different sea area. In: Seabed mining Vol. 4. Ocean economics and technology branch UN. V 4. 79 pp.

ARCHER A A (1985). The metal resources of manganese nodules. In: Marine mining a new beginning- Conference proceedings July 18-21, 1982. Hilo, Hawaii, Department of planning and economic development, Univ. of Hawaii. Seagrant Program. 13-22.

BANAKAR V K, PATTAN J N, JAUHARI P, PADMAVATI V K AND PARTHIBAN G (1989). Grade estimation of ferromanganese nodules collected during Nand Rachit cruises from Central Indian Basin. Internal report, PMN project NIO, Goa. 6 pp.

BATIZA R (1982). Abundance, distribution and size of volcanoes in the Pacific ocean and implications on origin of non hotspot volcanoes. Earth and Planetary Science letters, V 60. 195-206

BATIZA R, FOX P J, CANDE S C, GRINDLAY N R, MELSON W G AND O'HEARN (1989). Morphology, abundance and chemistry of near ridge seamounts in the vicinity of the Mid-Atlantic ridge $\sim 26^0$S. Journal of Geology, V 97, No. 2, 209-220.

BATIZA, R AND VENKO D (1983). Volcanic development of small oceanic central volcanoes on the flanks of East Pacific Rise inferred from narrow beam echosounder surveys. Marine Geology 54: 53-90.

BELDERSON R H, KENYON N H AND STRIDE A H. (1972). Comparison between narrow beam and conventional echosounding from Mediterranean ridge. Marine Geology. V 12,M11-M15.

BELL T H JR. (1975). Statistical features of seafloor topography. Deep Sea Research, V 22, No 12, 883-892.

BONNATI E AND NAIDU Y R (1965). Origin of manganese nodules on the ocean floor. American Journal of Science. V 263. 17-39.

BONNATI. E, KRAEMAR T, RYDELL H (1972). Classification and genesis of submarine manganese deposits. In: Horn B (Ed) Ferromanganese deposits on ocean floor. National Science Foundation, Washington. 149-166.

BORCH ET AL. (1972). Site 215 DSDP report US Govt. printing press, Washington. Vol 22. 193-200.

BOTT M H P (1981). Crustal doming and mechanism of continental rifting. Tectanophysics, V 73(1/3). 1-8.

CALVERT S E AND PIPER D Z (1984). Geochemistry of ferromanganese nodules from DOMES Site A, northern equatorial Pacific. Multiple diagenetic sources in the deep sea. Geochimica Cosmochimica Acta. V 48, 1913-1928.

CARTER D J T. (1980). Echosounding correction tables (formerly Mathews tables), Hydrographic Department, Ministry of Defence, Taunton.

CLOSS H, BUNGENSTOCK H AND HINZ K (1969). Ergebnisse seismischer untersuchungen im nordlichen Arabischer Untersuchungen zur internationalen Indischen Ozean expedition. "Meteor" Forschungsergebneisse. C(2). 1-28.

CRAIG J D (1975). The distribution of polymetallic nodules in the North Equatorial Pacific. Ph.D. Thesis Univ. of Hawaii. Unpublished. 104 pp.

CRAIG J D (1979). Relationship between bathymetry and Ferromanganese deposits in the north equatorial Pacific. Marine Geology. V 29. 165-186.

CRONAN D S (1972). Regional geochemistry of the ferromanganese nodules in the world oceans. In Horn D (Ed). Ferromanganese deposits on the ocean floor. National Science Foundation, Washington D C. 19-30

CRONAN D S, TOOMS J S (1967). Subsurface concentrations of manganese nodules in Pacific sediments, Deep Sea Research, 14, 117-119.

DAVIES T A, WIDE P AND CLAGUE P A (1972). Koko seamount, a major guyot at the southern end of the Emperor seamount chain. Marine Geology. V 13, 311-321.

EPP D AND SMOOT N C (1989). Distribution of seamounts in North Atlantic. Nature 337: 254-257.

EWING M, EITTREIM S, TRUCHAN M AND EWING J I (1969). Sediment distribution in Indian Ocean. Deep Sea Research, V 16. 231-248.

EWING M, SHIPLET M, CONNERY S D (1973). Intensive survey of manganese nodules region in N. Atlantic Ocean. Inter university program of research on Fe-Mn Deposits. National Science Foundation, Washington. 187-217.

FAGARLAND NILS (1983). Tectonic analyses of a Viking graben border fault. American Association of Petroleum Geologists Bulletin. V 67 (11). 2125-2136.

FAIRBRIDGE R W (1968). Encyclopedia of Oceanography. Reinhald Publishers, New York.

FELIX D. (1980). Some problems in making nodule abundance estimates from seafloor photographs. Marine Mining, V 2, 293-302.

FELLERER R. (1975). Methods and problems of exploration of manganese nodules- Oceanology International, V 75, 121-126.

FEWKES, R H, MCFARLAND W D, REINHART W R AND SOREM R K, (1979) . Development of a reliable method for evaluation of Deep sea manganese nodule deposits, NTIS reproduction, Bureau of Mines report no. 6480, 91 pp.

FISHER R L, SCLATER J G AND MCKENZIE D P (1971). Evolution of Central Indian Ridge, western Indian Ocean. Bulletin Geological Society of America. V 82, No.3, 553-562.

FORNARI D J, RYAN W B F AND FOX P J, (1984). Evolution of craters and calderas on young seamounts: Insights from SEAMARC I and seabeam sonar surveys of a small seamount group near the axis of East Pacific Rise at 10^0 N. Journal of Geophysical Research 89: 11069-11083

FORSYTH D, AND ROWLETT H (1979). Microearthquakes and recent faulting at the intersection of the Vema fracture zone and the Mid Atlantic ridge (abstract), Eos Trans. AGU,60,376.

FRANCIS, T J G., PORTER I T, AND LILWALL R C (1978). Microearthquakes near eastern end of St. Paul fracture zone, Geophys. J. R. Astron. Soc.,53,201-217.

FRAZER J AND FISK M B (1981). Geological factors related to characteristics of sea floor manganese nodule deposits. Deep sea Research, V 28 A, No.12, 1533-1551.

FRAZER, J Z; FISK M B, ELLIOT J, WHITE M AND WILSON L, (1978). Availability of Cu, Ni, Co and Mn from ocean ferromanganese nodules. SIO ref. no. 78 - 25, p. 138.

FROIDEFOND, J M AND BERTHOIS L (1984). Morphometric processing of sounding profiles and comparison with visual analysis. International Hydrographic Review. V 61, 17-34.

FRYER P AND SMOOT N C (1985). Process of subduction in Mariana and Izubonin trenches. Marine Geology. V 64, 67-90.

FUERSTENAU D W (1966). Metal recovery from manganese nodules. Office of research services, California- Berklay. 122 pp.

GALLO D G, FOX P J, AND MCDONALD K C, (1986). A Seabeam investigation of the Clipperton transform fault: The morphotectonic expression of a fast slipping transform boundary, Journal of Geophysical Research. V 91,3455-3467.

GANSSER A (1966). Indian Ocean and the Himalayas- a geological interpretation. Eclogae Geological Helvetiae. V59, 831-848.

GLASBY G P, (1976). Marine manganese deposits, Elsevier. Amsterdam.

GLASBY G P, (1973). Distribution of manganese nodules and lebensspuren in underwater photographs from the Carlsberg ridge, Indian Ocean. New Zealand J. Geol. and Geoph., 16(1),1-17.

GLASBY G P AND READ A J (1976). Deep sea manganese nodules. In: Handbook of strata-bound and stratiform ore deposits. Editor K.H. Wolf, Elsevier, Amsterdam. 295 - 340.

GOULD W T,HENDRY R AND HUPERT H E, (1981). An abyssal topographic experiment. Deep Sea Research 28:409-440.

GRANT J A AND SCHREIBER R, (1990). Modern Swathe sounding and subbottom profiling technique for research application: The Atlas Hydrosweep and Parasonde systems. Marine Geophysical Researches V 12. 9-19

GUTBERLET M AND SCHENKE H W, (1989). Hydrosweep- New era in high precision bathymetric surveying in deep and shallow waters. Marine Geodesy. V 33(1),1-24.

HALBACH P AND OZAKARA M (1979). Morphological and geochemical classification of deep sea ferromanganese nodules and it's genetic interpretation. In: La genes des nodules de manganese. CNRS, Paris. 77-89.

HALBACH P, SCHERHAG C, HEBISCH U AND MARCHIG V (1981). Geological and Mineralogical control of different genetic types of deep sea nodules from the Pacific ocean. Mineralium Deposita. V 16. 55-84.

HANDSCHUMACHER D (1973). Formation of Emperor seamount chain. Nature. V 244 (5412). 150-152.

HEEZEN B C AD THARP M (1966). Physiography of the Indian Ocean. Philosophical Transactions of Royal Society of London. A259, 137-149.

HEYE D (1978). Changes in growth rate of manganese nodules from central Pacific in area of a seamount as shown by the I_o method. Marine Geology. V 28. M59-M65.

HILLS E S. (1972) Elements of Structural geology, Chapman and Hills publishers. P 465-472.

HOLLISTER C D, GLENN M F AND LONSDALE P F,(1978). Morphology of Seamounts in western Pacific and Philippine basin from Multi Beam Sonar data. Earth and Planetary Science Letters 41:405-418.

HORN D R, HORN B AND DELACH M N, (1972). Worldwide distribution and metal content of deep-sea Manganese deposits. In: Manganese nodule deposits in the Pacific Symposium/ Workshop Proc., Hawaii, October 16 - 17, 1972.

State Center SCI. Policy Technol. Assess. Dep. Plan. Econ. Dev., State of Hawaii, 46 - 60.

HORN D R, HORN B AND DELACH M N, (1973). Factors which control the distribution of ferromanganese nodules and proposed research vessel's track in North Pacific. Tech. report off Int. Decade Ocean Exploration. 8- 20.

IRISH J D. (1976). Bathymetric and Magnetic survey of California seamount. Marine Geology V 21, No(3),M31-M35.

IYER S D AND SHARMA R, (1990). Correlation between occurrence of manganese. nodules and rocks in a part of the Central Indian Ocean Basin. Marine Geology, V 92. 127-138.

IYER S D AND KARISIDDAIAH S M, (1988). Morphology and petrography of pumice from the Central Indian Ocean Basin. Indian Jour. Mar. Sci., 17: 333 - 334.

JOHNSON D A (1972). Ocean floor erosion in the equatorial pacific. Geological Society of America Bulletin, V 83, 3121-3124.

JORDAN T H, MENARD H W AND SMITH D K, (1983). Density and size distribution of seamounts in the eastern Pacific inferred from wide beam sounding data. Journal of Geophysical Research V 88, 10508-10518.

KAMESH RAJU K A (1990). Magnetic and bathymetric studies in the vicinity of 73^0 E fracture zone, Central Indian Basin. Marine Geology , V 95, 147-153.

KAMESH RAJU K A AND RAMPRASAD T (1989). Magnetic lineations in the CIB for the period A24-A21: A study in relation to the Indian Ocean triple junction , Earth and Planetary Science Letters, V 95, 395-402.

KAMESH RAJU K A, RAMPRASAD T, KODAGALI V N AND NAIR R R (1992). Multibeam bathymetric, gravity and magnetic studies over 79^0 E fracture zone- Central Indian Basin. Journal of Geophysical Research (in Press).

KAUFMAN R, (1974). Selection and sizing of tracks comprising a manganese nodule ore body. OTC preprints, VII-OTC 2059. 283-293

KEATING B, (1989). Morphology of Central Pacific Seamounts: Implications for Mn-Crust mining. OTC Reprints, 189-200.

KODAGALI V N (1988). Influence of regional and local topography on the distribution of polymetallic nodules in the Central Indian Ocean Basin. Geo-Marine letters, V 8, 173-178.

KODAGALI V N, (1989a). Morphometric studies on a part of Central Indian Ocean. Journal of the Geol. Soc. of India, V 33,547- 555.

KODAGALI V N, (1989b). Morphology of an uncharted seamount from Central Indian Basin. Marine Geodesy, V 13, 89 - 94.

KODAGALI V N, (1990). Report on the 58th Oceanographic cruise of ORV Sagarkanya, NIO Report. PP 14.

KODAGALI V N, RAJU K A K, RAMPRASAD T, GEORGE P AND JAISHANKAR S, (1992). Detailed bathymetric surveys in the Central Indian Basin. International Hydrographic Review V- LXIX(69). 143-150.

LACEY A, OCKENDON J R AND TURCOTTE D L (1981). On the geometric form of volcanoes. Earth and Planetary Science Letters. V 54. 139-143.

LALOU C, BRICHET E AND RANQUE M (1973). Certains nodules de manganese trouves en surface des sediments sont-ils des formation contemporaines de la sedimentation. C R Acadamy of Science, Paris. V 276. 1661-1664.

LARINA N I (1975). Mountains of the Pacific Ocean. Oceanology. V 15, No. 1, 89-94.

LAUGHTON A S, MATHEWS D M AND FISHER R L (1971). Structure of Indian Ocean. In: The Sea, Vol.4 ' New concepts of seafloor evolution'. John Wiley and Sons, NY. 543-580.

LEPICHON X AND HEIRTZLER J R (1968). Magnetic anomalies in the Indian Ocean and seafloor spreading. Journal of Geophysical Research. V 73, 2101-2117.

LEPLY L K (1966). Ocean terrain analysis. International Hydrographic Review. V.43, 97-113.

LONSDALE P F AND SPEISS F N, (1979). A pair of young cratered volcanoes in the East Pacific Rise. Journal of Geology 87: 157-173.

MACDONALD, K C, CASTILLO D A, MILLER S P, FOX P J, KASTENS K, AND BONATTI E, (1986). Deep-Tow studies of the Vema fracture zone 1. Tectonics of a major slow slipping transform fault and its Intersection with the Mid-Atlantic ridge, Journal of Geophysical Research , V 91, 3334-3354.

MALHOFF A G, G M MCMURTRY, J C WILTSHIRE AND H W YEH.(1982). Geology and chemistry of Hydrothermal deposits from active submarine volcano Lohihi, Hawaii. Nature V 298. 234-239.

MARGOLIS S V AND BURNS R G (1976). Pacific deep sea manganese nodules- their distribution, composition and origin. Annual Review of Earth and Planetary Sciences. V 4, 229-263.

MCKENZIE D P, AND SCLATER J G, (1971). Evolution of Indian Ocean since Late Cretaceous, Geophysics Journal Royal Astronomical Society. V 25, 437-528

MENARD H W (1964). Marine Geology of the Pacific. McGraw Hill Newyork, 271 pp.

MENARD H W (1967). Seafloor spreading, topography and the second layer. Science, V 157, 923-924

MENARD H W AND ATWATER T (1969). Origin of Fracture zone topography. Nature, V 222, 1037-40.

MENARD H W AND FRAZER J (1978). Manganese nodules of sea floor inverse correlation between grade and abundance. Science, V 199, 869-971.

MERO J L (1965). The mineral resources of the sea. Elsevier, Amsterdam. 304 pp.

MEYER K (1973). Surface sediment and manganese nodule facies encountered on RV Valdivia cruises 72/73. In: Morgenstein M (Ed) Origin and distribution of manganese nodules in the Pacific and prospects for exploration. Dept. of Oceanography, University of Hawaii, Honolulu, Hawaii. 125-136.

MIZUNO A AND MORITANI T, (1977). Outline of GH76-1 cruise and it's results. In: Deep sea mineral resources investigation in Central eastern part of Central Pacific Basin- January to March 1976 (GH76-1 cruise). A Mizano and T Moritani (Eds). Geological survey of Japan cruise report No.8. pp 20.

MOLNAR P AND STOCK J, (1987). Relative motions of hotspots in the Pacific, Atlantic and Indian oceans since late Cretaceous time. Nature. V 337. 587-591.

MOORE J R AND CRUICKSHANK M J, (1973). Identification of technological gaps in exploration of marine ferromanganese deposits. In: Inter-University program of Research on ferromanganese deposits of ocean floor Phase I report-Seabed assessment programme IDOE, NSF, Washington, 279-335.

MOORE T C AND HEATH G R, (1966). Manganese nodules, topography and thickness of quarternary sediments. Nature V 212, 983-985.

MORGENSTEIN M, (1973). Sedimentary diagenesis and rates of manganese accretion on the Waho shelf, Kauai channel, Hawaii. In: Inter university program of research on ferromanganese deposits of the ocean floor. Phase I report. National Science Foundation., 121-135.

MOROV N A, (1982). Relationship between height of Pacific seamount and age of lithosphere. Oceanology. V 22, No.3, 320-324.

MUKHOPADHYAY R AND KHADGE N H, (1990). Seamounts in the Central Indian Ocean Basin: indicator of the Indian plate movement. Proc. of the Indian Academy of Sciences (E and PS), V 99, 357 - 365.

MUKHOPADHYAY R M AND NAGENDERNATH B, (1988). Influence of seamount topography on the local facies variation in ferro-manganese deposits in the Indian Ocean, Deep-Sea Research, V 35 no.8, 1431-1436

NAINI B AND LEYDEN B, (1973). Ganges cone: a wide angle seismic reflection and refraction study. Journal of Geophysical Research, V 78. 8711-8720.

PAOLA CHRIS, (1985). A method for spatially averaging small-scale bottom roughness. Marine Geology. V 66, 291-301

PASHO D W, (1979). Determining deep sea-bed mine site area requirements- a discussion.: In UN ocean economics office (Ed). Dimensions and perspectives: Boston Massachusetts USA. Reidel Publishing Co. 83-112.

PATRIAT P AND SEGOUFIN J, (1988). Reconstruction of Central Indian Ocean. Tectonophysics V 155, p 211-254.

PATRIAT P, AND ACHACHE J, (1984). India-Eurasia collision chronology has implications for crustal shortening and driving mechanism of plates, Nature, 155, 211-234

PATTAN J N AND KODAGALI V N, (1988). Seabed topography and distribution of manganese nodules in the Central Indian Ocean. Mahasagar, V 21,No (1), 7-12.

PEARSON J S, (1975). Ocean floor mining. Noyes data corporatiion, Park ridge, New Jersy. 201 pp.

PEUTOT G AND MELGUEN M, (1979). Influence of deep water circulation and sea floor morphology on the abundance and grade of S Pacific manganese nodules. IN: Bischoff H, Piper D (Eds). Marine Geology and oceanography of Pacific manganese nodule Province. Plenum, Newyork. 621-649.

PIKE R J AND WILSON S E, (1971). Elevation-relief ratio, hypsometric integral and geomorphic area-altitude analysis. Geol.Soci.of Amer. Bull. V 16, 275-292

PRATT R M, (1963). Great Meteor seamounts. Deep Sea Research. V 10. 17-25.

RAO V P, (1987). Mineralogy of polymetallic nodules and associated sediments from the Central Indian Basin. Marine Geology, V 74, 151-157.

RONA P A, HARBISON R N AND BUSH S A, (1974). Abyssal hills of the eastern central north Atlantic. Marine Geology, V 16, 275-292.

ROWLETT I, (1981). Seismicity at intersection of spreading centers and transform faults, J. Geophys. Res., V 86, 3815-3820.

SANDWELL D T, AND SCHUBERT G, (1982). Lithospheric flexure at fracture zones, J. Geophys. Res., V 87, 4657-4667.

SCHLICH R, (1982). Indian ocean: Aseismic ridges, spreading centers and oceanic basins. In: Ocean Basins and Margins. A E M Neirn and F G Stehli (Eds). Plenum Press, New York. V 6, 51-147.

SIAPNO W D, (1975). Exploration technology and ocean mining parameters. American mining congress convention, San fransisco. 28 th Sept-10 th Oct. reprint 1-24.

SEARLE R C, (1979). Side scan sonar studies of North Atlantic Fracture zones. Journal of Geological Society of London. V 136, 283-292.

SHARMA R, (1989). Effect of sediment-water interface boundary layer on exposure and abundance of nodules : A study from seabed photographs, Journal of Geologocal Society of India,V 34. 310-317.

SHARMA R AND KODAGALI V N, (1990). SPHINCS: A System for cataloguing and interpreting seabed photographs of nodules. Marine Geology, V 92. 139-146.

SIDDIQUIE H N, HASHIMI N H, VORA K H AND PATHAK M C, (1987). Exploration of the continental margins of India. International Hydrographic Review. LXIV(1), 91 - 110.

SKORNYAKOVA N S AND ANDRUSCHENKO P F, (1974). Ferromanganese in the Pacific Ocean. International Geology Review. V 16, 863-919.

SMITH D K, (1988). Shape analysis of Pacific seamounts. Earth and Planetary Science Letters V 90,457-466.

SMITH D K AND SHAW P R, (1989). Using topographic distributions to infer seafloor patterns. IEEE Journal of Ocean Engineering. 338-347.

SMOOT N C, (1981). Multibeam Sonar surveys of Guyots of the Gulf of Alaska. Marine Geology, V 43. M87-94.

SMOOT N C, (1982). Guyots of the Mid-Emperor chain mapped with multibeam sonar. Marine Geology V 47. 153-163.

SOREM R K, FEWKES R H, MCFARLAND W D AND REINHART W, (1979). Physical aspects of growth environment in Horn region, east equatorial Pacific region. In: La Geneses des nodules de manganese, CNRS, Paris, 61-76.

STACKELBERG VON U, (1982). Influence of hiatuses and volcanic rains on the origin of manganese nodules of the equatorial north Pacific (Valdivia cruises VA 13/2 and VA-18). Marine Mining. V 3 297-314.

SUDHAKAR M, (1988). Relation between grade and abundance of manganese nodules. Current Science V 57, No 12, 662-663.

TAYLOR P T, STANLEY D J, SIMKIN T AND JOHN W, (1975). Gilliss Seamount: Detailed bathymetry and modification by bottom currents. Marine Geology V 19. 139-157.

TAYLOR P T, WOOD C A AND O'HEARN T J, (1980). Morphological investigation of Henderson seamount. Geology (8):390-395.

UDINTSEV G B, (1975). Geological and Geophysical Atlas of the Indian Ocean. Moscow Academy of Sciences, 151pp

USUI A, NISHIMURA A, TANAHASHI M AND TERASHIMA S, (1987). Local variability of manganese nodule facies on small abyssal hills of the Central Pacific Basin. Marine Geology V 74. 237-275.

WALGATE R, (1984). Excitement on the seabed. Nature311(5982): 96

WHITTEN D G A AND BROOKS J R V, (1976). Eds. Dictionary of Geology Penguin Books Ltd., Harmondsworth, Middlesex, England. PP 495.

WOOD C A, (1984). Calderas: a planetary perspective. Journal of Geophyscial research, V 89. 8391-8407.

YOUNG A, (1972). Slopes. K M Clayton (Ed). Oliver Boyd, Edinburgh, 288 pp.

List of Publications of the author

PATTAN J N AND **KODAGALI V N, (1988).** Seabed topography and distribution of manganese nodules in the Central Indian Ocean. Mahasagar, V 21,No (1), 7-12.

KODAGALI V N (1988). Influence of regional and local topography on the distribution of polymetallic nodules in the Central Indian Ocean Basin. Geo-Marine letters, V 8, 173-178.

PARTICIPANTS OF FS SONNE CRUISES (1988). Exploration for hydrothermal activity near Rodrigues triple junction. °anadian Mineralogist, V 26. 721-736.

BANAKAR V K AND **KODAGALI V N (1988).** Nodules of Central Indian Basin. In: book ' First Nodule to First Mine site ' edited by S Z Qasim and R R Nair.

KODAGALI V N, (1989). Morphometric studies on a part of Central Indian Ocean. Journal of the Geol. Soc. of India, V 33,547- 555.

KODAGALI V N, (1989). Morphology of an uncharted seamount from Central Indian Basin. Marine Geodesy, V 13, 89 - 94.

SHARMA R and **KODAGALI V N, (1990).** SPHINCS: A System for cataloguing and interpreting seabed photographs of nodules. Marine Geology, V 92. 139-146.

KODAGALI V N, Raju K A K, Ramprasad T, George P and Jaishankar S, **(1992).** Detailed bathymetric surveys in the Central Indian Basin. International Hydrographic Review V- LXIX(69). 143-150.

Kodagali V N, (1992). Slope angle studies from multibeam sonar data on three seamounts in Central Indian Basin. Offshore Technology Conference May 4-7, 1992 Preprints 463-470.

KODAGALI V N, (1992). Morphological investigation of 'uncharted' seamount from Central Indian Basin Revisited with multibeam sonar system. Marine Geodesy. Vol 15. 47-56.

SHARMA R AND **KODAGALI V N, (1992).** Influence of seabed topography on the distribution of manganese nodules and associated features in the Central Indian Basin: A study based on Photographic observations. Marine Geology (in press).

KAMESH RAJU K A, RAMPRASAD T, **KODAGALI V N** AND NAIR R R (1992). Multibeam bathymetric, gravity and magnetic studies over 79^0 E fracture zone- Central Indian Basin. Journal of Geophysical Research (in Press)

RAO P S, **Kodagali V N,** RAMPRASAD T AND NAIR R R **(1992).** Morphology of a coral bank, Western Continental shelf of India: a multibeam study. Journal of Geological Society of India (in Press).

Technical/Cruise reports.... 09.

Papers presented at Syposia/Seminars..... 11.

T-138